

Polyelectrolyte-based Nanoparticles for Gene and Protein Delivery

By

Supang Khondee

Submitted to the graduate degree program in Pharmaceutical Chemistry and the
Graduate Faculty of the University of Kansas in partial fulfillment of the requirements
for the degree of Doctor of Philosophy.

Cory Berkland, Chairperson

C. Russell Middaugh

Teruna J. Siahaan

Laird Forrest

Prajna Dhar

Date Defended: April 14, 2011

The dissertation committee for Supang Khondee certifies that this is the approved version of the following dissertation:

Polyelectrolyte-based Nanoparticles for
Gene and Protein Delivery

Cory Berkland, Chairperson

Date approved: April 14, 2011

ABSTRACT

Polyelectrolytes have emerged as a versatile, simple and promising tool to deliver therapeutic payloads. Their ability to form complexes with oppositely charged polymers or biomacromolecules has led to various applications in the pharmaceutical and biotechnology industries. In this thesis, three different polyelectrolyte delivery systems have been developed and explored for potential uses in gene and protein delivery.

Polyvinylamine (PVAm) nanogels with different amounts of surface charge and degradability were used to systematically inspect gene transfection efficiency and cytotoxicity. Transfection efficiency of non-degradable nanogels increased with increasing amounts of positive charge. Intriguingly, acid-labile nanogels bearing low charge showed sustained gene transfection and low cytotoxicity. An intricate balance between transfection efficiency and cytotoxicity is crucial for gene vectors. These results led to an exploration of less toxic, small polycations.

Historically, polyplexes using small polycationic peptides such as TAT have shown relatively poor gene transfection, however, previous studies in our group showed that the transfection efficiency could be enhanced by condensing these large polyplexes using calcium. In this thesis, the LABL peptide targeting intercellular cell-adhesion molecule-1 (ICAM-1) was conjugated to TAT peptide using a polyethylene glycol (PEG) spacer. Though the transfection efficiency of TAT polyplexes was reduced by PEGylation, TAT complexes targeting ICAM-1 were able to restore high levels of gene transfection. Thus, targeted TAT polyplexes offer promise for gene delivery to sites of injury or inflammation. Next, other PEGylation strategies using polyelectrolytes were explored.

Repifermin, a truncated version of fibroblast growth factor-10 (FGF-10) also known as keratinocyte growth factor-2 (KGF-2), is a heparin-binding protein with potent regenerative properties. The protein unfolds and aggregates at relatively low temperature (~37 °C). The thermal stability of several FGFs was enhanced by electrostatic interactions with polyanions. PEG was grafted to the polyanions pentosan polysulfate (PPS) and dextran sulfate (DS). The potential uses of polyanion conjugates were explored using a variety of spectroscopic and calorimetric methods, and dynamic light scattering. PPS-PEG and DS-PEG conjugates were able to stabilize KGF-2 by increasing the melting temperature of the protein complexes. Though there are several parameters that could be optimized to improve the protein structure upon binding, polyanion-PEG conjugates, however, are encouraging reagents that can improve the thermal stability of heparin-binding proteins via electrostatic PEGylation.

Dedicated to:

*My parents,
Supan Khondee and Supat Dachata*

ACKNOWLEDGEMENTS

I would like to express my earnest gratitude to my mentor and advisor, Dr. Cory Berkland, for his continued guidance, encouragement and support. These projects would never have been possible without his vision. It has been a pleasure to work for him and with him over the years. I would like to special thank Cory for his patience, understanding and kindness throughout the years. I will always respect your advice to think out of the box and to balance between personal and professional lives, Cory.

I am grateful to Drs. Russ Middaugh, Teruna Siahaan, Laird Forrest, and Prajna Dhar for taking the time to serve on my dissertation committee and for pushing me toward excellence. I especially want to thank Drs. Middaugh and Siahaan for their helpful and insightful comments as readers.

My time here would not have been this enjoyable if it were not for all the wonderful friendships I have had. I would like to thank all of my past and present colleagues at the University of Kansas for all of their help and support which helped me get through my research and several dead-end times: Lianjun Shi, Tatyana Yakovleva, Sheng-Xue Xie, Huili Guan, Christopher Olsen, Yuhong Zeng, Kristin Aillon, Abdulgader Baoum, Joshua Sestak, Taryn Bagby, Rungsinee Phongpradist, Sharadvi Thati, Nadya Galeva, and Heather Shinogle. I would also like to thank my roommates for their friendship and support throughout the years: Chuda Chittasupho and Warangkana Pornputtapitak. Thank you to all my Thai friends in Lawrence for making the town a fun and enjoyable place to live.

I would also like to thank the entire faculty in the Department of Pharmaceutical Chemistry for their outstanding instruction and mentorship over the years. I feel fortunate to have a chance to study here, one of the premiere institutions

in the field. Many thanks go to all staff in the Department of Pharmaceutical Chemistry for their assistance and support.

I would like to extend a sincere thank you to the graduate scholarship from Naresuan University, Thailand for financial support during the first three years of my study.

I never could have made it to where I am now without the love, support and continuous encouragement from my family. I owe my deepest gratitude to my parents for their support throughout my education and especially to my mom for being my 'number one fan' throughout the years. I would like to special thank my brothers for their humor, motivation and faith during difficult times. Finally, I would like to thank God for blessing my life with health, opportunity and wonderful people.

Supang Khondee

April 2011

TABLE OF CONTENTS

Chapter 1: Polyelectrolytes as therapeutic delivery systems	1
1.1 Introduction.....	2
1.2 Background and general properties.....	3
1.1.1 Classifications	3
1.1.1.1 Synthetic polyelectrolytes	3
1.1.1.2 Natural polyelectrolytes	5
1.1.2 Polyelectrolyte properties	14
1.3 Biomedical applications of polyelectrolytes	19
1.3.1 Drug and nucleic acid delivery	19
1.3.2 Protein stabilization, immobilization and controlled release...	23
1.3.3 Responsive drug delivery systems	28
1.4 Thesis goal, outline and specific aims	29
1.4.1 The effect and relationship of surface charge and degradability of polyvinyl amine (PVAm) nanogel on transfection efficiency	30
1.4.2 Calcium-crosslinked LABL-TAT complexes effectively target gene delivery to ICAM-1 expressing cells	30
1.4.3 Non-covalent PEGylation by polyanion complexation as a novel means to stabilize Keratinocyte Growth Factor-2 (KGF-2).....	30
1.5 Bibliography	32
Chapter 2: The effect and relationship of surface charge and degradability of polyvinyl amine (PVAm) nanogel on transfection efficiency	39
2.1 Introduction.....	40
2.2 Materials and methods.....	42
2.2.1 Materials	42
2.2.2 Synthesis of polyvinylamine nanogel	42

2.2.3 Cell culture and plasmid DNA preparation	43
2.2.4 Formation of polyvinylamine /DNA complexes	44
2.2.5 Gel electrophoresis	44
2.2.6 <i>In vitro</i> transfection assay	44
2.2.7 Particle size and zeta-potential measurements	45
2.2.8 Cell viability assay	45
2.3 Results	46
2.3.1 PVAm nanogel synthesis	46
2.3.2 Complex formation	51
2.3.4 Cytotoxicity test	56
2.3.5 Transfection	58
2.4 Discussion	61
2.5 Conclusions	64
2.6 Bibliography	65
Chapter 3: Calcium-crosslinked LABL-TAT complexes effectively target gene delivery to ICAM-1 expressing cells	70
3.1 Introduction.....	71
3.2 Materials and methods.....	73
3.2.1 Materials	73
3.2.2 Complex formation	75
3.2.3 Size and morphology	75
3.2.4 Agarose gel electrophoresis	76
3.2.5 Cytotoxicity assay	76
3.2.6 Relative ICAM-1 expression on A549 cells	77
3.2.7 Transfection studies	77

3.2.8 Confocal microscopy of internalization	78
3.2.9 Statistic analysis	79
3.3 Results	79
3.3.1 Purification and characterization of TAT, TAT-PEG, and TAT-PEG-LABL	79
3.3.2 Physicochemical characterization of complexes	79
3.3.3 Cytotoxicity, transfection efficiency, and intracellular accumulation of complexes	88
3.4 Discussion	96
3.5 Conclusions	102
3.6 Bibliography	103
Chapter 4: Non-covalent PEGylation by polyanion complexation as a novel means to stabilize keratinocyte growth factor-2 (KGF-2).....	108
4.1 Introduction.....	109
4.2 Materials and methods.....	112
4.2.1 Materials.....	112
4.2.2 Synthesis of carboxymethyl dextran sulfate (CMDS).....	112
4.2.3 Synthesis of dextran sulfate-PEG 5 kDa and 20 kDa.....	113
4.2.4 Synthesis of pentosan sulfate-PEG 5 kDa and 20 kDa.....	114
4.2.5 Characterization of polyanion conjugates.....	114
4.2.6 Cytotoxicity assay.....	116
4.2.7 Formulation of KGF-2:polyanion complexes.....	116
4.2.8 Biophysical characterization of KGF-2 complexes.....	117
4.3 Results	119
4.3.1 Synthesis and characterization of polyanion-PEGs.....	119
4.3.2 Cytotoxicity test.....	126

4.3.3 Differential scanning calorimetry	126
4.3.4 Circular dichroism	128
4.3.5 Intrinsic tryptophan fluorescence spectroscopy	133
4.3.6 Heat induced aggregation studies.....	136
4.3.7 Isothermal titration calorimetry	143
4.3.8 Competitive binding study	144
4.4 Discussion	144
4.5 Conclusions	148
4.6 Bibliography	149
Chapter 5: Conclusions	152
5.1 Summary and conclusions	153
5.2 Future directions	155
5.3 Bibliography	157

INDEX OF FIGURES

<u>Figure</u>	<u>Page(s)</u>	<u>Caption</u>
1.1	14	(A) An uncharged polymer molecule in a random coil shape (B) an anionic polyelectrolyte in salt-free solution.
1.2	18	A representative scheme of PEC formation when the two constituent polyelectrolytes have very different molecular weights.
2.1	47	Reaction scheme for (A) non-degradable and (B) acid-labile PVAm nanogel synthesis.
2.2	50	Conversion rate of non-degradable PVAm nanogels with (A) 0.1 N NaOH (B) 0.5 N NaOH and degradable PVAm nanogels with (C) 0.1 N NaOH (D) 0.5 N NaOH at 80 °C over time.
2.3	52	¹ H-NMR spectra of (A) non-degradable PNVF and (B) non-degradable PVAm nanogels after hydrolysis with 0.1 N NaOH at 80 °C for 6 h and (C) acid-labile PNVF and (D) acid-labile PVAm nanogels after hydrolysis with 0.5 N NaOH at 80 °C for 3 h.
2.4	53	Gel electrophoresis of non-degradable PVAm/DNA complexes made from (a) 158 nm, +8.2 mV, (b) 116 nm, +18 mV, and acid-labile PVAm/DNA complexes made from (c) 308 nm, +3.5 mV (d) 228 nm, +11 mV.
2.5	54	Effective diameter of non-degradable (a, b) and acid-labile (c, d) PVAm/DNA complexes at different polymer-to-DNA ratios ($n = 3 \pm \text{SD}$).
2.6	55	Stability of (A) non-degradable and (B) acid-labile PVAm/DNA complexes at different nanogel-to-DNA ratios in serum free medium and (C) non-degradable and (D) acid-labile PVAm/DNA complexes at different nanogel-to-DNA ratios in growth medium over time.
2.7	57	Cytotoxicity of PEI, non-degradable (a, b) and acid-labile (c, d) PVAm nanogels in A549 cells.
2.8	59	Transfection efficiency of non-degradable PVAm complexes made from (A) PVAm, 158 nm, +8 mV (B) PVAm, 116 nm, +18 mV and acid-labile complexes made from (C) PVAm, 308 nm, +3.5 mV (D) PVAm, 228 nm, +11 mV at different nanogel-to-DNA ratios 2 and 4 day post-transfection in A549 cells.
3.1	80	HPLC chromatograms for TAT, TAT-PEG, and TAT-PEG-LABL confirmed purity > 95%.

<u>Figure</u>	<u>Page(s)</u>	<u>Caption</u>
3.2	81	Electrospray ionization (ESI) mass spectra of (A) TAT, (B) TAT-PEG, and (C) TAT-PEG-LABL were in agreement with calculated masses.
3.3	83	Gel electrophoresis of (A) TAT/DNA and (B) TAT-PEG/DNA complexes at different N/P ratios. (C) TAT-PEG-LABL/DNA complexes at an N/P ratio of 30 with different amounts of TAT-PEG-LABL combined with TAT-PEG. All complexes at all N/P ratios limited the mobility of DNA.
3.4	84	DLS was used to determine the size of TAT/DNA, TAT-PEG/DNA, 25% TAT-PEG-LABL/DNA, and 50% TAT-PEG-LABL/DNA complexes at an N/P ratio of 30 with different concentration of CaCl ₂ . (A) The hydrodynamic diameters of complexes were determined in deionized water and (B) in serum-free F12K media. (C) The hydrodynamic diameter of complexes (formed with 150 mM CaCl ₂) in F12K media were stable over time. For missing data points, diameter was >1 μm.
3.5	86	Transmission electron micrographs of (A) TAT/DNA, (B) TAT/DNA-Ca, (C) TAT-PEG/DNA, (D) TAT-PEG/DNA-Ca, (E) 25% TAT-PEG-LABL/DNA, (F) 25% TAT-PEG-LABL/DNA-Ca (G) 50% TAT-PEG-LABL/DNA, and (H) 50% TAT-PEG-LABL/DNA-Ca complexes. Complexes were formed at an N/P ratio of 30 without CaCl ₂ (left panel) or with 75 mM of CaCl ₂ (right panel). Scale bars are 500 nm.
3.6	87	A heparin displacement assay for (A) TAT/DNA, (B) TAT-PEG/DNA, (C) 25% TAT-PEG-LABL/DNA, and (D) 50% TAT-PEG-LABL/DNA complexes was used to assess the effect of calcium chloride concentration (0, 30, 75, 150, 300 mM) on complex stability. Complexes were formed at an N/P of 30 and incubated for 30 min with increasing heparin concentrations (0.05-0.35 U). Free DNA is shown as a control (C) to the left.
3.7	89	TAT peptide and derivatives showed low cytotoxicity in comparison to PEI (A) in unactivated and (B) in activated A549 cells, which overexpress ICAM-1.
3.8	90	Transfection efficiencies of TAT peptide derivative/DNA complexes in A549 cells. (A) TAT/DNA and TAT-PEG/DNA complexes at an N/P ratio of 30 with different concentrations of calcium chloride (B) TAT/DNA complexes at different N/P ratios (C) TAT-PEG/DNA complexes at different N/P ratios. L= Lipofectamine.

<u>Figure</u>	<u>Page(s)</u>	<u>Caption</u>
3.9	92	Relative ICAM-1 expression level in A549 cells after activation with TNF- α for 24 h and 48 h (* = $p < 0.05$, <i>t</i> -test).
3.10	94	Transfection efficiencies of TAT peptide derivative/DNA complexes in activated A549 cells (overexpressing ICAM-1) at different concentrations of calcium chloride. Complexes were formed at an N/P ratio of 30. L= Lipofectamine (* = $p < 0.05$, one-way ANOVA, Tukey post test).
3.11	95	Transfection efficiencies of TAT/DNA and 50% TAT-PEG-LABL/DNA complexes in activated A549 cells (overexpressing ICAM-1) after incubation with free LABL peptide or anti-ICAM-1 mAb prior to exposure to TAT complexes. Complexes were formed at an N/P ratio of 30 and 150 mM CaCl ₂ (* = $p < 0.05$, ** = $p < 0.01$, one-way ANOVA, Tukey post test).
3.12	97	Transfection efficiencies of 25% and 50% TAT-PEG-LABL/DNA complexes in normal and activated A549 cells. Complexes were formed at an N/P ratio of 30 and 150 mM CaCl ₂ (* = $p < 0.05$, <i>t</i> -test).
3.13	98	Micrographs of (A) TAT-PEG/DNA complexes and (B) 50% TAT-PEG-LABL/DNA complexes in A549 cells (activated with TNF- α) after 4 h of incubation at 37 °C. Complexes were formed at an N/P ratio of 30 and a CaCl ₂ of 150 mM (1 = DAPI fluorescence (cell nuclei), 2 = TOTO-3 fluorescence (DNA), 3 = Merged DAPI and TOTO-3 fluorescence, 4 = Merged DAPI, TOTO-3 fluorescence, and bright field transmission).
4.1	111	Representative structures of (A) pentosan polysulfate (PPS) and (B) dextran sulfate (DS).
4.2	120	DSC thermograms of KGF-2 and KGF-2:polyanion complexes at different molar ratios for (A) chromotropic acid (B) acid fuchsin (C) pyridoxal-phosphate-6-azophenyl-2',4'-disulfonate (PPADS) (D) congo red (E) trypan blue (F) PPS and (G) DS (upward = endothermic).
4.3	123	Size exclusion chromatography showed (A) polymers with different MW, structure, and charge exhibiting different retention times (numbers indicate MW (kDa)) (B) Chromatograms of PPS and PPS-conjugates and (C) chromatograms of DS and DS-conjugates.
4.4	124	SDS-PAGE analysis of polyanions and conjugates compared to PEG standards.

<u>Figure</u>	<u>Page(s)</u>	<u>Caption</u>
4.5	125	(A) The depletion of methylene blue absorbance (664 nm) upon binding with increasing amount of polyanions and (B) standard curves of PPS and DS.
4.6	127	Cytotoxicity of (A) PPS and (B) DS and polyanion conjugates in HUVEC compared to PEI.
4.7	129	DSC thermograms of KGF-2 and KGF-2:polyanion complexes at different molar ratios for (A) PPS and (B) DS and polyanion conjugates (upward = endothermic).
4.8	130	Far-UV CD spectra of KGF-2 and KGF-2:polyanion complexes at different molar ratios (scanned at 10 °C) for (A) PPS and (B) DS and polyanion conjugates.
4.9	131	(A) Far-UV CD spectra of unfolded KGF-2 (scanned at 10 °C) (B) melting curves of unfolded KGF-2 by monitoring fluorescence emission maximum position shifts.
4.10	132	Effect of temperature on the molar ellipticity of KGF-2 and KGF-2:polyanion complexes (monitored at 229 nm) at different molar ratios for (A) PPS and (B) DS and polyanion conjugates.
4.11	134	Effect of temperature on the fluorescence emission maximum positions of KGF-2 and KGF-2:polyanion complexes at different molar ratios for (A) PPS and (B) DS and polyanion conjugates.
4.12	135	Effect of temperature on light-scattering intensity (monitored at 295 nm) of KGF-2 and KGF-2:polyanion complexes at different molar ratios for (A) PPS and (B) DS and polyanion conjugates.
4.13	137	Temperature induced aggregation of KGF-2 and selected KGF-2:polyanion complexes monitored using (A) optical density (OD) at 350 nm and (B) dynamic light scattering (DLS).
4.14	139	The hydrodynamic diameter of KGF-2:PPS-PEG20 complexes at 20 °C.
4.15	141	Representative ITC binding isotherm of KGF-2 (20 μM) titrated with DS (500 μM) at 25 °C.

INDEX OF TABLES

<u>Table</u>	<u>Page(s)</u>	<u>Caption</u>
1.1	5	Representative synthetic polyelectrolytes.
1.2	9	Representative natural polyelectrolytes.
2.1	49	(A) Representative properties of PNVF and PVAm nanogels and (B) statistical analysis (one-way ANOVA, Tucky post test)
4.1	121	Characteristics of polyanion conjugates.
4.2	138	The hydrodynamic diameter of KGF-2 and selected KGF-2 complexes at 10 °C.
4.3	140	Transition midpoint of KGF-2 alone and in the presence of polyanions and polyanion-PEGs.
4.4	142	Thermodynamic parameters of most KGF-2 interactions with polyanions or conjugates using a two-site model and a one-site model for KGF-2:PPS-PEG20 complexes ($^*\Delta G = \Delta H - T\Delta S$, T = 298 K).

Chapter 1

Polyelectrolytes as therapeutic delivery systems

1.1 Introduction

Many of the pharmacological and therapeutic properties of drugs can be improved through the use of drug delivery systems (DDSs) such as lipid- and polymer-based nanoparticles. DDSs are often designed to alter pharmacokinetics, biodistribution, or to serve as drug reservoirs. Polymers have been used intensively in DDSs and recently have emerged as an essential component of novel therapeutics. These therapeutics include macromolecular drugs, polymer-drug and polymer-protein conjugates, and polymeric drug delivery systems such as polymeric micelles and polycation complexes with DNA or RNA (polyplexes).

Several improvements have been reported when using polymers in DDSs. First, conjugation of polyethylene glycol (PEG) has resulted in the improved stability and pharmacokinetic properties of many therapeutic proteins. Several PEGylated protein products are commercially available. For example, PEGylated asparaginase (Onspar®), PEGylated adenosine deamidase (Adagen®) and PEGylated interferon (PEG-Intron™ and PEG-Asys®).¹ Second, conjugation of low-molecular weight anticancer drugs to polymers has improved the therapeutic index of several anticancer drugs. Some anticancer drug conjugates are in clinical trials. For example, polyglutamate-paclitaxel (CT-2103; XYOTAX™), N-(2-hydroxypropyl) methacrylamide (HPMA)-doxorubicin (PK1; FCE28068) and HPMA-doxorubicin-galactosamine (PK2; FCE28069).² Other novel polymer-based DDSs are well-defined multivalent and dendritic polymers such as the microbicide VivaGel, a dendritic polyanion that can potentially reduce or prevent transmission of HIV.³

There are several approaches to incorporate therapeutics to and/or into polymers including covalent conjugation, entrapment or encapsulation, and electrostatic complexation. Covalent conjugation usually involves harsh chemicals

and/or organic solvents and often, a reduction in biological activity has been reported.¹ Meanwhile, polymerization reactions can require multiple preparation and purification steps. As a result, this thesis focuses on electrostatic interactions between oppositely charged biomacromolecules such as nucleic acids or model proteins and polyelectrolytes, to explore various polyelectrolyte-based DDSs.

1.2 Background and general properties

Polyelectrolytes are polymers carrying ionizable groups along the polymer chain. Polyelectrolytes may be anionic, cationic or amphiphilic and they may be synthetic or natural. Examples of polyelectrolytes include poly(acrylic acid), poly(methacrylic acid), poly(vinyl amine), poly(4-vinyl pyridine), and many biological molecules such as polypeptides, proteins, nucleic acids, and polysaccharides. Polyelectrolytes are used in a variety of industries such as papermaking, food processing, medicine and pharmaceuticals, water purification, oil field exploration, and cosmetic formulation. This chapter will briefly overview polyelectrolytes, classifications, general properties, and polyelectrolyte-polyelectrolyte and polyelectrolyte-surfactant interactions, then focus will shift to biomedical applications of polyelectrolytes.

1.2.1 Classification of polyelectrolytes

Polyelectrolytes are available in a wide range of chemistries, molecular weights and charge densities. For biomedical applications, certain polyelectrolytes reviewed here have the potential to be translated to the clinic such as biodegradable synthetic polyelectrolytes or natural polyelectrolytes.

1.2.1.1 Synthetic polyelectrolytes

Polyelectrolytes can be synthesized by polymerization of ionized monomers, incorporating ionizable groups into a polymer chain, or by chemical modification of

existing polymers (Table 1.1). These methods have been reviewed extensively elsewhere (see Scranton *et al.*⁴, Jiang *et al.*,⁵ and Bohrisch *et al.*⁶). Generally, polymerization is more prevalent since the properties of final products can be controlled easily. However, the method of choice depends upon the type of added functional groups and the nature of parent polymers.

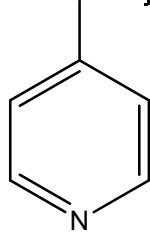
For the first method, polymerization of ionizable monomers, polyelectrolytes are commonly synthesized by free-radical polymerization of monomers containing a carbon-carbon double bond. Crosslinked polymers may be produced by including a small amount of a crosslinking agent. Step-growth polymerization reactions may be used to synthesize polyelectrolytes, but this method is less common. This reaction is a type of polymerization in which monomers react to form dimers, trimers, longer oligomers and eventually long chain polymers and initiators or terminators are not usually required.

The second method employs post-polymerization modifications of nonionic polymers. Sulfonation can produce anionic polyelectrolytes containing sulfonic acid groups. Addition or substitution reactions may be used to produce polyelectrolytes. In addition, hydrolysis or oxidation of labile bonds may also be used to functionalize nonionic polymers.

Both of these methods have been successfully employed to create homopolymer or random copolymer polyelectrolytes. In addition, amphiphilic block copolymers which contain both anionic and cationic blocks can be synthesized by using free-radical polymerization, by modifying one block of a block copolymer, or by coupling two blocks that were synthesized *a priori*. More advanced polyelectrolyte architectures such as branched, conjugated or star-shape polyelectrolytes have been

widely studied to achieve desired properties. Several authors have reported these methods elsewhere.^{5,7}

Table 1.1. Representative synthetic polyelectrolytes

Name	Structure
Poly(acrylic acid)	$\left[\text{CH}_2\text{CH} \begin{array}{c} \\ \text{COOH} \end{array} \right]_n$
Poly(methacrylic acid)	$\left[\text{CH}_2\text{C} \begin{array}{c} \\ \text{CH}_3 \\ \\ \text{COOH} \end{array} \right]_n$
Poly(ethylenimine)	$\left[\text{CH}_2\text{CHNH} \begin{array}{c} \\ \text{H} \end{array} \right]_n$
Poly(vinylamine)	$\left[\text{CH}_2\text{CH} \begin{array}{c} \\ \text{NH}_2 \end{array} \right]_n$
Poly(4-vinylpyridine)	$\left[\text{CH}_2\text{CH} \begin{array}{c} \\ \text{C}_5\text{H}_4\text{N} \end{array} \right]_n$ 

1.2.1.2 Natural polyelectrolytes

Among polymeric materials, natural polymers are ideal candidates for therapeutic formulation, since they are generally non-cytotoxic even at high

concentrations.⁸ They also often contain reactive sites that are amendable to conjugation, crosslinking and other modifications. Natural polyelectrolytes have emerged as therapeutics in molecular medicines (e.g. proteins, nucleic acids, and peptides) or as essential components of carriers or platforms in drug and gene delivery, vaccination, and tissue engineering (e.g. polysaccharides and polypeptides). For example, chitosan has been successful in oral and nasal delivery due to the mucoadhesive property. Collagen, gelatin, chitosan, alginate, and their derivatives have been extensively studied in gene therapy.

Nucleic acids

Nucleic acids including deoxyribonucleic acid (DNA) and ribonucleic acid (RNA) have emerged as promising therapeutics in cancers, cardiovascular, inflammatory, and infectious diseases as well as organ transplantation.⁹ Nucleic acids can be synthesized via polymerase chain reaction (PCR) or solid phase synthesis. Nucleic acid-based therapeutics include plasmids containing transgenes for gene therapy and vaccines, oligonucleotides for antisense and antigene applications, ribozymes, DNazymes, aptamers, small interfering RNAs (siRNAs) and others. Plasmids are high molecular weight, double-stranded DNAs containing transgenes, which encode specific proteins.¹⁰ Oligonucleotides are short single-stranded segments of DNA that can selectively inhibit the expression of a single protein after being internalized.¹¹ Ribozymes are RNA molecules which can cleave mRNA molecules in a sequence specific manner.¹² DNazymes are analogs of ribozymes which have greater biological stability.¹³ SiRNAs are short doublestranded RNAs with typically 21-23 nucleotides that are complementary to the targeted mRNA intended for knockdown.¹⁴⁻¹⁵

Poly(amino acid)s or polypeptides

Amino acid-based polymers have received much attention due to their biocompatibility and biodegradability and the accuracy of their synthesis. Poly(amino acid)s can be biosynthesized from microorganisms or chemically synthesized. Some of these polymers have unique properties and functions derived from the amino acid moiety. For example, poly(glutamic acid) is a poly(amino acid) with carboxyl groups on the side chain which allow conjugation with several chemotherapeutic agents such as doxorubicin, daunorubicin, mephalan, paclitaxel, and camptothecin.¹⁶ In addition, poly(L-lysine) and poly(arginine) have been widely used as non-viral carriers. These poly(amino acid)s are protonated in a physiological environment and are able to form complexes with negatively charged DNA. Some poly(amino acid)s such as TAT peptide have the ability to cross cellular membranes allowing the intracellular delivery of various molecules ranging from low molecular weight drugs to nanosized particles.¹⁷

Polysaccharides

Polysaccharides are polymers formed from repeating monosaccharides or disaccharides which are linked together by glycosidic bonds. Polysaccharides are often heterogenous, containing slight modifications of repeating units. Polysaccharides can be produced via microbial fermentation, animal and plant extraction. Polysaccharides have emerged as a class of biomaterials with enormous potential applications including protein interactions, cell and tissue engineering, vaccine delivery, and cancer treatment.¹⁸⁻¹⁹ Some selected natural polysaccharides which are of interest in this thesis are listed below.

Chitin and chitosan: Chitin is a major component of crustacean shells such as crab, shrimp and crawfish shells and is a byproduct of the shell-fish industry. It is a

copolymer of β -1,4 linked D-glucosamine and N-acetyl D-glucosamine. Chitosan is modified from chitin, by partial deacetylation of the N-acetyl D-glucosamine residues. Chitosan is insoluble in water, but soluble in weak organic solutions such as acetic acid and formic acid.²⁰

Alginate: Alginate is a linear anionic polysaccharide. It is a block copolymer of β -1,4 linked D-manuronic acid (M) and α -1,4 linked L-guluronic acid (G) residues, produced by algae. The monomers can be arranged in consecutive MM blocks, consecutive GG blocks, alternating MG blocks or randomly organized blocks.²¹ It has abundant hydroxyl and carboxyl groups (one carboxylic group per saccharide unit). Alginate absorbs water quickly.

Dextran and dextran sulfate: Dextran is a complex, branched glucan in which the straight chain consists of α -1,6 glycosidic linkages of glucopyranose units and branches begin from α -1,3 linkages. Dextran can be synthesized either chemically or by certain lactic-acid bacteria from sucrose.²² Dextran sulfate is a negatively charged polymer that can be synthesized by sulfonation of dextran.²³ It typically contains approximately 17% sulfur, which is equivalent to approximately 2.3 sulfate groups per glucosyl residue, although the degree of sulfonation can vary.

Chondroitin sulfate: Chondroitin sulfate is a sulfated glycosaminoglycan (GAG) composed of a chain of alternating sugars N-acetylgalactosamine (GalNAc) and glucuronic acid (GlcA). Each sugar residue can be sulfated in variable positions and quantities. For example, chondroitin-4-sulfate is sulfated at carbon 4 of GalNAc sugar, chondroitin-6-sulfate is sulfated at carbon 6 of GalNAc sugar, chondroitin-2,6-sulfate is sulfated at carbon 2 of GlcA and 6 of GalNAc sugar and chondroitin-4,6-sulfate is sulfated at carbon 4 and 6 of GalNAc sugar.

Heparin and heparan sulfate: Heparin and heparan sulfate are linear polysaccharides which have similar structures, but heparan sulfate is less sulfated. Heparin and heparan sulfate consist of variably sulfated repeating disaccharide units that can be combined into a large variety of different sequences. The most common disaccharide unit is composed of a glucuronic acid (GlcA), N-acetylglucosamine (GlcNAc), 2-O-sulfated iduronic acid and 6-O-sulfated and N-sulfated glucosamine.

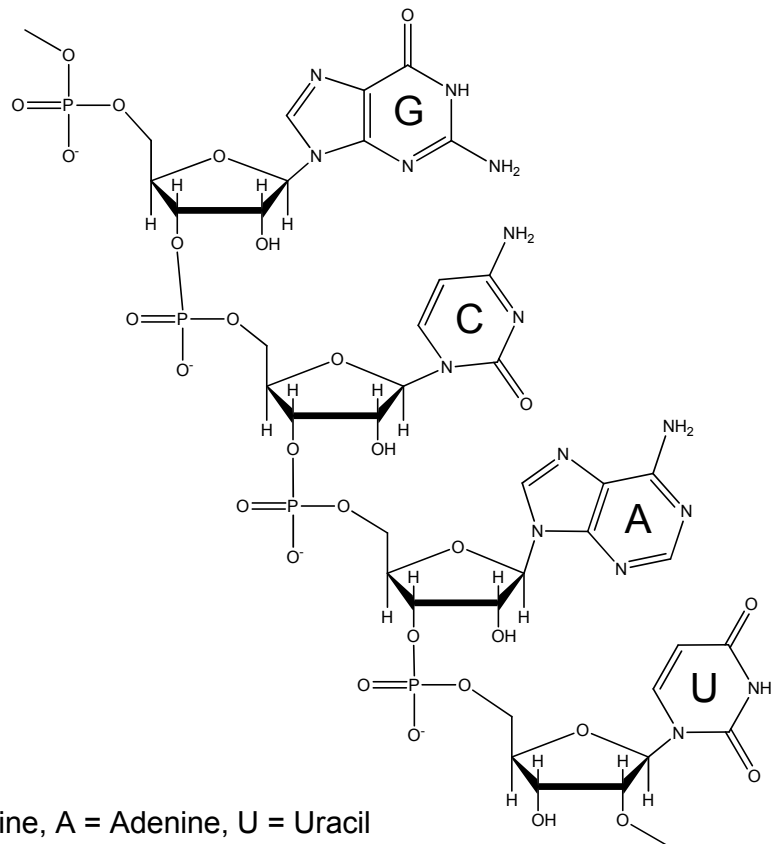
Sucrose octasulfate: Sucrose octasulfate (SOS) is a sulfated disaccharide. Sucrose octasulfate was found to mimic heparin action by supporting fibroblast growth factor (FGF)-induced neovascularization and cell proliferation *in vitro*.²⁴⁻²⁶ SOS is also a precursor of Sucrafate, an anti-ulcer drug that mediates its action through interaction with FGFs.²⁷⁻²⁸

Table 1.2. Representative natural polyelectrolytes

Name	Structure
<i>Nucleic acids:</i>	
Deoxyribonucleic acid (DNA)	<p>The diagram illustrates a segment of a DNA double helix. It shows two antiparallel sugar-phosphate backbones. The sugar units are deoxyribose, and the phosphate groups are linked by phosphodiester bonds. The nitrogenous bases are Adenine (A), Thymine (T), Cytosine (C), and Guanine (G). Hydrogen bonds are shown as red dashed lines between the bases: A pairs with T (two bonds), and C pairs with G (three bonds).</p>
	C = Cytosine, G = Guanine, A = Adenine, T = Thymine

Name	Structure
------	-----------

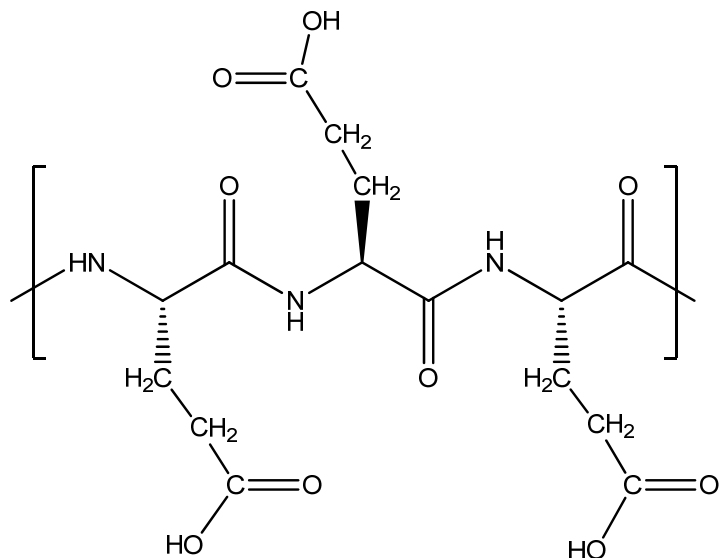
Ribonucleic acid (RNA)



C = Cytosine, G = Guanine, A = Adenine, U = Uracil

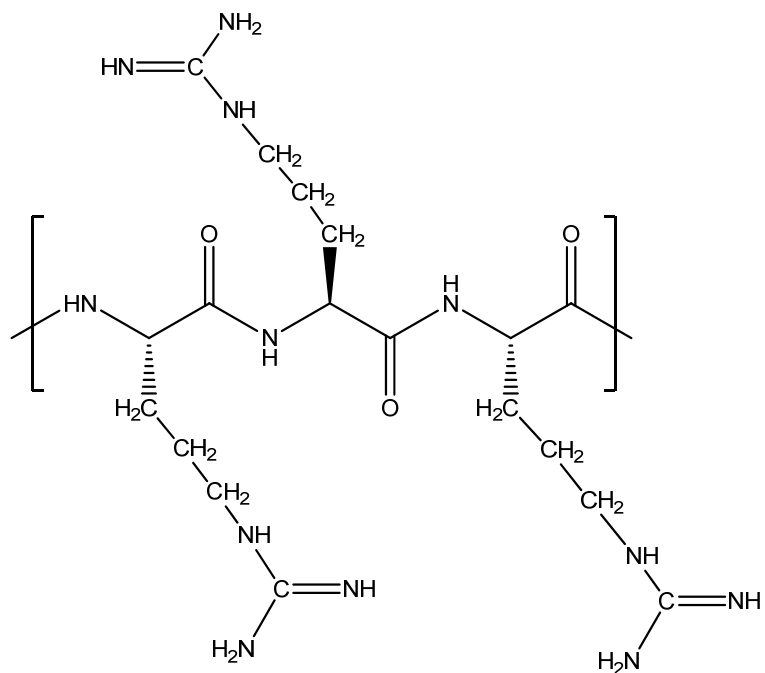
Poly(amino acid)s:

Poly(glutamic acid)

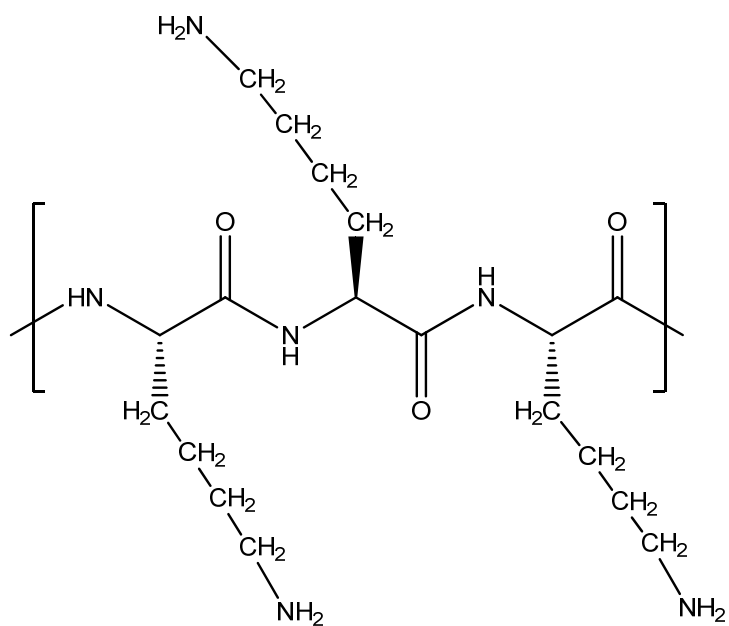


Name	Structure
------	-----------

Polyarginine



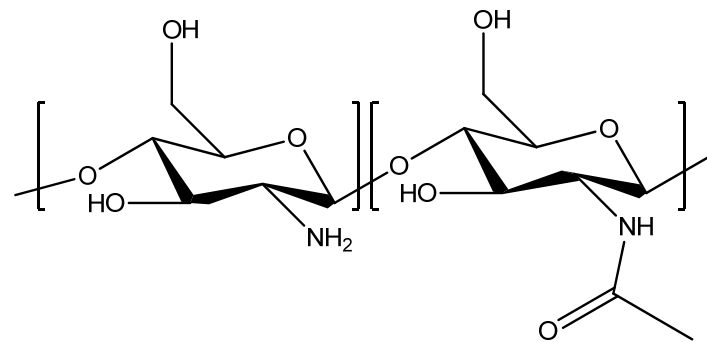
Poly(lysine)



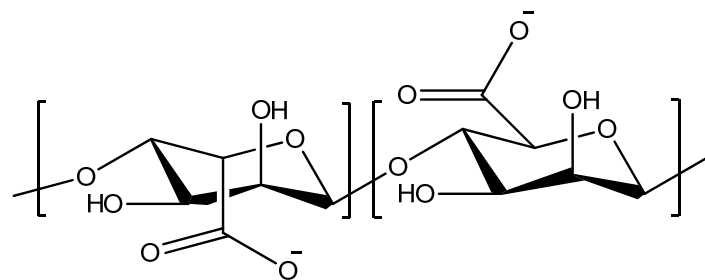
Name	Structure
------	-----------

Polysaccharides:

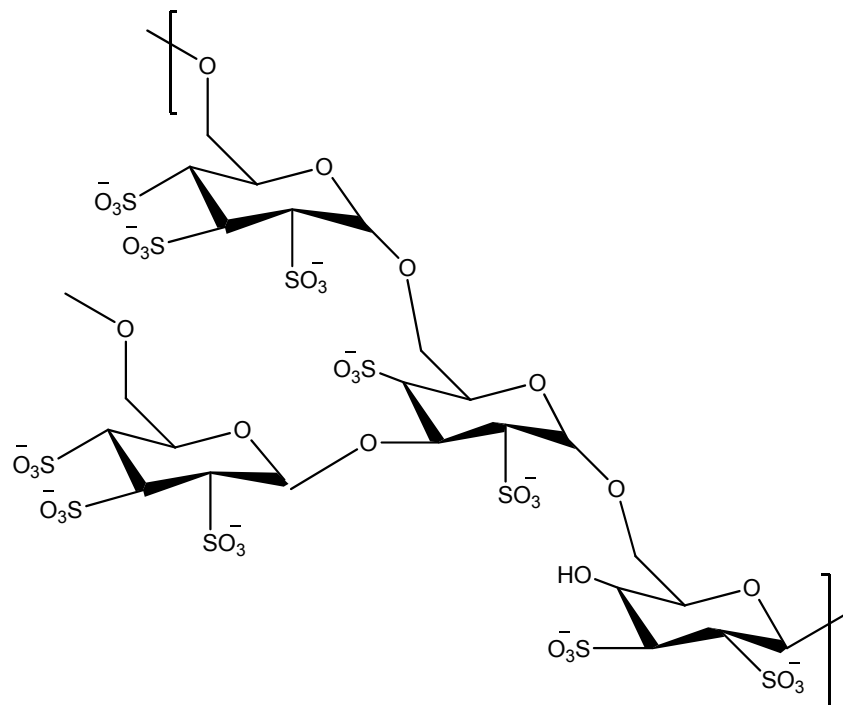
Chitin and chitosan



Alginate



Dextran sulfate



Name	Structure
Chondroitin-4-sulfate	
Chondroitin-6-sulfate	
Heparin and heparan sulfate	<p data-bbox="691 1294 1015 1368"> $X = \text{OH}, \text{OSO}_3^-$ $Y = \text{NHAc}, \text{NH}_2, \text{NHSO}_3^-$ </p>
Sucrose octasulfate	

1.2.2 Polyelectrolyte properties

In solution, polyelectrolytes exhibit interesting behavior different from that of uncharged polymers. For example, the conformation of polyelectrolytes depends on the degree of ionization. An uncharged linear polymer is often found in a “random coil” conformation in solution (Figure 1.1A). The charges on a linear polyelectrolyte chain will repel each other, which can cause the chain to expand to a “rigid-rod-like” conformation (Figure 1.1B).²⁹

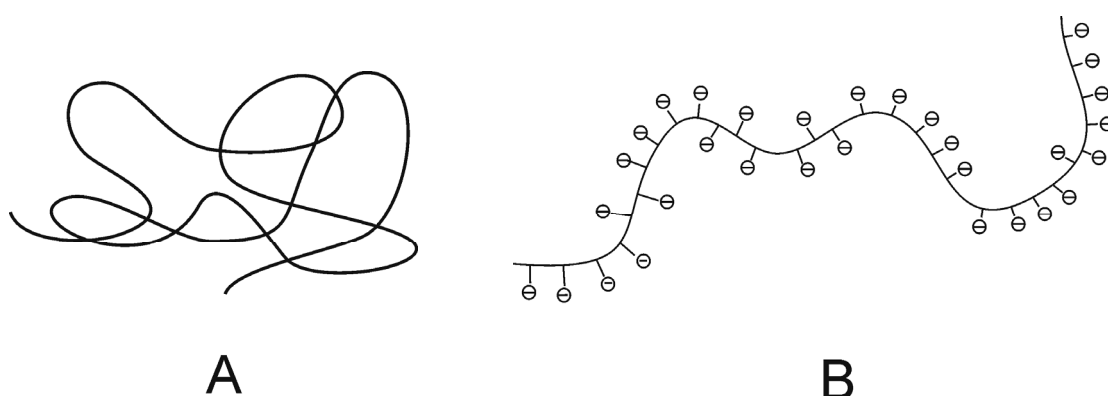


Figure 1.1. (A) An uncharged polymer molecule in a random coil shape (B) an anionic polyelectrolyte in salt-free solution.

The ionic groups of a polyelectrolyte may interact with one another or with mobile charges in the solution. Therefore, solution properties of polyelectrolytes such as viscosity and light scattering depend strongly on the degree of ionization (which depends on their structures and the pH of the solution), polyelectrolyte concentration and ionic strength. For example, under ideal conditions the viscosity of polyelectrolyte solutions is proportional to the square root of polymer concentration (Fouss law), whereas the viscosity of uncharged polymers is proportional to the polymer concentration.³⁰ Additionally, the osmotic pressure of polyelectrolytes in salt-free solutions can be several orders of magnitude higher than the osmotic pressure of neutral polymer at similar polymer concentrations.³¹ Medium conditions such as

pH also have an effect on polyelectrolyte viscosity. For example, at low pH, aqueous solution of a weak acid polyelectrolyte will exhibit a relatively low viscosity when the polymer is in its neutral form and a higher viscosity in its ionized form at intermediate pH. If salt is added to the solution, the polyelectrolyte chain will collapse due to screening effects and this phenomenon leads to a decrease in the viscosity. In summary, polyelectrolytes generally exhibit higher water solubility, expanded hydrated dimensions and a higher sensitivity to ionic strength and pH compared to nonionic polymers.

Polyelectrolytes in solution can form stable polyelectrolyte complexes (PECs). PECs can be formed using either oppositely charged polyelectrolytes, or a polyelectrolyte-surfactant pair. The PEC formation process is usually entropically driven by the release of counter ions and water from the hydrated polyelectrolyte molecules.³²⁻³³ However, other forces such as hydrogen bonding, hydrophobic interactions, van der Waals forces or dipole-charge transfer may be involved in the formation of PECs.³⁴ Even though the formations of polyelectrolyte and polyelectrolyte-surfactant complexes are similar, their solid-state structures are different. Polyelectrolyte-surfactant complexes commonly have highly ordered solid state structures such as frozen liquid crystals, whereas, PECs show somewhat fuzzy structures, for example, ladder and scrambled-eggs structures. Polyelectrolyte-surfactant complexes have order because of cooperative binding of surfactant molecules onto polyelectrolyte chains and the amphiphilicity of surfactant molecules.³⁴

Synthetic polyelectrolytes are generally used in PEC formation studies since key parameters such as molecular weight and charge density can be precisely controlled. PEC formation leads to different structures, depending on the

characteristics of polyelectrolytes used, mixing regime, and media conditions such as ionic strength and pH.³⁴⁻³⁵ Historically, mechanisms of PEC formation were studied in the 1970s by Tasuchida and Kabanov.³⁴⁻³⁶ In early studies, PEC formation of strong polyelectrolytes with a high charge density at a stoichiometric charge ratio (1:1) led to precipitated PECs which were insoluble in all common solvents. PECs formed at non-stoichiometric mixing ratios under certain conditions such as solutions $< 1 \times 10^{-3}$ g/mL did not precipitate and resulted in a stable dispersion of PEC particles.³⁶ In addition, an appropriate amount of salt in the solution was found to shift kinetically formed complexes toward the thermodynamically favored component since salt weakens the electrostatic interaction and enables rearrangement.³⁷ The role of salt in the formation of 'soluble' PECs (stable suspensions) was extensively studied in the 1990s.^{33,38-40} In general, particle flocculation was reduced at low ionic strength. Further increasing ionic strength at first led to a shrinking of PECs due to charge shielding by the electrolyte. When a critical ionic strength was exceeded, PECs were again precipitating. At even higher ionic strength, the precipitate dissolved and both components existed as free polyelectrolyte chains in solution.

To date, PEC structures may be categorized into two main types according to the structure of constituent polyelectrolytes. First, water-soluble PECs are formed using weak polyelectrolytes having very different molecular weights and mixed in non-stoichiometric ratios.³⁸ These PECs usually consist of a long host molecule sequentially bound with shorter, oppositely charged guest molecules according to the ladder model. Second, insoluble and aggregated PECs can form using polyelectrolytes having a high charge density and/or relatively high molecular weights, especially when mixed at or near a 1:1 charge ratio. These structures follow the scramble-eggs model.³⁹ This PEC formation at high concentration ($> 1 \times 10^{-2}$ g/mL) will tend towards

flocculation whatever the mixing ratio, but the formation at very low concentration ($< 1 \times 10^{-4}$ g/mL) and non-stoichiometric mixing ratios will give stable suspensions.^{34,39}

Several groups have studied the formation of water-soluble PECs at different mixing ratios, buffers and pH in order to examine colloidal stability and degree of hydration and to develop optimized nanoparticles for biomedical applications. In general, the formation of stable PECs requires the non-stoichiometric mixing of two constituent polyelectrolyte solutions. The constituent solutions can be mixed by slow titration of the default polymer into the polymer in excess or by rapid addition. Variations of particle size due to charge mixing ratios were found to be similar for both modes of addition, but rapid addition was less sensitive to order of mixing.⁴⁰ Additionally, rapid addition may result in more stable particles than slow titration when the charge mixing ratios are close to 1:1.⁴⁰

PECs tend to have very broad size distributions and not all constituent polyelectrolytes are consumed in the formation of stable PECs.⁴¹⁻⁴² Polymer charge density is an important factor in PEC stability, but, in the presence of salt, charge density by itself can not control the structure and stability of PECs.⁴³ Chain length (or molecular weight) and composition also influence the PEC particle size and colloidal stability. Schatz *et al.* and Drogoz *et al.* have studied PEC formation using different molecular weights of cationic chitosan and anionic dextran sulfate mixed via dropwise addition. Two situations could be identified (Figures 1.2).^{40,42} First, when the polyelectrolytes in excess have high molecular weight and could act as host and accommodate several of shorter guest polyelectrolyte molecules, stable PECs consisting of a hydrophobic core and a large hydrophilic corona were formed. Addition of short guest polyelectrolytes led to a limited size reduction. Second, when the polyelectrolytes in excess are smaller than the titrant, the outcome depended on

the capacity of the excess polyelectrolytes for charge neutralization. If the excess polyelectrolytes were too small and weakly charged, flocculation occurred. If the excess polyelectrolytes were not too small, dense particles stabilized by unpaired charges was observed.

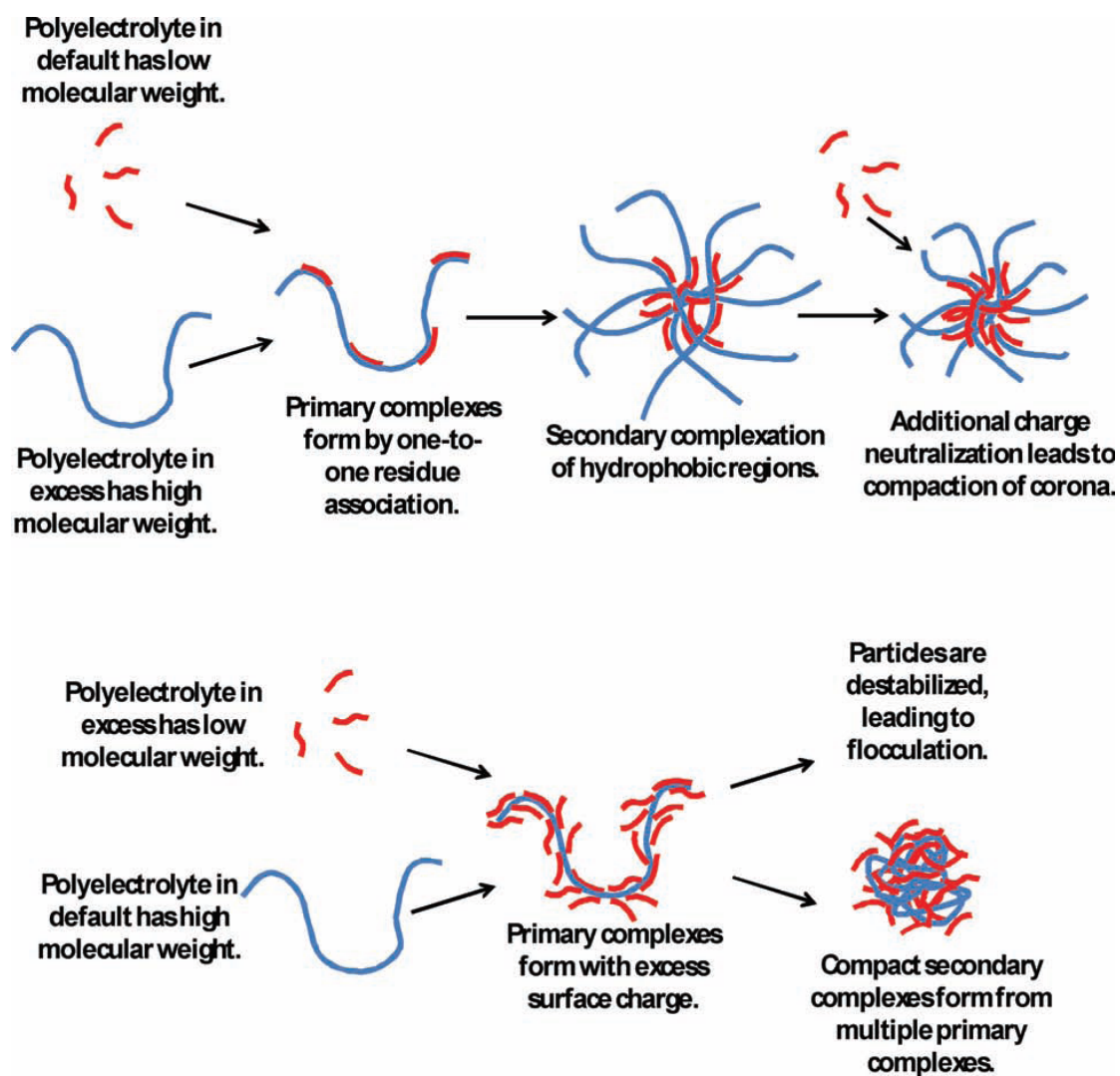


Figure 1.2. A representative scheme of PEC formation when the two constituent polyelectrolytes have very different molecular weights.³³

1. 3 Biomedical applications of polyelectrolytes

Polyelectrolytes can be used to deliver a number of therapeutics ranging from small molecule drugs to macromolecules. Polyelectrolyte complexes offer several potential benefits such as stabilizing therapeutics during formulation and storage, targeting therapeutics to desired sites of action, releasing therapeutics with controllable kinetics, and minimizing toxicity and side effects of therapeutics. Moreover, some polyelectrolyte properties such as swelling can be controlled by external stimuli, which can enable environmentally responsive delivery systems. In particular, for fragile therapeutics such as proteins and nucleic acids, nanoparticle synthesis using polymerization or solvent removal techniques (e.g. precipitation) may expose the therapeutic to harsh temperature and/or solvent conditions. In contrast, nanoparticle formation by polyelectrolyte complexation can be done in aqueous solutions at or near physiological pH and ionic strength, and at room temperature or lower. Such conditions can preserve conformation and biological activity of therapeutics. As a result, development of polyelectrolyte nanoparticle-based delivery systems for proteins, nucleic acids, and vaccines has been widely explored.

1.3.1 Drug and nucleic acid delivery

Amphotericin B (AmB) is an antifungal agent that has poor oral bioavailability due to its low solubility. There are two forms of intravenous preparations available; liposomal and lipid complex formulations. The lipid complex formulation (Ampholip®) has serious nephrotoxicity. Liposomal formulations (AmBisome® and Fungisome®) have reduced toxicity, but are quite expensive. Therefore, developing safer and more affordable formulations is desirable. Tiyaboonchai and others have developed AmB-loaded polyethylenimine (PEI)-dextran sulfate (DS) PEC nanoparticles. The AmB-loaded nanoparticles showed high

drug loading efficiency, low cytotoxicity and high efficacy against *Candida Albicans* compared to free drug.⁴⁴ In a separate publication, the same author has recently developed AmB-loaded nanoparticles using chitosan (CH) and dextran sulfate (DS). This system was expected to be less toxic and more biocompatible compared to the first system which contained PEI. AmB-CH NPs showed reduced renal toxicity *in vivo* compared to Fungisome®.⁴⁵

Complexation of negatively charged DNA and RNA with various cationic polymers has been utilized as a means to deliver nucleic acids to treat genetic diseases, and infectious diseases as well as cancers. Electrostatic binding of DNA has some advantages over other techniques. The method is simple, uses mild preparation conditions, and requires no purification, whereas polymeric nanoparticles and lipid/liposome formulations may involve multiple preparation and purification procedures. Complexation with polycations commonly prevents DNA and RNA degradation by nucleases. Polycations can form small and stable nanoparticles with DNA and RNA. Additionally, they may promote cellular uptake, endosomal escape and nuclear entry.

Among synthetic polycations, the use of PEI is common. It can have transfection efficiency comparable to viral vectors.⁴⁶ Theoretically, branched PEI has primary, secondary and tertiary amines in a 1:2:1 ratio. Due to a large number of amines, PEI exhibits high buffer capacity. This feature leads to a proposed proton-sponge character which leads to osmotic swelling and endosomal membrane rupture, ultimately resulting in high transfection efficiency. Although PEI is efficacious, high toxicity is still a major concern. Various chemical modifications have been pursued to make PEI translatable. Partial acetylation, cleavable linkers, imidazole conjugation, hyaluronic acid (HA) conjugation, chitosan conjugation, and PEGylation have all been employed to reduce toxicity, modify biodistribution and enhance the transfection

efficiency of PEI.⁴⁷⁻⁵⁶ Some PEI-mediated vectors have been evaluated in clinical trials including jetPEI, PEG-PEI-Cholesterol and PEI-mannose and dextrose.⁵⁷

Alternatively, natural cationic polymers such as chitosan, poly(glycoamidoamine), schizophyllan, and dextran derivatives, can be used to deliver nucleic acids to avoid the relatively high toxicity of many synthetic cationic polymers. Several modifications were made to increase transfection levels of these polymers. For example, terminal amines of chitosan were N-quaternized to increase charge density which resulted in high transfection efficiency, albeit with higher cytotoxicity.⁵⁸ In a later study, the same group was able to reduce this higher cytotoxicity by conjugation of trimethyl chitosan with PEG.⁵⁹ Other examples to improve transfection efficiency and stability of chitosan include crosslinking with disulfide linkages, introducing imidazole groups, and conjugation with hydrophobic moieties such as deoxycholic acid, stearic acid, and alkyl chains.⁶²⁻⁶⁷

Another efficient and biodegradable construct that can be used to complex nucleic acids involves the use of cell penetration peptides (CPPs). CPPs are short peptides (<30 amino acids) that usually contain basic amino acids and are protonated at physiological pH. Certain CPPs have been reported to cross cell membranes within seconds or minutes at micromolar concentrations. Therefore, CPPs are interesting carriers that may be used to transport electrostatically or covalently bound cargo across the cell membrane.

CPPs can be classified into three groups; primary, secondary, and non-amphipathic CCPs.⁶⁰ Primary amphipathic CCPs contain both hydrophobic and cationic regions (> 20 amino acids). Examples of primary amphipathic CCPs are SP-NLS, MPG, transportan, TP10, pep-1, and P (α)/(β). Secondary amphipathic CCPs, such as, penetratin, KLAL and RL16, are shorter and only present their amphipathic

properties after binding with lipids or glycosaminoglycans (GAGs). Non-amphipathic CCPs, for example, TAT and R9, are short and contain only cationic amino acids.

To date, internalization mechanisms of CPPs remain elusive. It was suggested that a single CPP may use multiple modes to enter cells depending on experimental conditions. CPP cellular entry modes can be categorized into two groups: energy-independent direct translocation and energy-dependent endocytosis. Historically, the penetration mechanism has been reported to be an energy- and receptor-independent process.⁶¹⁻⁶² Additionally, an inverted micelle mechanism has been proposed.⁶² However, with the rapid development of molecular techniques, a number of recent reports have indicated that endocytotic mechanisms including macropinocytosis, clathrin-coated pits, and lipid rafts all occurred.⁷¹⁻⁷⁶ It appears that pathways may vary with peptide properties (e.g. molecule length and charge delocalization), peptide concentration, cell types, cargo size and charge, and physiological conditions.⁶³⁻⁶⁶ Descriptions of these phenomena have received less attention than their potential applications in drug and gene delivery.

MPG (acetyl-GALFLGFLGAAGSTMGAWSQPKKKRKVCysteamide), a primary amphipathic CCP, contains a hydrophobic N-terminal region and a hydrophilic nuclear localizing signal (NLS) region. MPG has been used to complex with and deliver plasmid DNA and siRNA to a number of adherent and suspension cells. MPG was shown to improve DNA nuclear entry in primary cell lines and non-dividing cells.⁶⁷⁻⁶⁸ Interestingly, MPG^{ΔNLS}, a mutant having a single mutation in the NLS region, was shown to deliver fluorescently labeled siRNA specifically to the cytoplasm and resulted in greater biological response, whereas MPG-transfected siRNA migrated rapidly to the nucleus.⁶⁸ Thus, modifying the NLS of MPG allowed delivery of siRNA to the desired compartment, the cytoplasm. MPG has also been

used to deliver siRNA into mouse blastocytes and the transfected blastocytes were reimplanted in mice.^{67,69}

In addition to direct complexation, encapsulation or adsorption of nucleic acids in PEC formulations offers an alternative delivery method. Tiyaboonchai *et al.* have encapsulated DNA into PEI-DS particles (>95% entrapment efficiency). DNA remained in a supercoiled-B form after incorporation in the complexes. PEI-DS/DNA particles showed higher transfection efficiency compared to PEI/DNA complexes and dextran sulfate seemingly reduced the cytotoxicity of PEI.⁷⁰ In another study, Hong *et al.* have adsorbed smad3 antisense oligonucleotides onto chitosan/ alginate complexes. A smad3-PEC lyophilized disk was administered topically to mice. The results suggested that the lyophilized disk healed wounds faster than other formulations.⁷¹

1.3.2 Protein stabilization, immobilization and controlled release

Polyelectrolyte-protein binding can happen in both cognate and non-cognate systems. Polyelectrolytes such as GAGs can interact with their cognate proteins to carry out physiological functions. There has also been increasing interest in using non-cognate polyelectrolytes to improve protein efficacy and stability or to extend the circulation half-life of therapeutic proteins. Like nucleic acids, proteins are often fragile. Polyelectrolyte binding offers a simple approach to stabilize, immobilize and control the release of therapeutic proteins. Unlike polymerization and/or conjugation reactions, electrostatic binding between polyelectrolytes and proteins may be done under mild conditions that preserve protein conformation and biological activity. Polyelectrolytes and proteins can bind via a number of non-covalent forces, for example, hydrogen bonding, salt bridges and ion pairs, and/or hydrophobic interactions.

α -Amylase, a major enzyme used in digestive enzyme supplements, has a relatively short shelf-life (up to 1 year when refrigerated). Sankalia *et al.* encapsulated α -amylase in chitosan-alginate PECs with 90% entrapment efficiency. The PECs were filled into capsules which then underwent stability testing according to the International Conference on Harmonization (ICH) guidelines. The stability data suggested that α -amylase chitosan-alginate PEC had extended the shelf-life to 3.68 years.⁷²

In addition to encapsulating a small molecule drug and a nucleic acid in PEI-DS PECs, Tiyaboonchai *et al.* also encapsulated insulin as a model protein drug in PEI-DS PECs (80-90% entrapment efficiency). The complexes had a rapid release profile, no insulin degradation product was detected during *in vitro* tests, and no significant conformational change was observed for insulin. Additionally, the insulin complexes showed an extended hypoglycemic effect in streptozotocin-induced diabetic rats.⁷³

Growth factors are secreted by a variety of cells and they regulate cellular activities such as migration, differentiation, and proliferation. Secreted growth factors bind to specific receptors and the binding subsequently initiates signal transduction pathways such as tissue regenerative processes. Growth factors generally have a short circulation half-life and undergo rapid degradation *in vivo* which makes it difficult to maintain local therapeutic concentrations.⁷⁴⁻⁷⁵ In addition, repeated administration can lead to negative side effects. As a result, there have been efforts to develop delivery systems for growth factors including lipid- and polymer-based systems including liposomes, solid lipid particles, lipid nanocapsules, dendrimers, polymeric nanoparticles, and micelles. Here, we will focus only on polyelectrolyte-based systems.

Heparin, heparin sulfates, and heparan and chondroitin sulfate proteoglycans are known to protect heparin binding growth factors (HBGFs) from proteolytic degradation and potentiate their *in vitro* biological effects.⁷⁶⁻⁷⁸ Interestingly, the binding appears to be non-specific via electrostatic interactions although with high affinity.⁷⁹ As a result, heparin-like materials and/or polyanions have been utilized to promote activity or to stabilize HBGFs.⁷⁹⁻⁸²

Vascular endothelial growth factor (VEGF) is a potent angiogenic cytokine that requires localized and sustained delivery to generate blood vessels. VEGF also has a short circulation half-life. Therefore, developing a sustained released formulation is of interest. VEGF has a heparin binding domain that can bind polyanions. Huang *et al.* complexed VEGF bound to dextran sulfate (DS) with the polycations, polyethylenimine, chitosan, or poly(L-lysine). The complexes had good encapsulation efficiencies (50-85%), extended VEGF release (up to 10 days), and the released VEGF remained active at day 10 of the release study.⁸³

Fibroblast growth factor-10 (FGF-10), also known as keratinocyte growth factor-2 (KGF-2), is involved in angiogenesis, wound healing and embryonic development. KGF-2 has been a candidate for treatment of chemotherapy- or radiotherapy-induced mucositis, ulcerative colitis, and cutaneous wounds.⁸⁴ Derrick *et al.* examined the effect of polyanions on the structure and stability of KGF-2 and found that polyanions such as heparin, sucrose octasulfate (SOS) and inositol hexaphosphate (IHP) stabilized KGF-2 by increasing the unfolding temperature by 9-15°C.⁷⁹ In a separate study, Huang *et al.* bound KGF-2 to DS and then complexed bound KGF-2 with polyethylenimine, chitosan, or poly(L-lysine). The unfolding temperature of bound KGF-2/DS was increased ~10°C. The KGF-2 bound to DS was packaged in PECs (entrapment efficiency 70-80%). The complexes had a sustained

release profile of KGF-2 up to 10 days. The mitogenic activity of the complexes on vascular endothelial cells was significantly enhanced.⁸¹

In an attempt to reduce the initial burst release of human growth hormone (hGH) from a thermosensitive poly(organophosphazene) hydrogel, hGH (pI = 5.27), was complexed with polycations (poly-L-arginine or poly-L-lysine). Then, the bound hGH and organophosphazene polymer were heated to 37°C to convert the polymer solution into a hydrogel. The hGH complexed to poly-L-arginine better than poly-L-lysine. All PECs loaded into the hydrogel showed slow release profiles compared to the release of hGH alone. A single subcutaneous injection of the hydrogel in Sprague-Dawley rats showed a sustained release profile of hGH up to 5 days.⁸⁵

Polyelectrolyte multilayers: Layer-by-layer (LbL) deposition is an alternative method of using polyelectrolytes for controlled release. This technique has been widely used in tissue engineering and implantable materials. But, in this short section, only drug delivery applications are briefly reviewed. Polyelectrolyte multilayers (PEMs) are formed by alternately depositing oppositely charged polyelectrolytes onto surfaces of materials. The driving forces behind polyelectrolyte deposition are very similar to the forces involved in the formation of PECs. These forces include electrostatic and non-electrostatic interactions including short-range interactions such as hydrophobicity, hydrogen bonds, Van der Waals forces, charge transfer halogen interactions, and covalent bonds formed by 'click' chemistry.⁸⁶ In addition, entropy gained due to the release of counterions is another force involved in multilayer formation.

Various methods have been used to form PEM films such as dip coating, spin coating and spraying. The most common method is dip coating since it is both efficient and economical. The spraying method was found to be effective under

conditions where dipping could not produce homogeneous films. Rinsing could be skipped in the spraying method to accelerate the process. PEM formation exhibits two growth patterns; a linear and an exponential one. The exponential pattern occurs when one of the polyelectrolytes can diffuse in and out of the film during the deposition and rinsing steps.⁸⁷ The chemical composition, thickness and mechanical properties of PEMs are important to the biological response of PEMs and these parameters can be controlled by changing processing conditions such as the ionic strength and pH of the polymer solutions.⁸⁸⁻⁸⁹ Various drugs including biomolecules such as polypeptides, polysaccharides, DNA, proteins, viruses and cells have been incorporated into PEM films. These therapeutics can be incorporated into PEMs by addition during PEM formation, adsorption or diffusion into the films after formation or by covalently binding to the constituent polymer before or after PEM formation.³³

PEM microcapsules have been used as a carrier and an adjuvant to deliver antigen (OVA) to the lungs. OVA was mixed with CaCl_2 and NaCO_3 to form OVA-loaded CaCO_3 microcapsule cores. Dextran sulfate/ poly-L-arginine PEMs were then alternately adsorbed onto CaCO_3 particles. The capsule cores were washed away leaving OVA-filled PEM microcapsules. OVA-loaded microcapsules, soluble OVA/microcapsule mixture, soluble OVA in phosphate buffered saline (PBS) or PBS alone were administered to C57BL/6 mice by intratracheal instillation. FITC-dextran-loaded microcapsules were used to track the uptake and degradation of PEM microcapsules. The microcapsules were taken up efficiently by pulmonary antigen presenting cells (APCs) and degraded completely 2 weeks after instillation. Moreover, OVA PEM microcapsules enhanced APC activation thus demonstrating adjuvant properties. Immunization with encapsulated OVA clearly stimulated a much stronger local Th17 response than the soluble OVA microcapsule mixture.⁹⁰ In a separate

study, the same dextran sulfate/ poly-L-arginine PEM constructs were formulated with p24 antigen from human immunodeficiency virus type 1 (HIV-1) and/ or the Toll-like receptor ligand 3 (TLR3) ligand poly I:C, a maturation factor. The *in vitro* and *in vivo* data suggested that both antigen and DC maturation signals can be delivered as a complex with PEM capsules to stimulate a virus-specific immune response.⁹¹

1.3.3 Responsive drug delivery systems

Responsive drug delivery systems can be categorized into two major types; externally regulated or open-loop systems and self-regulated or closed-loop systems. The externally regulated system uses external triggers such as ultrasonic, magnetic, electric, photonic or chemical agents to control delivery of therapeutics from the system. Meanwhile, self-regulated systems control and adjust the system output according to external variables and the release rate is controlled by a feedback reaction. Chen *et al.* has developed glucose-sensitive LbL multilayer films for self-regulated release of insulin. The LbL multilayer film consisted of positively charged poly[2-(dimethylamino)ethyl methacrylate] (PDMAEMA) star polymer and negatively charged insulin and glucose oxidase (GOD). Star PDMAEMA bearing tertiary amine groups was protonated and fully extended at low pH. Under high glucose conditions, GOD converts glucose into gluconic acid which changes the pH within the film. Low pH will induce star PDMAEMA to rearrange the film morphology resulting in an “open” status of the film to release insulin. *In vitro* release studies showed that the film released insulin differently, depending on glucose concentration. *In vivo* data in streptozotolin (STZ)-induced diabetic rats showed that the insulin-loaded multilayer film effectively reduced blood glucose levels.⁹²

The studies reviewed in this section demonstrated various biomedical applications of polyelectrolytes. Therapeutics ranging from small molecule drugs to macromolecules such as proteins and DNA have been delivered using a variety of polyelectrolyte constructs including polyelectrolyte complexes and multilayers. In addition to the ease of production and mild preparation conditions, polyelectrolyte-based DDSs often offer attractive benefits such as improved drug stability during formulation and storage, modulation of pharmacokinetics, controlled release, and reduction of toxicity and side effects. More well defined and precise polyelectrolyte-based DDSs are under development to enhance performance and ultimately maximize patient benefits.

1.4 Thesis goal, outline and specific aims

The overall goal of this work was to develop improved polyelectrolyte-based DDSs for gene and protein delivery. Macromolecular therapeutics have emerged as important drugs, but could often benefit from enhanced delivery. Therefore, three different projects have been devised to investigate potential use of polyelectrolyte-based DDSs for gene and protein delivery. For the first project, the goal was to investigate the effect and relationship of surface charge and degradability of synthetic polymeric nanoparticles on transfection efficiency. Building upon this previous work, the synthetic polycation was replaced with a small cell penetration peptide (TAT peptide) which has very low cytotoxicity and could be optimized to have high transfection efficiency. In addition, LABL peptide targeting intercellular cell-adhesion molecule-1 (ICAM-1) was conjugated to the TAT peptide to explore targeted transfection as part of the second project. The third project involved development of anionic block copolymers that could be used to stabilize and PEGylate proteins bearing a heparin binding groove such as growth factors.

1.4.1 The effect and relationship of surface charge and degradability of polyvinyl amine (PVAm) nanogel on transfection efficiency

The data presented in Chapter 2 systematically investigates the relationship of surface charge and degradability to transfection efficiency. Synthetic polymeric particles were chosen since degradability and surface charge could be precisely controlled. Crosslinked poly(N-vinylformamide) (PNVF) nanogels with different degradability were synthesized using free-radical chain polymerization. The nanogels were hydrolyzed to produce different degrees of polyvinyl amine (PVAm) content. The cytotoxicity of PVAm nanogels and the transfection efficiency of PVAm/DNA complexes were evaluated in human alveolar basal epithelial cells (A549).

1.4.2 Calcium-crosslinked LABL-TAT complexes effectively target gene delivery to ICAM-1 expressing cells

Chapter 3 details the development of a new transfection agent targeted to ICAM-1 on cells. The upregulation of ICAM-1 is associated with diverse diseases. Thus, elevated ICAM-1 has been used as a target for various drugs and gene delivery. Synthetic versions of polycations such as PVAm (Chapter 2) were replaced with the CPP TAT, which was observed to yield high transfection after complexing with DNA and condensing with calcium. TAT, TAT-PEG, and TAT-PEG-LABL block peptides were synthesized. The cytotoxicity and the transfection efficiency of DNA complexed with these block peptides were evaluated in A549 cells overexpressing ICAM-1. The specificity of the targeted TAT-PEG-LABL blockpeptide was also examined.

1.4.3 Non-covalent PEGylation by polyanion complexation as a novel means to stabilize Keratinocyte Growth Factor-2 (KGF-2)

In this chapter (4), we presented a new approach to stabilize a model HBGF, KGF-2, through ionic interactions with PEGylated polyanions. Repifermin® is a truncated form of recombinant KGF-2 and was used for the treatment of

chemotherapy- or radiotherapy-induced mucositis, ulcerative colitis and cutaneous wound healing. However, Repifermin® encounters several difficulties such as poor *in vitro* stability ($T_m \sim 37^\circ\text{C}$) and a relatively short half-life *in vivo*. Thus, a simple non-covalent PEGylation using ionic interaction between readily PEGylated polyanions (dextran sulfate and pentosan polysulfate) and KGF-2 was investigated. The potential use of these PEGylated polyanions was examined through spectroscopic, calorimetric and light scattering techniques.

1.5 Bibliography

1. Haag R, Kratz F 2006. Polymer therapeutics: concepts and applications. *Angewandte Chemie International Edition* 45(8):1198-1215.
2. Vicent M, Duncan R 2006. Polymer conjugates: nanosized medicines for treating cancer. *Trends in biotechnology* 24(1):39-47.
3. Rupp R, Rosenthal S, Stanberry L 2007. VivaGel(tm)(SPL7013 Gel): A candidate dendrimer-microbicide for the prevention of HIV and HSV infection. *International journal of nanomedicine* 2(4):561.
4. Scranton A, Rangarajan B, Klier J 1995. Biomedical applications of polyelectrolytes. *Biopolymers* 11:1-54.
5. Jiang H, Taranekar P, Reynolds J, Schanze K 2009. Conjugated Polyelectrolytes: Synthesis, Photophysics, and Applications. *Angewandte Chemie International Edition* 48(24):4300-4316.
6. Bohrisch J, Eisenbach C, Jaeger W, Mori H, Müller A, Rehahn M, Schaller C, Traser S, Wittmeyer P 2004. New polyelectrolyte architectures. *Polyelectrolytes with Defined Molecular Architecture* 1:277-296.
7. Jenkins D, Hudson S 2001. Review of vinyl graft copolymerization featuring recent advances toward controlled radical-based reactions and illustrated with chitin/chitosan trunk polymers. *Chem Rev* 101(11):3245-3274.
8. Dang J, Leong K 2006. Natural polymers for gene delivery and tissue engineering. *Advanced drug delivery reviews* 58(4):487-499.
9. Opalinska J, Gewirtz A 2002. Nucleic-acid therapeutics: basic principles and recent applications. *Nature Reviews Drug Discovery* 1(7):503-514.
10. Uherek C, Wels W 2000. DNA-carrier proteins for targeted gene delivery. *Advanced drug delivery reviews* 44(2-3):153-166.
11. Crooke S 1999. Molecular mechanisms of action of antisense drugs. *Biochimica et Biophysica Acta (BBA)-Gene Structure and Expression* 1489(1):31-43.
12. Stull R, Szoka J, FC 1995. Antigene, ribozyme and aptamer nucleic acid drugs: progress and prospects. *Pharmaceutical research* 12(4):465-483.
13. Akhtar S, Hughes M, Khan A, Bibby M, Hussain M, Nawaz Q, Double J, Sayyed P 2000. The delivery of antisense therapeutics. *Advanced drug delivery reviews* 44(1):3-21.
14. Bertrand J, Pottier M, Vekris A, Opolon P, Maksimenko A, Malvy C 2002. Comparison of antisense oligonucleotides and siRNAs in cell culture and in vivo. *Biochemical and biophysical research communications* 296(4):1000-1004.
15. Scherr M, Morgan M, Eder M 2003. Gene silencing mediated by small interfering RNAs in mammalian cells. *Current medicinal chemistry* 10(3):245-256.
16. Li C 2002. Poly (-glutamic acid)-anticancer drug conjugates. *Advanced drug delivery reviews* 54(5):695-713.
17. Said Hassane F, Saleh A, Abes R, Gait M, Lebleu B 2010. Cell penetrating peptides: overview and applications to the delivery of oligonucleotides. *Cellular and molecular life sciences* 67(5):715-726.
18. Alper J 2003. Glycobiology: turning sweet on cancer. *Science* 301(5630):159.
19. Kilcoyne M, Joshi L 2007. Carbohydrates in therapeutics. *Cardiovascular & Hematological Agents in Medicinal Chemistry (Formerly Current Medicinal Chemistry-Cardiovascular & Hematological Agents)* 5(3):186-197.

20. Schatz C, Viton C, Delair T, Pichot C, Domard A 2003. Typical physicochemical behaviors of chitosan in aqueous solution. *Biomacromolecules* 4(3):641-648.
21. Yang J, Xie Y, He W 2010. Research Progress on Chemical Modification of Alginate: A Review. *Carbohydrate Polymers*.
22. Van Tomme S 2007. Self-assembling microsphere-based dextran hydrogels for pharmaceutical applications.
23. Hatanaka K, Yoshida T, Miyahara S, Sato T, Ono F, Uryu T, Kuzuhara H 1987. Synthesis of new heparinoids with high anticoagulant activity. *Journal of medicinal chemistry* 30(5):810-814.
24. Arunkumar A, Kumar T, Kathir K, Srisailam S, Wang H, Leena P, Chi Y, Chen H, Wu C, Wu R 2002. Oligomerization of acidic fibroblast growth factor is not a prerequisite for its cell proliferation activity. *Protein Science* 11(5):1050-1061.
25. Middaugh C, Mach H, Burke C, Volkin D, Dabora J, Tsai P, Bruner M, Ryan J, Marfia K 1992. Nature of the interaction of growth factors with suramin. *Biochemistry* 31(37):9016-9024.
26. Volkin D, Verticelli A, Marfia K, Burke C, Mach H, Middaugh C 1993. Sucralfate and soluble sucrose octasulfate bind and stabilize acidic fibroblast growth factor. *Biochimica et Biophysica Acta (BBA)-Protein Structure and Molecular Enzymology* 1203(1):18-26.
27. Nagashima R 1981. Development and characteristics of sucralfate. *Journal of clinical gastroenterology* 3(Suppl 2):103.
28. Volkin DB, Verticelli AM, Marfia KE, Burke CJ, Mach H, Middaugh CR 1993. Sucralfate and soluble sucrose octasulfate bind and stabilize acidic fibroblast growth factor. *Biochimica et Biophysica Acta (BBA)-Protein Structure and Molecular Enzymology* 1203(1):18-26.
29. Mortimer D 1991. Synthetic polyelectrolytes—a review. *Polymer international* 25(1):29-41.
30. Rubinstein M, Colby R, Dobrynin A 1994. Dynamics of semidilute polyelectrolyte solutions. *Physical review letters* 73(20):2776-2779.
31. Dobrynin A, Rubinstein M 2005. Theory of polyelectrolytes in solutions and at surfaces. *Progress in Polymer Science* 30(11):1049-1118.
32. Gummel J, Cousin F, Bou F 2007. Counterions release from electrostatic complexes of polyelectrolytes and proteins of opposite charge: a direct measurement. *J Am Chem Soc* 129(18):5806-5807.
33. Boddohi S, Kipper M 2010. Engineering Nanoassemblies of Polysaccharides. *Advanced Materials*.
34. Thunemann A, Müller M, Dautzenberg H, Joanny J, Löwen H 2004. Polyelectrolyte complexes. *Polyelectrolytes with Defined Molecular Architecture II*:19-33.
35. Dautzenberg H 1997. Polyelectrolyte complex formation in highly aggregating systems. 1. Effect of salt: polyelectrolyte complex formation in the presence of NaCl. *Macromolecules* 30(25):7810-7815.
36. Zezin A, Kabanov V 1982. A New Class of Complex Water-soluble Polyelectrolytes. *Russian Chemical Reviews* 51(9):833-855.
37. Karibyants N, Dautzenberg H 1998. Preferential binding with regard to chain length and chemical structure in the reactions of formation of quasi-soluble polyelectrolyte complexes. *Langmuir* 14(16):4427-4434.
38. Kabanov V, Zezin A 1984. Soluble interpolymeric complexes as a new class of synthetic polyelectrolytes. *Pure and applied chemistry* 56(3):343-354.

39. Schatz C, Lucas J, Viton C, Domard A, Pichot C, Delair T 2004. Formation and properties of positively charged colloids based on polyelectrolyte complexes of biopolymers. *Langmuir* 20(18):7766-7778.
40. Schatz C, Domard A, Viton C, Pichot C, Delair T 2004. Versatile and efficient formation of colloids of biopolymer-based polyelectrolyte complexes. *Biomacromolecules* 5(5):1882-1892.
41. Boddohi S, Moore N, Johnson P, Kipper M 2009. Polysaccharide-based polyelectrolyte complex nanoparticles from chitosan, heparin, and hyaluronan. *Biomacromolecules* 10(6):1402-1409.
42. Drogoz A, David L, Rochas C, Domard A, Delair T 2007. Polyelectrolyte complexes from polysaccharides: Formation and stoichiometry monitoring. *Langmuir* 23(22):10950-10958.
43. Dautzenberg H, Jaeger W 2002. Effect of charge density on the formation and salt stability of polyelectrolyte complexes. *Macromolecular Chemistry and Physics* 203(14):2095-2102.
44. Tiyaboonchai W, Woiszwilllo J, Middaugh C 2001. Formulation and characterization of amphotericin B-polyethylenimine-dextran sulfate nanoparticles. *Journal of pharmaceutical sciences* 90(7):902-914.
45. Tiyaboonchai W, Limpeanchob N 2007. Formulation and characterization of amphotericin B-chitosan-dextran sulfate nanoparticles. *International journal of pharmaceutics* 329(1-2):142-149.
46. Abdallah B, Hassan A, Benoist C, Goula D, Behr J, Demeneix B 1996. A powerful nonviral vector for in vivo gene transfer into the adult mammalian brain: polyethylenimine. *Human gene therapy* 7(16):1947-1954.
47. Forrest M, Koerber J, Pack D 2003. A degradable polyethylenimine derivative with low toxicity for highly efficient gene delivery. *Bioconjugate Chem* 14(5):934-940.
48. Forrest M, Meister G, Koerber J, Pack D 2004. Partial acetylation of polyethylenimine enhances in vitro gene delivery. *Pharmaceutical research* 21(2):365-371.
49. Gabrielson N, Pack D 2006. Acetylation of polyethylenimine enhances gene delivery via weakened polymer/DNA interactions. *Biomacromolecules* 7(8):2427-2435.
50. Kloeckner J, Wagner E, Ogris M 2006. Degradable gene carriers based on oligomerized polyamines. *European Journal of Pharmaceutical Sciences* 29(5):414-425.
51. Peng Q, Zhong Z, Zhuo R 2008. Disulfide cross-linked polyethylenimines (PEI) prepared via thiolation of low molecular weight PEI as highly efficient gene vectors. *Bioconjugate chemistry* 19(2):499-506.
52. Swami A, Aggarwal A, Pathak A, Patnaik S, Kumar P, Singh Y, Gupta K 2007. Imidazolyl-PEI modified nanoparticles for enhanced gene delivery. *International journal of pharmaceutics* 335(1-2):180-192.
53. Swami A, Kurupati R, Pathak A, Singh Y, Kumar P, Gupta K 2007. A unique and highly efficient non-viral DNA/siRNA delivery system based on PEI-bisepoxide nanoparticles. *Biochemical and biophysical research communications* 362(4):835-841.
54. Thomas M, Ge Q, Lu J, Chen J, Klivanov A 2005. Cross-linked small polyethylenimines: while still nontoxic, deliver DNA efficiently to mammalian cells in vitro and in vivo. *Pharmaceutical research* 22(3):373-380.

55. Wong K, Sun G, Zhang X, Dai H, Liu Y, He C, Leong K 2006. PEI-g-chitosan, a novel gene delivery system with transfection efficiency comparable to polyethylenimine in vitro and after liver administration in vivo. *Bioconjugate Chem* 17(1):152-158.
56. Yao J 2010. Amphoteric hyaluronic acid derivative for targeting gene delivery. *Biomaterials*.
57. Mintzer M, Simanek E 2008. Nonviral vectors for gene delivery. *Chemical reviews* 109(2):259-302.
58. Kean T, Roth S, Thanou M 2005. Trimethylated chitosans as non-viral gene delivery vectors: cytotoxicity and transfection efficiency. *Journal of Controlled Release* 103(3):643-653.
59. Germershaus O, Mao S, Sitterberg J, Bakowsky U, Kissel T 2008. Gene delivery using chitosan, trimethyl chitosan or polyethylenglycol-graft-trimethyl chitosan block copolymers: establishment of structure-activity relationships in vitro. *Journal of Controlled Release* 125(2):145-154.
60. Ziegler A 2008. Thermodynamic studies and binding mechanisms of cell-penetrating peptides with lipids and glycosaminoglycans. *Advanced drug delivery reviews* 60(4-5):580-597.
61. Zorko M, Langel Ü 2005. Cell-penetrating peptides: mechanism and kinetics of cargo delivery. *Advanced drug delivery reviews* 57(4):529-545.
62. Derossi D, Calvet S, Trembleau A, Brunissen A, Chassaing G, Prochiantz A 1996. Cell internalization of the third helix of the Antennapedia homeodomain is receptor-independent. *Journal of Biological Chemistry* 271(30):18188.
63. Foerg C, Merkle H 2008. On the biomedical promise of cell penetrating peptides: limits versus prospects. *Journal of pharmaceutical sciences* 97(1):144-162.
64. Ignatovich I, Dizhe E, Pavlotskaya A, Akifiev B, Burov S, Orlov S, Perevozchikov A 2003. Complexes of plasmid DNA with basic domain 47-57 of the HIV-1 Tat protein are transferred to mammalian cells by endocytosis-mediated pathways. *Journal of Biological Chemistry* 278(43):42625.
65. Mueller J, Kretzschmar I, Volkmer R, Boisguerin P 2008. Comparison of cellular uptake using 22 CPPs in 4 different cell lines. *Bioconjugate chemistry* 19(12):2363-2374.
66. Torchilin V 2008. Tat peptide-mediated intracellular delivery of pharmaceutical nanocarriers. *Advanced drug delivery reviews* 60(4-5):548-558.
67. Crombez L, Charnet A, Morris M, Aldrian-Herrada G, Heitz F, Divita G 2007. A non-covalent peptide-based strategy for siRNA delivery. *Biochemical Society Transactions* 35:44-46.
68. Simeoni F, Morris M, Heitz F, Divita G 2003. Insight into the mechanism of the peptide based gene delivery system MPG: implications for delivery of siRNA into mammalian cells. *Nucleic acids research* 31(11):2717.
69. Zeineddine D, Papadimou E, Chebli K, Gineste M, Liu J, Grey C, Thurig S, Behfar A, Wallace V, Skerjanc I 2006. Oct-3/4 dose dependently regulates specification of embryonic stem cells toward a cardiac lineage and early heart development. *Developmental cell* 11(4):535-546.
70. Tiyaboonchai W, Woiszwilllo J, Middaugh C 2003. Formulation and characterization of DNA-polyethylenimine-dextran sulfate nanoparticles. *European Journal of Pharmaceutical Sciences* 19(4):191-202.
71. Hong H, Jin S, Park J, Ahn W, Kim C 2008. Accelerated wound healing by smad3 antisense oligonucleotides-impregnated chitosan/alginate polyelectrolyte complex. *Biomaterials* 29(36):4831-4837.

72. Sankalia M, Mashru R, Sankalia J, Sutariya V 2007. Reversed chitosan-alginate polyelectrolyte complex for stability improvement of alpha-amylase: Optimization and physicochemical characterization. *European journal of pharmaceuticals and biopharmaceutics* 65(2):215-232.
73. Tiyaboonchai W, Woiszwilllo J, Sims R, Middaugh C 2003. Insulin containing polyethylenimine-dextran sulfate nanoparticles. *International journal of pharmaceuticals* 255(1-2):139-151.
74. Zhang S, Uluda H 2009. Nanoparticulate systems for growth factor delivery. *Pharmaceutical research* 26(7):1561-1580.
75. Street J, Bao M, DeGuzman L, Bunting S, Peale F, Ferrara N, Steinmetz H, Hoeffel J, Cleland J, Daugherty A 2002. Vascular endothelial growth factor stimulates bone repair by promoting angiogenesis and bone turnover. *Proceedings of the National Academy of Sciences of the United States of America* 99(15):9656.
76. Ruoslahti E, Yamaguchi Y 1991. Proteoglycans as modulators of growth factor activities. *Cell* 64(5):867.
77. Saksela O, Moscatelli D, Sommer A, Rifkin D 1988. Endothelial cell-derived heparan sulfate binds basic fibroblast growth factor and protects it from proteolytic degradation. *The Journal of cell biology* 107(2):743.
78. Sommer A, Rifkin D 1989. Interaction of heparin with human basic fibroblast growth factor: protection of the angiogenic protein from proteolytic degradation by a glycosaminoglycan. *Journal of cellular physiology* 138(1):215-220.
79. Derrick T, Grillo A, Vitharana S, Jones L, Rexroad J, Shah A, Perkins M, Spitznagel T, Middaugh C 2007. Effect of polyanions on the structure and stability of repifermin(tm)(keratinocyte growth factor 2). *Journal of pharmaceutical sciences* 96(4):761-776.
80. Blanquaert F, Barritault D, Caruelle J 1999. Effects of heparan-like polymers associated with growth factors on osteoblast proliferation and phenotype expression. *Journal of Biomedical Materials Research Part A* 44(1):63-72.
81. Huang M, Berkland C 2009. Controlled release of Repifermin(R) from polyelectrolyte complexes stimulates endothelial cell proliferation. *Journal of pharmaceutical sciences* 98(1):268-280.
82. Kamerzell T, Unruh J, Johnson C, Middaugh C 2006. Conformational flexibility, hydration and state parameter fluctuations of fibroblast growth factor-10: Effects of ligand binding. *Biochemistry* 45(51):15288-15300.
83. Huang M, Vitharana S, Peek L, Coop T, Berkland C 2007. Polyelectrolyte complexes stabilize and controllably release vascular endothelial growth factor. *Biomacromolecules* 8(5):1607-1614.
84. Sung C, Parry T, Riccobene T, Mahoney A, Roschke V, Murray J, Gu M, Glenn J, Caputo F, Farman C 2002. Pharmacologic and pharmacokinetic profile of repifermin (KGF-2) in monkeys and comparative pharmacokinetics in humans. *The AAPS Journal* 4(2):24-33.
85. Park M, Chun C, Ahn S, Ki M, Cho C, Song S 2010. Sustained delivery of human growth hormone using a polyelectrolyte complex-loaded thermosensitive polyphosphazene hydrogel. *Journal of Controlled Release*.
86. Boudou T, Crouzier T, Ren K, Blin G, Picart C 2010. Multiple functionalities of polyelectrolyte multilayer films: New biomedical applications. *Advanced Materials* 22(4):441-467.
87. Lavallo P, Picart C, Mutterer J, Gergely C, Reiss H, Voegel J, Senger B, Schaaf P 2004. Modeling the Buildup of Polyelectrolyte Multilayer Films Having Exponential Growth. *J Phys Chem B* 108(2):635-648.

88. Boddohi S, Killingsworth C, Kipper M 2008. Polyelectrolyte multilayer assembly as a function of pH and ionic strength using the polysaccharides chitosan and heparin. *Biomacromolecules* 9(7):2021-2028.
89. Fu J, Ji J, Yuan W, Shen J 2005. Construction of anti-adhesive and antibacterial multilayer films via layer-by-layer assembly of heparin and chitosan. *Biomaterials* 26(33):6684-6692.
90. De Koker S, Naessens T, De Geest B, Bogaert P, Demeester J, De Smedt S, Grooten J 2010. Biodegradable polyelectrolyte microcapsules: antigen delivery tools with Th17 skewing activity after pulmonary delivery. *The Journal of Immunology* 184(1):203.
91. De Haes W, De Koker S, Pollard C, Atkinson D, Vlieghe E, Hoste J, Rejman J, De Smedt S, Grooten J, Vanham G 2010. Polyelectrolyte capsules-containing HIV-1 p24 and poly I: C modulate dendritic cells to stimulate HIV-1-specific immune responses. *Molecular Therapy* 18(7):1408-1416.
92. Chen X, Wu W, Guo Z, Xin J, Li J 2010. Controlled insulin release from glucose-sensitive self-assembled multilayer films based on 21-arm star polymer. *Biomaterials*.

Chapter 2

The effect and relationship of surface charge and degradability of polyvinyl amine (PVAm) nanogel on transfection efficiency

2.1 Introduction

Gene therapy represents a promising method to prevent, treat, or cure diseases. A major challenge of gene delivery is the balance between safety and efficiency. Viruses are highly efficient vectors, but often exhibit immunogenicity and mutagenicity. In addition, they can be difficult and expensive to produce. Non-viral vectors including cationic lipids and polymers have received attention due to their simplicity of production and gene-carrying capacity; however, they often have limited transfection efficiency and can exhibit significant toxicity.¹

Over the past two decades, many types of cationic polymers have been developed and studied as an alternative to viral vectors due to their versatility of physicochemical properties and easy manipulation. Charge is a key parameter of the polymer for DNA binding, interaction with the cell surface, endolysosomal escape, and subcellular localization. The nature of the polymer charge can enhance the transfection efficiency²⁻⁴, but may also result in undesirable cytotoxicity.

Cytotoxicity of polymeric vectors depends upon material composition, exposure time, and dose.⁵ Besides charge density, cytotoxicity also depends on molecular weight and degradability of vectors.⁵⁻⁶ Low molecular weight polyethylenimine (PEI) and polylysine exhibited low toxicity in previous studies.⁷⁻⁹ As a result, many groups have used low molecular weight PEI to try to avoid toxicity.¹⁰⁻¹² Highly cationic vectors cause cytotoxicity by destabilizing the plasma membrane, interacting with cellular components, and inhibiting normal cellular processes, which can induce necrosis and/or apoptosis.^{5,13-14} Many strategies have been employed to reduce undesirable toxicity of polymers containing high cation density such as using hydrophilic, tertiary amine-based polymers¹⁵, reducing the number of primary amines by acetylation¹⁶, or conjugating with cyclodextrins.¹⁷

Degradability is also an intriguing property which may be incorporated into polymers. It is known that some degradable carriers can release free DNA into the cytosol rapidly and some have been shown to exhibit low cytotoxicity.⁶ Several groups have used biodegradable polymers such as chitosan¹⁸⁻²⁰ and poly(lactic-co-glycolic acid) (PLGA)²¹ as gene carriers. A number of pH-responsive linkers such as imine²², diacrylate²³, ketal²⁴⁻²⁵ or disulfide²⁶ linkers have also been explored to achieve degradability of synthetic vectors.

The balance between transfection efficiency and toxicity is crucial. For example, fully deacetylated PEI exhibiting only moderate *in vitro* transfection efficiency and low cytotoxicity have shown improved performance *in vivo* when compared to unmodified PEI.²⁷ Many structure-bioactivity studies have been conducted to find suitable gene carriers. Previous findings have revealed the structural impact of vectors on transfection efficiency and cytotoxicity. For example, the proximity of amine units in polymer chains can enhance both gene expression and cytotoxicity.²⁸ In contrast, liposome:DNA weight ratios had a greater impact on transfection efficiency than lipoplex structures.²⁹ In another study, polylysine-graft-imidazoleacetic acid conjugates bearing high imidazole content exhibited high gene expression.³⁰ Recent studies show that amino alcohol polymers possess appreciable *in vitro* gene expression among other poly(β -amino ester)s, and terminal functionality had great effect on *in vivo* transfection efficiency.³¹⁻³² Further structure-function studies should be performed systematically in order to better define efficient, non-toxic and *in vivo* stable vectors.

Hydrogels have been widely used as delivery vehicles for vaccines, proteins, peptides and nucleic acids due to their hydrophilic nature and biocompatibility.³³⁻³⁵ Here, hydrophilic polyvinylamine (PVAm) nanogels were synthesized with controlled

amounts of primary amines. This system provides a means to assess cytotoxicity and transfection efficiency as a function of particle charge. PVAm nanogels were derived from Poly(N-vinylformamide) PNVF nanogels which were previously reported as protein carriers.³⁶ The effect of particle degradability on transfection efficiency was also assessed. PVAm nanogels were crosslinked using a non-degradable crosslinker or an acid-labile crosslinker which contains a central ketal subject to rapid degradation in acidic compartments, such as in lysosomes.^{25,37} We anticipated that PVAm nanogels with different charge densities and/or degradability would provide different transfection efficiencies. The findings from this well-controlled polymer system will add to literature defining relationships between transfection efficiency and structure, which shall aid in the future development of gene carriers.

2.2 Materials and methods

2.2.1 Materials

N-vinylformamide (NVF; Aldrich) 2, 2'-Azobis(2,4-dimethylpentanitrile (Vazo-52, DuPont). Tween-80, Span-80, and 25 kDa branched PEI were purchased from Aldrich. All other materials were used as received. 2-(N-vinylformamido) ethyl ether (NVEE) and 2-Bis[2, 2'-di(N-vinylformamido)ethoxy]propane (BDEP) were synthesized according to the procedure previously reported.³⁸⁻³⁹

2.2.2 Synthesis of polyvinylamine nanogel

Polyvinylamine nanogels with controlled charge densities, derived from polyvinylformamide, were synthesized using inverse emulsion polymerization. Briefly, in the aqueous phase, vinylformamide (350 mg) was mixed with 16 mg of the low temperature free radical initiator, VAZO-52. Then 50 mg of crosslinker, NVEE or BDEP, was added and mixed. Water 165 μ L (or 160 μ L of 10 mM phosphate buffer pH 8.0, when BDEP is used) was added and mixed. The water phase then was

mixed with 100 mL of hexane, containing VAZO-52 (30 mg), Tween-80 (3.0 g) and Span-80 (4.1 g). The mixture was homogenized to form an inverse emulsion and purged with nitrogen gas. The polymerization reaction was carried out under nitrogen atmosphere at 50 °C for 24 h. PNVF nanogels were purified by centrifugation at 15,000 rpm for 45 min, redispersed in water or 10 mM phosphate buffer (pH 8.0), and dialyzed (Spectrapor; MWCO 10,000 Da, Spectrum Laboratories Inc., CA). PNVF nanogels were converted to PVAm nanogels by hydrolysis using 0.1 or 0.5 N NaOH at 80 °C for various times as indicated in the results. PVAm nanogels were dialyzed to remove NaOH (Spectrapor; MWCO 2,000 Da, Spectrum Laboratories Inc., CA) and lyophilized (Labconco Corp., MO). Non-degradable and acid-labile PVAm nanogels were redispersed in water or 10 mM phosphate buffer (pH 8.0), respectively, to a final concentration of ~1 mg/mL. Nanogel size and zeta potential analysis was performed by dynamic light scattering (ZetaPALS; Brookhaven Instruments Corp., NY). To track the conversion of formamide side groups to amines, aliquots of non-degradable and acid-labile nanogels were collected at preselected time points, purified by size exclusion chromatography (Sephadex G-25, Chemsavers Inc., VA) and lyophilized. Dried nanogels were dissolved in D₂O (10 mg/mL), and ¹H-NMR spectra were acquired (Avance 400 MHz with an H/C/P/N QNP gradient probe, probe temperature 25 °C, 64 scans).

2.2.3 Cell culture and plasmid DNA preparation

Human alveolar basal epithelial cells (A549) were purchased from the American Type Culture Collection (ATCC) and maintained according to ATCC protocols, at 37 °C and 5% CO₂. The 5-kilobase pair expression vector pGL3 (Promega Corp., WI), containing the luciferase gene driven by the SV40 promoter and enhancer, was used. Plasmids were grown in *Escherichia coli* cell in Lubris

Bertani (LB) agar broth supplemented with 60 µg/mL ampicillin and purified using QIAGEN plasmid Giga Kits (Valencia, CA) according to the manufacturer's instructions. The DNA concentration was determined by measuring UV absorbance at 260 nm (Agilent 8453/Agilent 89090A, Agilent Technologies Inc., CA). The DNA purity was determined by measuring absorbance (A). DNA with an A_{260}/A_{280} ratio of 1.8 or greater was used.

2.2.4 Formation of polyvinylamine /DNA complexes

DNA-nanogel complexes were prepared by adding 10 µL DNA solution (0.1 µg/µL) into 15 µL of nanogel suspension, and mixing intensively by repeated pipetting and vortexing. Next, 15 µL of water was added, mixed, and incubated at room temperature for 30 min for complex formation.

2.2.5 Gel electrophoresis

Complexes were prepared by adding 10 µL DNA solution (0.1 µg/µL) into 15 µL of nanogel suspension as before, after which 4 µL of Tris-acetate-EDTA (TAE) buffer (Promega Corp., WI) and 4 µL of SYBR Green I (Invitrogen, CA) was added into the mixture. The mixture was incubated at room temperature for 30 min, and 7 µL of DNA loading buffer (Takara Bio Inc., Japan) was added. Then, 6 µL of the mixture was loaded on to a 1% agarose gel (Fisher, NJ), and electrophoresed (110 V, 30 min). A 1 kb DNA ladder (Promega Corp., WI) was used as a marker. DNA bands were visualized and photographed with an Alpha Imager (Alpha Innotech Corp., CA).

2.2.6 In vitro transfection assay

Cells were cultured in F-12 K medium (Mediatech Inc., VA) supplemented according to ATCC protocol and seeded in 96-well plates at 8,000 cells per well for 24 h before transfection. Immediately before transfection, the growth medium was removed, cells were washed with 100 µL of phosphate buffered saline (PBS) (MP

Biomedicals, LLC, OH), and 100 μ L of complexes (500 ng plasmid per well) in serum free medium was added to each well. Transfection medium was replaced with growth medium 5 h post-transfection. Luciferase expression was measured 48 and 96 h later using a luciferase assay (Promega Corp., WI). Luciferase activity was quantified in relative light units (RLUs) using a microplate reader (SpectraMax M5; Molecular Devices Corp., CA), and normalized by total cell protein which was determined using a bicinchoninic acid (BCA) assay (Thermo scientific, IL). Experiments were conducted in triplicate.

2.2.7 Particle size and zeta-potential measurements

Non-degradable and acid-labile PVAm nanogels were redispersed in water or 10 mM phosphate buffer (pH 8.0), respectively, to a final concentration of \sim 1 mg/mL. Nanogel size and zeta potential analysis was performed by dynamic light scattering (ZetaPALS; Brookhaven Instruments Corp., NY).

The size and stability of complexes was tested in serum free and growth medium. Complex size was determined using a dynamic light scattering system (BT 9000AT; Brookhaven Instruments Corp., Holtsville, NY). The mean diameter of the sample was obtained from the Stoke-Einstein equation using the method of cumulants. Complexes were then diluted with an equal volume of each medium and incubated at 37 $^{\circ}$ C for 4 h. The size of complexes in media over time was determined in the same fashion.

2.2.8 Cell viability assay

Cytotoxicity was characterized using a CellTiter 96 AQueous Cell Proliferation assay kit (Promega Corp., WI). A549 cells were seeded in 96-well plates at an initial density of 8,000 cells per well in 100 μ L of growth medium for 24 h. The growth medium was replaced with fresh, serum-free medium containing

nanogel samples. Cells were incubated with nanogels for 24 h, and the medium was replaced with complete growth medium. Then, 20 μ L of MTS ([3-(4,5-dimethylthiazol-2-yl)-5-(3-carboxymethoxyphenyl)-2-(4-sulfophenyl)-2H-tetrazolium]) and PMS (phenazine methosulfate) were added to each well, and the samples were incubated for 2 h. The absorbance was read at 490 nm, relative to blank wells prepared without cells, using a microplate reader (SpectraMax M5; Molecular Devices Corp., CA). Cell viability was expressed as the percentage of absorbance relative to the control (cells not exposed to the nanogels). Experiments were performed in triplicate.

2.3 Results

Structure-transfection relationships of polycationic gene delivery vectors have received significant attention due to the massive demand to rationalize efficient vector structure.^{16-17,23} Charge density and degradability are well known effectors of transfection efficiency and cytotoxicity. PVAm nanogels represent an attractive model for systematically studying DNA delivery. An important feature is that PVAm nanogels can be hydrolyzed from PNVF nanogels to yield different charge densities. This allows one to examine transfection efficiency of vectors as a function of particle charge, which also plays a primary role in cytotoxicity. The effect of degradability on transfection efficiency may also be assessed by crosslinking PVAm nanogels with non-degradable or acid-labile crosslinkers. Two sets of PVAm nanogels, non-degradable and acid-labile, with various charge densities were examined to correlate these chemical properties to transfection efficiency and cytotoxicity.

2.3.1 PVAm nanogel synthesis

Non-degradable and acid-labile PNVF nanogels were synthesized using inverse emulsion polymerization under nitrogen atmosphere at 50 °C for 24 h. The

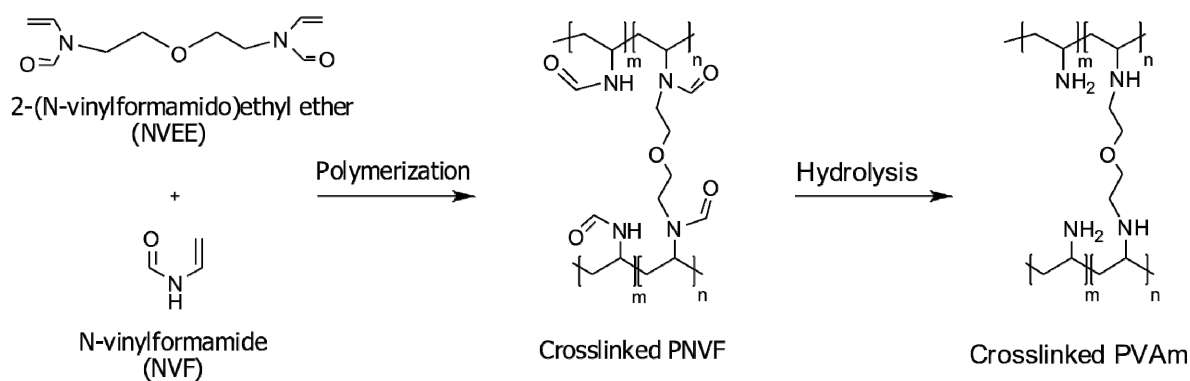
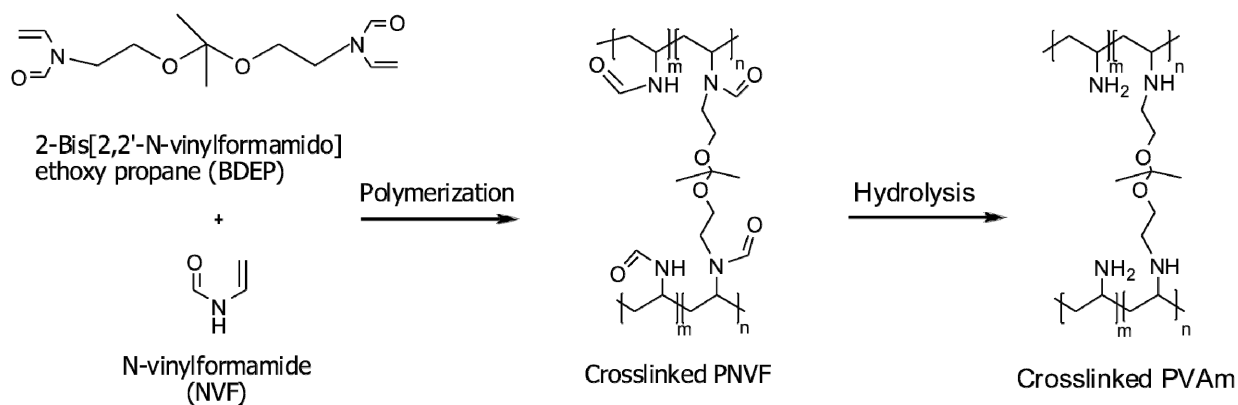
A**B**

Figure 2.1. Reaction scheme for (A) non-degradable and (B) acid-labile PVAm nanogel synthesis.

size of nanogels and the hydrolysis rate of acid-labile nanogels was controlled by the monomer: crosslinker ratio.^{36,38} The monomer: crosslinker ratio 7:1 and high temperature (50 °C) were selected based on previous experimentation.³⁶ These conditions yield small and stable nanogels and offer high yields at short reaction times. After purification, PNVF nanogels were converted to PVAm nanogels by hydrolysis of formamide side groups using NaOH at 80 °C. Nanogels were collected at different hydrolysis times in order to produce PVAm nanogels bearing different charge densities. The overall synthesis schemes for non-degradable and acid-labile PVAm nanogels are shown in Figure 2.1.

The size, size distribution, and surface charge of PNVF and PVAm nanogels were measured by dynamic light scattering in water or 10 mM phosphate buffer pH 8 for non-degradable and acid-labile PVAm nanogels, respectively (Table 2.1). Particle size and zeta potential of PVAm nanogels hydrolyzed with 0.1 and 0.5 N NaOH at 80 °C were monitored over time (Figure 2.2). Zeta potential measurements was used to detected the conversion from PNVF to PVAm nanogels. The conversion rate was controlled by the concentration of NaOH and hydrolysis time. PVAm nanogel charge and size tended to increase as a function of hydrolysis time. The increase of osmotic pressure inside the polymer network due to counter ions coordinating with an increasing number of positively charged amines probably accounted for the marked size increase.⁴⁰ Of course, the protonation of amine groups as pH decreases further propagates the observed size increase.⁴¹ Gradual charge increase was obtained during formamide hydrolysis using 0.1 N NaOH for both non-degradable and acid-labile PVAm. In comparison, 0.5 N NaOH, yielded a more rapid charge increase resembling a second order reaction, where the rate of reaction tended to strongly depend on the concentration of reactants. Non-degradable nanogels appeared to be less prone to size

Table 2.1. (A) Representative properties of PNVF and PVAm nanogels and (B) statistical analysis (one-way ANOVA, Tukey post test)

A

Nanogels	Type	Hydrolysis condition	Effective diameter (nm±SD)*	Polydispersity	Zeta potential (mV±SD)*
PNVF	Non-degradable	-	129 ± 2.7	0.09	-11 ± 1.7
PVAm a	Non-degradable	20 min, 80 °C, 0.5 M NaOH	158 ± 4.3	0.17	+8.2 ± 1.7
PVAm b	Non-degradable	3 h, 80 °C, 0.5 M NaOH	116 ± 6.9	0.01	+18 ± 3.7
PNVF	Acid-labile	-	177 ± 11	0.23	-0.45 ± 2.8
PVAm c	Acid-labile	1 h, 80 °C, 0.1 M NaOH	308 ± 40	0.32	+3.5 ± 0.8
PVAm d	Acid-labile	6 h, 80 °C, 0.1 M NaOH	260 ± 48	0.43	+10 ± 0.4

SD = Standard deviation

B

Effective diameter		Zeta potential	
One-way analysis of variance	P<0.0001	One-way analysis of variance	P<0.0001
<i>Tukey's Multiple Comparison Test</i>		<i>Tukey's Multiple Comparison Test</i>	
PNVF non-degradable vs PVAm c	P < 0.001	PNVF non-degradable vs PVAm a	P < 0.001
PNVF non-degradable vs PVAm d	P < 0.001	PNVF non-degradable vs PVAm b	P < 0.001
PVAm a vs PVAm c	P < 0.001	PNVF non-degradable vs PNVF acid-labile	P < 0.001
PVAm a vs PVAm d	P < 0.01	PNVF non-degradable vs PVAm c	P < 0.001
PVAm b vs PVAm c	P < 0.001	PNVF non-degradable vs PVAm d	P < 0.001
PVAm b vs PVAm d	P < 0.001	PVAm a vs PVAm b	P < 0.01
PNVF acid-labile vs PVAm c	P < 0.001	PVAm a vs PNVF acid-labile	P < 0.01
PNVF acid-labile vs PVAm d	P < 0.05	PVAm b vs PNVF acid-labile	P < 0.001
		PVAm b vs PVAm c	P < 0.001
		PVAm b vs PVAm d	P < 0.01
		PNVF acid-labile vs PVAm d	P < 0.001
		PVAm c vs PVAm d	P < 0.05

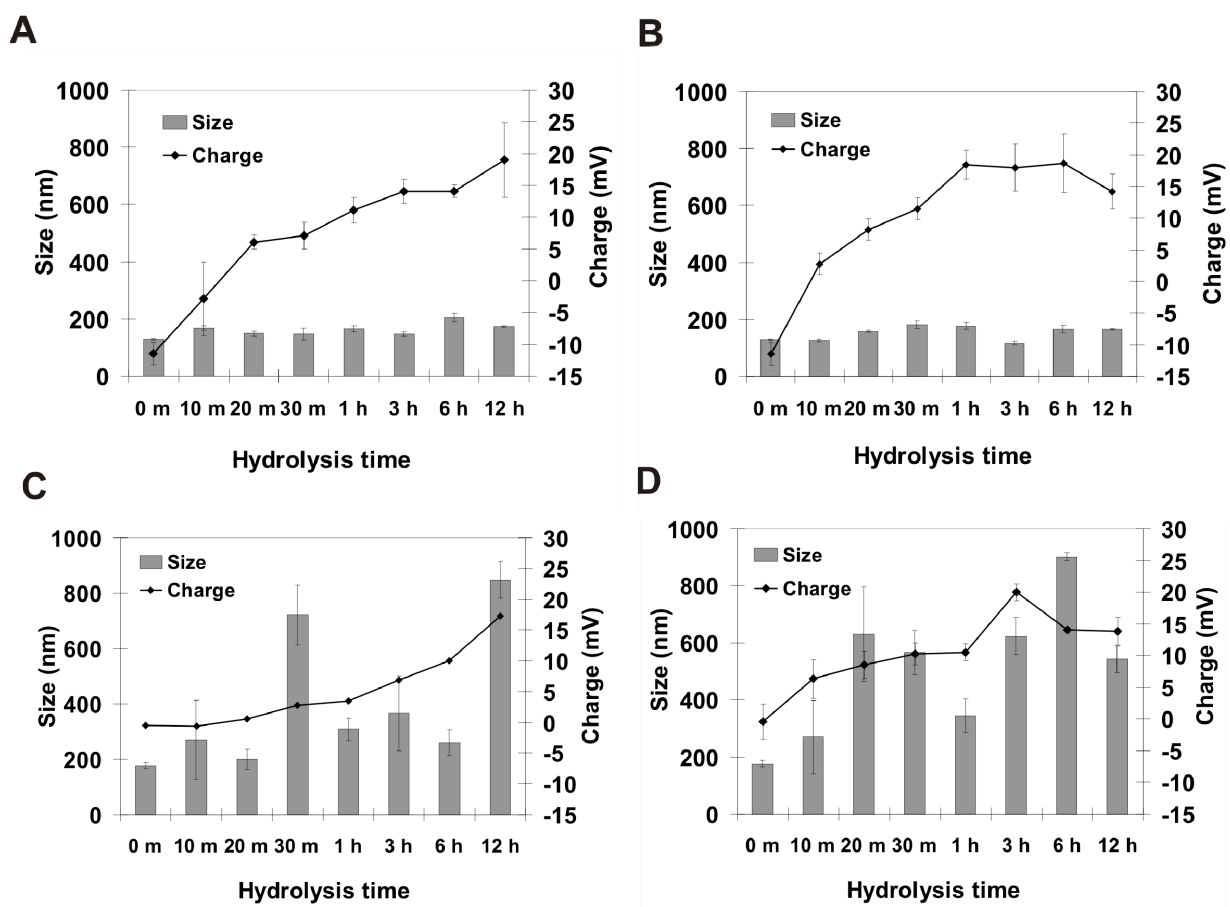


Figure 2.2. Conversion rate of non-degradable PVAm nanogels with (A) 0.1 N NaOH (B) 0.5 N NaOH and degradable PVAm nanogels with (C) 0.1 N NaOH (D) 0.5 N NaOH at 80 °C over time.

change than acid-labile nanogels. The larger observed size increase may be due to some cleavage of the acid-labile crosslinker during the purification.³⁶ As previously reported, the half-lives of acid-labile nanogels were 10 and 90 min and ~57 h in solution at pH 4.7, 5.8 and 7.4, respectively. Even though the pH of the dialysis medium was controlled (pH~8) in the purification step, acid-labile crosslinkers still hydrolyzed slowly which might have led to the larger observed size of degradable nanoparticles. The conversion of formamides to amines was confirmed by ¹H-NMR for both non-degradable and acid-labile PVAm nanogels (Figure 2.3). The decrease in intensity of the formamide chemical shift (-CHO, ~8 ppm) was observed in both non-degradable and acid-labile nanogel formulations.

2.3.2 Complex formation

The electrostatic interaction between DNA and different nanogel formulations as a function of nanogel: DNA mass ratio was examined by gel electrophoresis. In general, both non-degradable and acid-labile PVAm with low and high surface charge formed complexes efficiently with plasmid DNA at nanogel: DNA ratios greater than 3. The higher nanogel: DNA ratios bound the DNA more completely, and, eventually, eliminated the electrophoretic mobility of the DNA (Figure 2.4). Non-degradable and acid-labile nanogels bearing the more highly charged surface showed improved DNA condensation compared to nanogels bearing lower charge as expected.

Dynamic light scattering was used to determine the size of the complexes. PVAm complexes exhibited sizes from 180-560 nm in diameter (Figure 2.5). For polymer: DNA complexes (e.g. PEI: DNA), the complex sizes have been reported to be a function of the DNA: polymer ratio.⁴²⁻⁴³ Data for PVAm complexes suggested that the size was related to the original size of the nanogels, thus suggesting that the DNA was adsorbing to the nanogel surface and not causing significant flocculation.

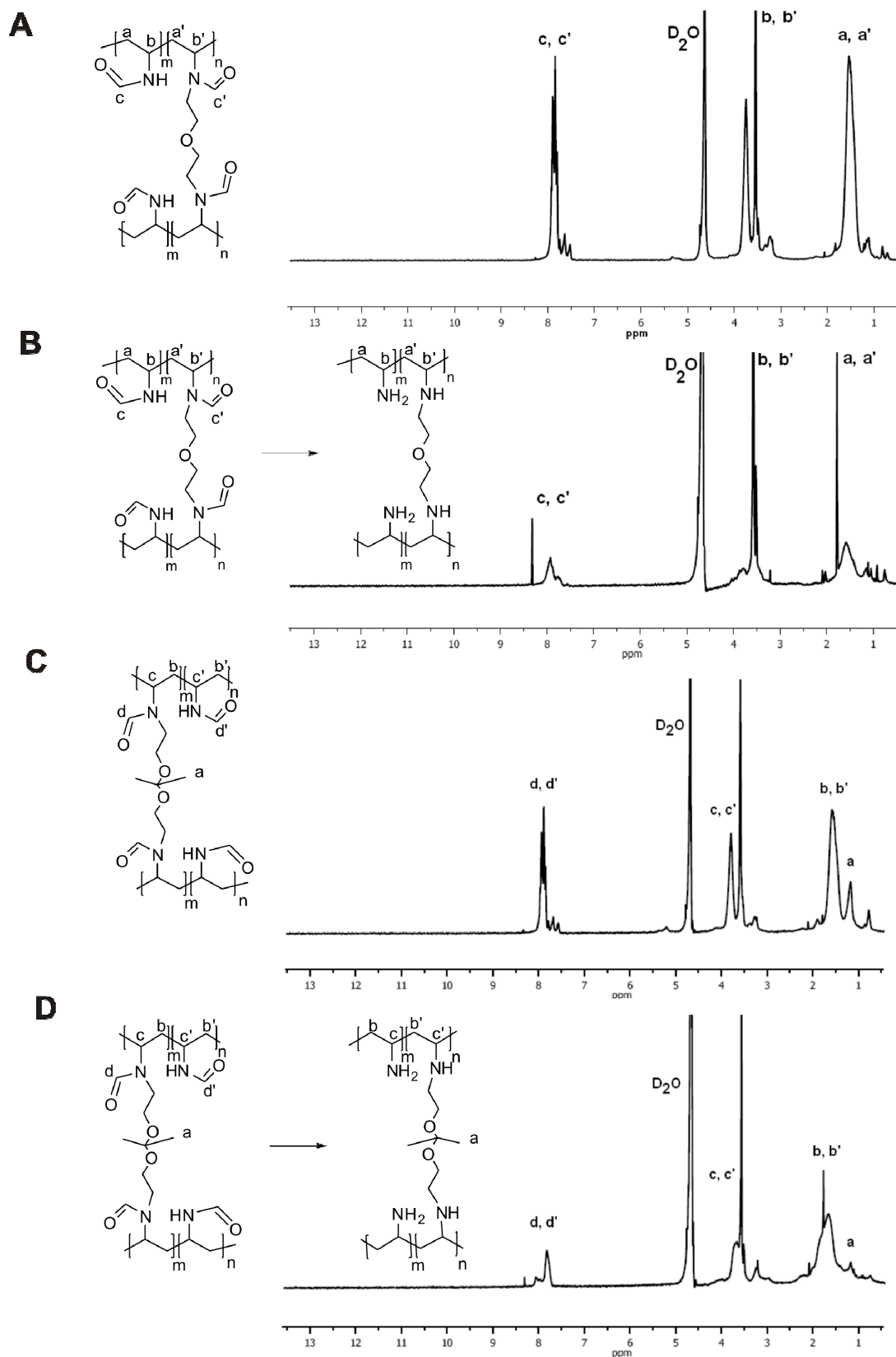


Figure 2.3. $^1\text{H-NMR}$ spectra of (A) non-degradable PNVF and (B) non-degradable PVAm nanogels after hydrolysis with 0.1 N NaOH at 80 °C for 6 h and (C) acid-labile PNVF and (D) acid-labile PVAm nanogels after hydrolysis with 0.5 N NaOH at 80 °C for 3 h.

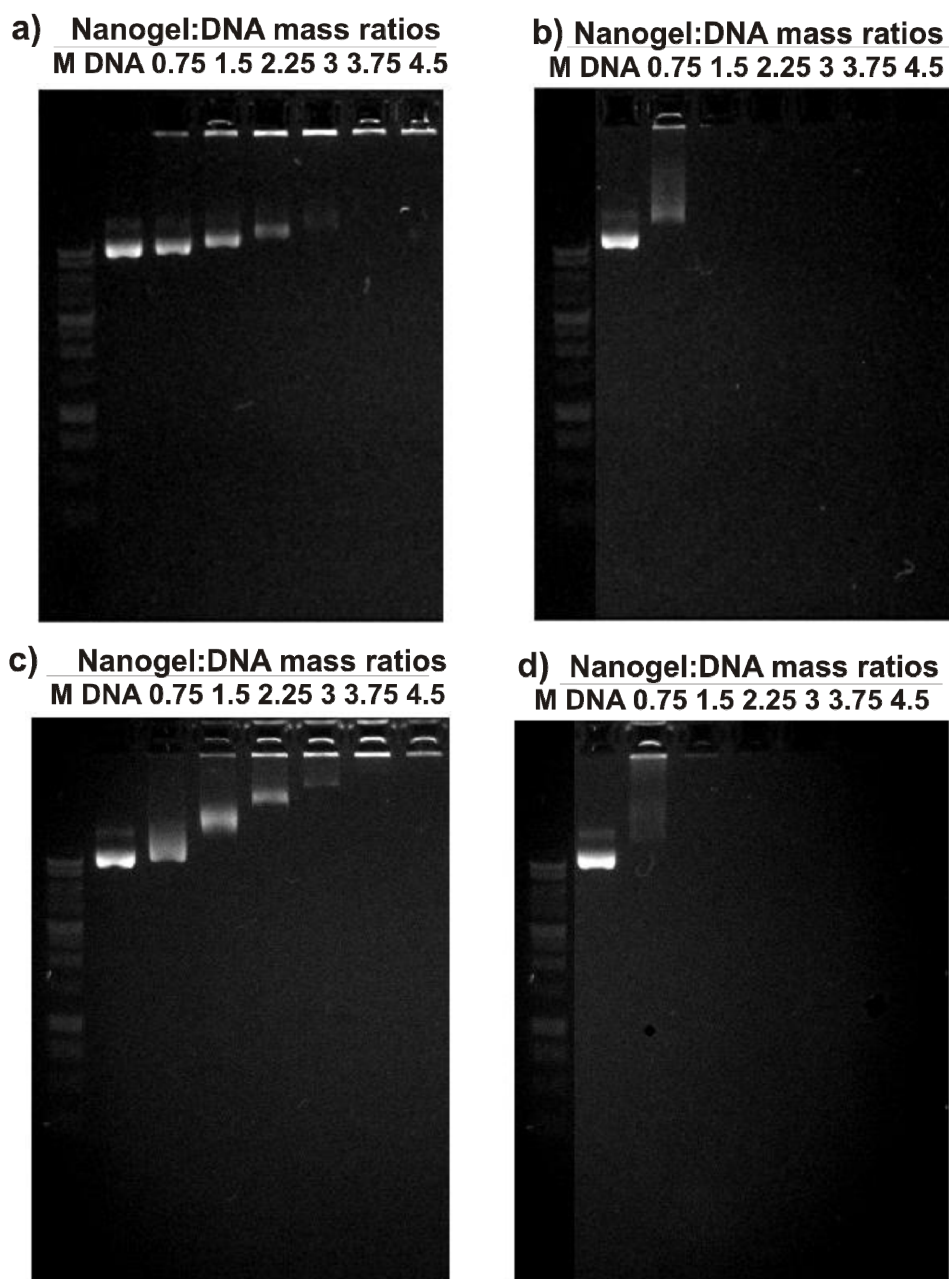


Figure 2.4. Gel electrophoresis of non-degradable PVAm/DNA complexes made from (a) 158 nm, +8.2 mV, (b) 116 nm, +18 mV, and acid-labile PVAm/DNA complexes made from (c) 308 nm, +3.5 mV (d) 228 nm, +11 mV.

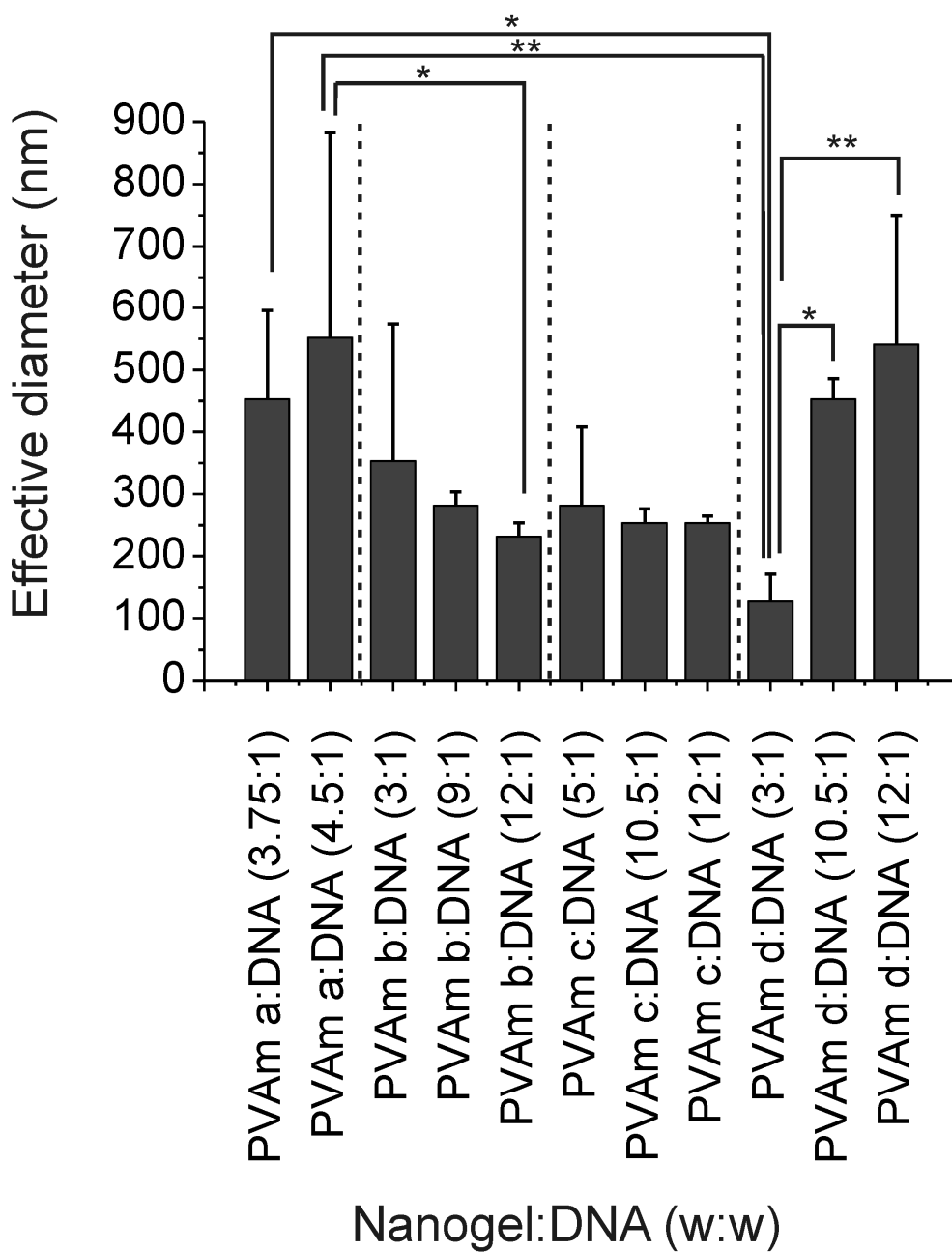


Figure 2.5. Effective diameter of non-degradable (a, b) and acid-labile (c, d) PVAm/DNA complexes at different polymer-to-DNA ratios ($n = 3 \pm SD$) (* = $p < 0.05$, ** = $p < 0.01$, one-way ANOVA, Tukey post test).

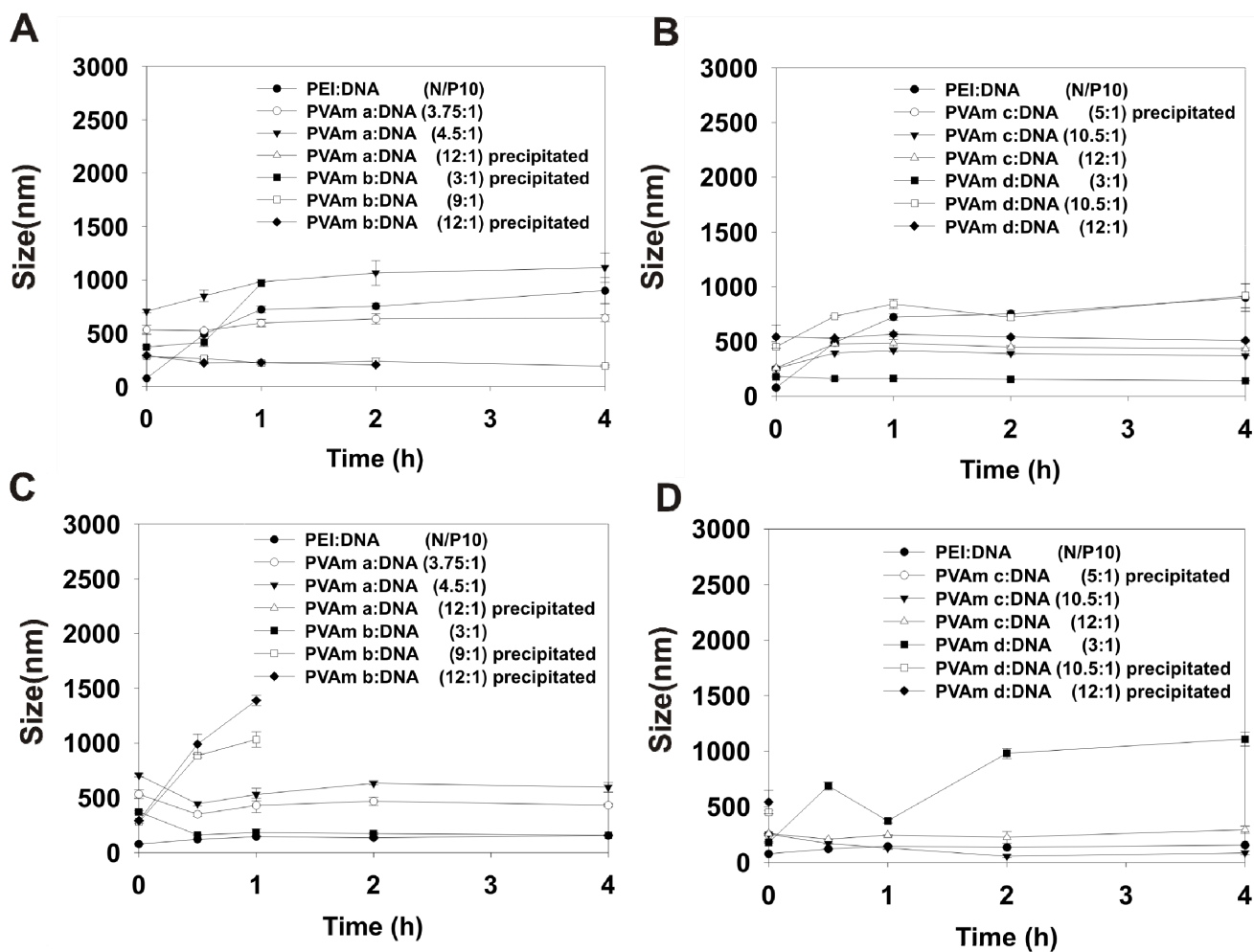


Figure 2.6. Stability of (A) non-degradable and (B) acid-labile PVAm/DNA complexes at different nanogel-to-DNA ratios in serum free medium and (C) non-degradable and (D) acid-labile PVAm/DNA complexes at different nanogel-to-DNA ratios in growth medium over time.

The stability of the complexes in serum-free and growth medium was also monitored over time (Figure 2.6). The complexes with high nanogel: DNA ratios, bearing high zeta potential, exhibited an increase in particle size in growth medium. The ionic interaction between serum protein and excess positive charge was a likely cause of the observed size increase and agglomeration.⁴⁴ Interestingly, PEI complexes and PVAm complexes with low nanogel: DNA ratios retained small sizes in growth medium for longer periods of time.

2.3.4 Cytotoxicity test

The *in vitro* cytotoxicity of non-degradable and acid-labile PVAm nanogels each exhibiting low or high charge was measured using an MTS assay. Results indicated that cytotoxicity increased with increasing accessible charge (Figure 2.7). The IC₅₀ of PEI was extremely low (~5 µg/mL). The IC₅₀ of non-degradable PVAm nanogels bearing charge +8.2 and +18 mV, were ~400 and 10 µg/mL, whereas acid-labile PVAm nanogels bearing charge +3.5 and +10 mV, were ~300 and 10 µg/mL, respectively. Acid-labile nanogels bearing lower charges (e.g. +10 mV) had almost the same level of cytotoxicity compared to non-degradable nanogels bearing higher charges (e.g. +18 mV). Charge density resulting from the number and the arrangement of cationic residues is a key factor for cytotoxicity.⁵ Non-degradable nanogels have a globular shape, whereas acid-labile nanogels gradually degrade to linear oligomers as dictated by the pH of the microenvironment over time. As reported previously, the half-lives of acid-labile nanogels were 10 and 90 min and ~57 h in solution at pH 4.7, 5.8 and 7.4, respectively, and the size of oligomers after degradation was ~14,000 Da.³⁶ Therefore, acid-labile nanogels were expected to be degraded rapidly once they were endocytosed. Upon degradation, PVAm oligomers are linear and have more accessible cationic charges than non-degradable

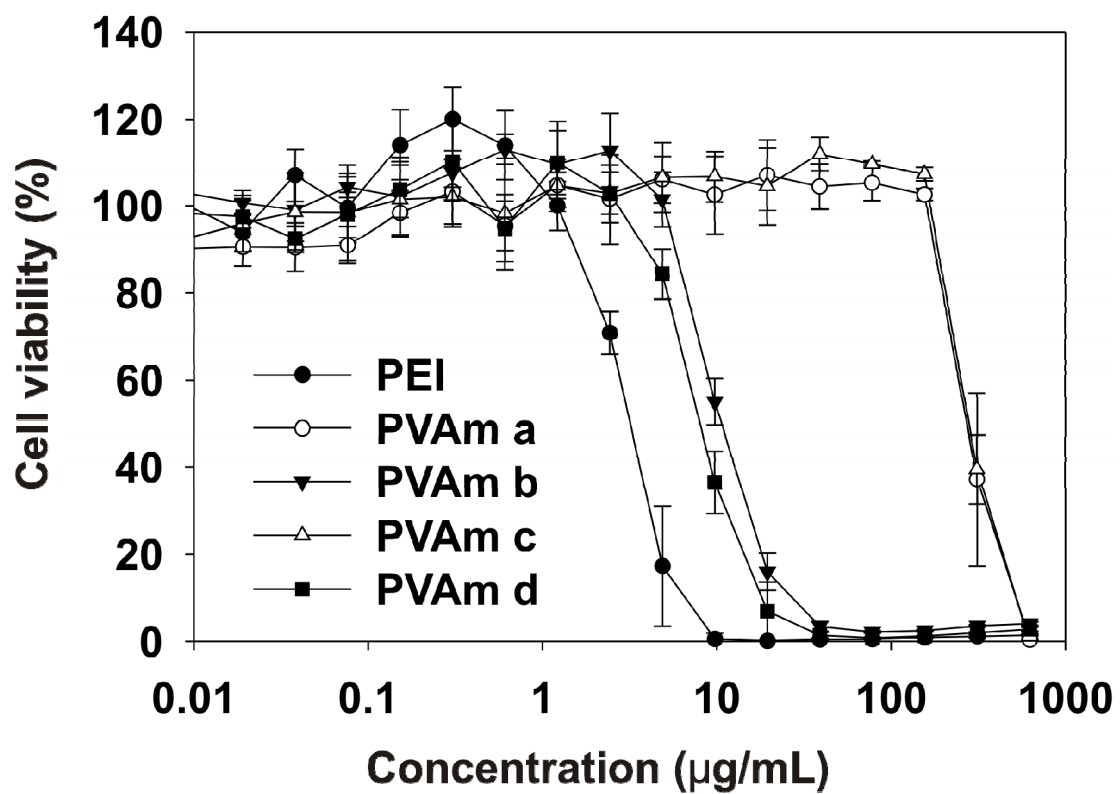


Figure 2.7. Cytotoxicity of PEI, non-degradable (a, b) and acid-labile (c, d) PVAm nanogels in A549 cells.

nanogels. Therefore, highly flexible cationic oligomers (degradation products) could interact and crosslink anionic microtubules or motor proteins and perhaps lead to the observed cytotoxicity.⁴⁵ In addition, flexible molecules have potentially greater interactions with membranes than rigid molecules.⁴⁶ Our results also support this hypothesis; globular non-degradable nanogels bearing almost the same charge (+8.2 mV, IC₅₀ ~400 µg/mL) had lower cytotoxicity compared to acid-labile nanogels (+10 mV, IC₅₀ ~10 µg/mL). The results suggest that accessible cationic charge density dictate the relative cytotoxicity of nanogels in this system.

2.3.5 Transfection

In vitro transfection efficiency in A549 cells was systematically studied as a function of the nanogel: DNA ratio. Overall, the transfection efficiencies of non-degradable and acid-labile PVAm nanogels were moderate compared to PEI (Figure 2.8). However, this system of nanogels with similar structure, but different charge densities and degradability, provided a tunable model to track the relationship between these properties and transfection efficiency. Most PVAm nanogels exhibited the highest transfection efficiency after 48 h of incubation. The nanogels bearing higher surface charge typically yielded higher transfection efficiencies at 48 h. This is presumably a result of improved electrostatic interaction with cell surfaces.⁴⁷ Acid-labile complexes made from PVAm bearing a lower surface charge exhibited higher transfection efficiencies on day 4 compared to all other formulations. Acid-labile PVAm nanogels bearing high surface charge mediated markedly lower gene expression. The observed reduction in gene expression for highly charged particles may have resulted from ineffective dissociation of DNA and relatively high cytotoxicity. Negligible transfection efficiency was observed at day 4 for all complexes made from non-degradable nanogels. Other rate limiting processes such as nuclear localization or

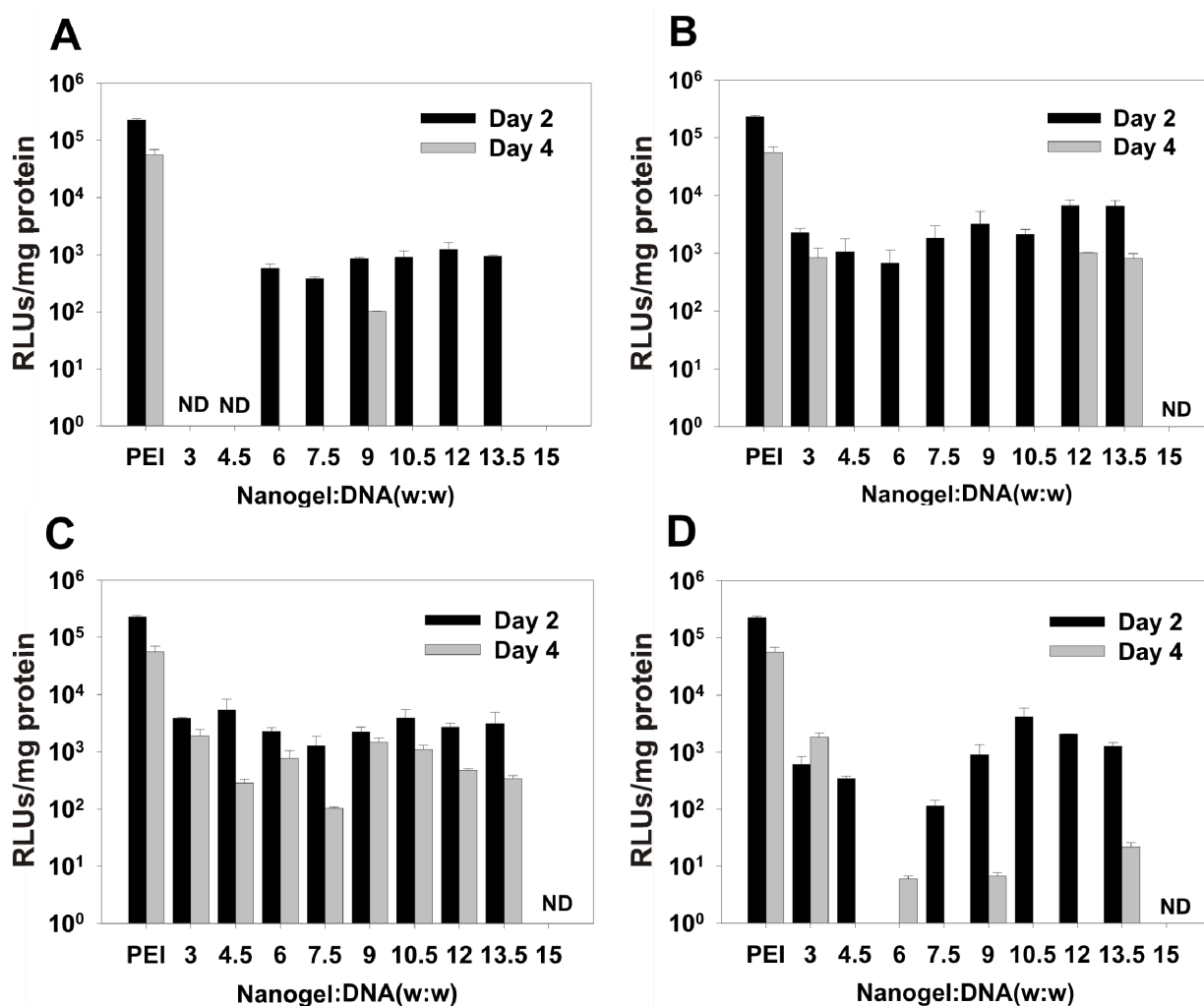


Figure 2.8. Transfection efficiency of non-degradable PVAm complexes made from (A) PVAm, 158 nm, +8 mV (B) PVAm, 116 nm, +18 mV and acid-labile complexes made from (C) PVAm, 308 nm, +3.5 mV (D) PVAm, 228 nm, +11 mV at different nanogel-to-DNA ratios 2 and 4 day post-transfection in A549 cells.

transcription may also be affected by the relative ability of these complexes to release DNA.⁴⁸⁻⁵¹

Size of complexes is known to be an important parameter effecting the endocytic pathway. It is reported that latex beads ≤ 200 nm (e.g. 50 nm and 100 nm and 80% of 200 nm) are exclusively taken up by clathrin-mediated endocytosis. With increasing size, the caveolae-mediated pathway becomes apparent. Larger beads (500 nm) are internalized predominantly via caveolae-mediated endocytosis, a non-degradative pathway reported to result in productive transfection.⁵²⁻⁵⁴ Even though non-degradable nanogels were smaller than 200 nm, both non-degradable and acid-labile nanogels were 200-500 nm in size when complexed with DNA, thus suggesting the use both endocytosis pathways.

Relatively high transfection efficiencies were observed at low and high nanogel: DNA ratios compared to medium ratios. It may be that moderate nanogel: DNA ratios (e.g. 6:1 and 7.5:1) formed tight complexes, impeding the dissociation of DNA to permit transcription. At low polymer: DNA ratios (e.g. 3:1 and 4.5:1) it is probable that looser complexes were formed allowing DNA to dissociate from the complexes more easily. At high nanogel: DNA ratios (e.g. 10.5:1), it may be that the increased positive charge improved recruitment of the complexes to the negatively charged cell surface resulting in higher transfection efficiencies despite the tight DNA binding. Similar results have been reported for cationic lipid/ DNA complexes and the results have been explained in terms of the interactions between complexes and cells.^{29,55}

Transfection efficiency of non-degradable complexes seemed to be directly related to the toxicity of nanogels, especially at high nanogel: DNA ratios. Non-degradable PVAm nanogels having higher cytotoxicity yielded higher transfection

efficiencies. Conversely, there was no apparent correlation between cytotoxicity and transfection efficiency for acid-labile complexes. Acid-labile nanogels bearing low charge exhibited higher transfection efficiency than acid-labile nanogels bearing high charge. In previous reports, particles bearing degradable bonds tended to release DNA rapidly regardless of the charge density.⁶ The ability to release DNA and overall low cytotoxicity were likely key factors leading to sustained gene expression levels at day 4.

2.4 Discussion

Gene delivery vectors should have high transfection efficiency and low toxicity in order to facilitate translation into the clinic. These properties have rarely been found in one vector. Polymers or lipids bearing high charge have improved DNA packaging, enhanced cell surface interaction that facilitates uptake by endocytosis, and improved endolysosomal escape.^{6,56} All of these features lead to high gene expression. However, it is well known that highly charged materials often have high cytotoxicity, aggregate readily in bodily fluids and may induce an inflammatory response. For example, systemic administration of lipoplexes activates the innate immune system rapidly and induces proinflammatory cytokines.⁵⁷

Several approaches have been reported to produce less toxic vectors. Generally, lower molecular weight polymers are preferred due to their corresponding reduction in toxicity. Many chemical modifications have been assessed to produce highly efficient and safe vectors. Forrest and others acetylated primary and secondary amines of branched, 25 kDa PEI to secondary and tertiary amides, respectively.¹⁶ The 43% acetylated PEI showed a 26-fold higher transfection efficiency compared to unmodified PEI. The decrease in the number of protonable nitrogens would be expected to decrease endolysosomal escape via the proton-sponge mechanism.

However, it was suspected that the improved performance was compensated by more DNA release from looser complexes and an overall reduction in cytotoxicity.

Polymer degradability is another important factor for effective gene delivery vehicles. Crosslinking strategies have also been utilized for producing a number of degradable polymers. Taking advantage of pH differences between physiological pH (~7) and lysosomal pH (~4-5), pH-responsive crosslinkers have been synthesized and incorporated into polymer backbones yielding a variety of degradable vectors.^{22,24-25}

Using naturally degradable polymers offers an alternative way to reduce toxicity. Cationic polysaccharides are water-soluble and biodegradable. Two main groups that have been investigated for gene delivery are chitosan derivatives and cationic dextrans (e.g. dextran-spermine). These materials have generally shown good DNA condensing ability and relatively low cytotoxicity compared to traditional vectors. In one study, chitosan and trimethylated chitosan showed appreciable transfection in two cell lines compared to PEI.²⁰ In addition, dextran-spermine polyplexes showed more mild tissue and systemic toxicity in mice in comparison to PEI.⁵⁸

In this study, hydrophilic PVAm nanogels bearing different cationic charge exhibited different gene expression levels. For non-degradable nanogels, high charge densities yielded higher gene expression compared to nanogels with low charge densities as expected. The observed gene expression may result from properties of these nanogels such as charge density which effects complex size and stability as well as cell binding. Highly charged non-degradable nanogels were able to condense DNA into smaller complexes compared to non-degradable nanogels with lower charge. The small size and complex stability under physiological conditions are important factors for efficient gene delivery.⁵⁹ The overall net positive surface charge also enhances

interaction with cellular membrane surface which promotes endocytosis. For example, highly cationic polymers were previously described to possess high transfection efficiency.^{5,60-61} Nagasaki *et al* reported cationic derivatives of Schizophyllan, a natural polysaccharide, showing superior transfection efficiency with an increased degree of amination.⁶² These materials also showed higher cytotoxicity as expected.

Interestingly, acid-labile nanogels with low charge densities yielded extended gene expression while maintaining lower cytotoxicity. The primary effector of the observed transfection efficiencies for complexes made from low charge nanogels may be the small complex size. A secondary effector for sustained gene expression might be the low toxicity of the low charge density nanogels. Even though higher charge polymers had higher efficiency at the same dose, they were more toxic and had lower efficiency with increased dose (presumably due to increased cytotoxicity).⁶⁰ Our results are also in accordance with findings by Miyata *et al.*, where poly (ethylene glycol)-poly(L-lysine) block copolymer with reduced charge density produced by thiolation was found to have high transfection efficiency compared to high charge density copolymers with the same degree of thiolation.⁶³

The data reinforced the idea that degradability and cationic charge are important properties of gene vectors. Balancing the two features, low charge and degradability, can give rise to improved transfection efficiency without compromising cytotoxicity. Finally, the data reiterate the need to study gene expression for longer periods of time, as compared to the typical 1-2 day transfection and 1 day cytotoxicity studies that are common today.

Gene therapy continues to hold promise to cure a number of diseases and to improve disease management. But, clinical applications are not yet realized since there are several confounding barriers. Overcoming one barrier (e.g. cytotoxicity) has

typically amplified another barrier (e.g. transfection efficiency). Understanding polymer structural effects on transfection will help us to optimize nonviral vector formulations. It is probable that carefully balancing transfection efficiency and toxicity is a key that should be further explored to develop suitable gene vectors.

2.5 Conclusions

PVAm nanogels having similar chemical structure and bearing discrete combinations of charge densities and degradability offered a means to assess structure-transfection relationships for this material. PNVF nanogels were synthesized and crosslinked with non-degradable or acid-labile crosslinkers via an inverse emulsion polymerization reaction. PNVF nanogels were then hydrolyzed to PVAm nanogels exhibiting different charge densities. The cytotoxicity of PVAm nanogels increased with increasing charge accessibility. Non-degradable nanogels yielded high initial gene expression. Interestingly, acid-labile nanogels bearing lower charge exhibited more sustained gene expression offering the highest cumulative gene expression of any nanogel formulation. These observations suggested that transfection efficiency may be improved by balancing charge and degradability without compromising cytotoxicity.

2.6 Bibliography

1. Glover DJ, Lipps HJ, Jans DA 2005. Towards safe, non-viral therapeutic gene expression in humans. *Nature Reviews Genetics* 6(4):299-310.
2. Sakurai F, Inoue R, Nishino Y, Okuda A, Matsumoto O, Taga T, Yamashita F, Takakura Y, Hashida M 2000. Effect of DNA/liposome mixing ratio on the physicochemical characteristics, cellular uptake and intracellular trafficking of plasmid DNA/cationic liposome complexes and subsequent gene expression. *Journal of Controlled Release* 66(2-3):255-269.
3. Khalil IA, Kogure K, Futaki S, Hama S, Akita H, Ueno M, Kishida H, Kudoh M, Mishina Y, Kataoka K 2007. Octaarginine-modified multifunctional envelope-type nanoparticles for gene delivery. *Gene Therapy* 14(8):682-689.
4. Kneuer C, Ehrhardt C, Bakowsky H, Ravi Kumar MNV, Oberle V, Lehr CM, Hoekstra D, Bakowsky U 2006. The Influence of Physicochemical Parameters on the Efficacy of Non-Viral DNA Transfection Complexes: A Comparative Study. *Journal of Nanoscience and Nanotechnology* 6(9-10):2776-2782.
5. Fischer D, Li Y, Ahlemeyer B, Kriegelstein J, Kissel T 2003. In vitro cytotoxicity testing of polycations: influence of polymer structure on cell viability and hemolysis. *Biomaterials* 24(7):1121-1131.
6. Pack DW, Hoffman AS, Pun S, Stayton PS 2005. Design and development of polymers for gene delivery. *Nature Reviews Drug Discovery* 4:581-593.
7. Kunath K, von Harpe A, Fischer D, Petersen H, Bickel U, Voigt K, Kissel T 2003. Low-molecular-weight polyethylenimine as a non-viral vector for DNA delivery: comparison of physicochemical properties, transfection efficiency and in vivo distribution with high-molecular-weight polyethylenimine. *Journal of Controlled Release* 89(1):113-125.
8. Wolfert MA, Dash PR, Nazarova O, Oupicky D, Seymour LW, Smart S, Strohal J, Ulbrich K 1999. Polyelectrolyte Vectors for Gene Delivery: Influence of Cationic Polymer on Biophysical Properties of Complexes Formed with DNA. *Bioconjugate Chemistry* 10:993-1004.
9. Wolfert MA, Seymour LW 1996. Atomic force microscopic analysis of the influence of the molecular weight of poly (L) lysine on the size of polyelectrolyte complexes formed with DNA. *Gene therapy(Basingstoke)* 3(3):269-273.
10. Werth S, Urban-Klein B, Dai L, Höbel S, Grzelinski M, Bakowsky U, Czubayko F, Aigner A 2006. A low molecular weight fraction of polyethylenimine (PEI) displays increased transfection efficiency of DNA and siRNA in fresh or lyophilized complexes. *Journal of Controlled Release* 112(2):257-270.
11. Shin JY, Suh D, Kim JM, Choi HG, Kim JA, Ko JJ, Lee YB, Kim JS, Oh YK 2005. Low molecular weight polyethylenimine for efficient transfection of human hematopoietic and umbilical cord blood-derived CD34+ cells. *BBA-General Subjects* 1725(3):377-384.
12. Lampela P, Raisanen J, Mannisto PT, Yla-Herttuala S, Raasmaja A 2002. The use of low-molecular-weight PEIs as gene carriers in the monkey fibroblastoma and rabbit smooth muscle cell cultures. *J Gene Med* 4(2):205-214.
13. Clamme JP, Krishnamoorthy G, Mély Y 2003. Intracellular dynamics of the gene delivery vehicle polyethylenimine during transfection: investigation by two-photon fluorescence correlation spectroscopy. *BBA-Biomembranes* 1617(1-2):52-61.
14. Bieber T, Meissner W, Kostin S, Niemann A, Elsasser HP 2002. Intracellular route and transcriptional competence of polyethylenimine–DNA complexes. *Journal of Controlled Release* 82(2-3):441-454.

15. Van de Wetering P, Moret EE, Schuurmans-Nieuwenbroek NME, Van Steenberghe MJ, Hennink WE 1999. Structure-Activity Relationships of Water-Soluble Cationic Methacrylate/Methacrylamide Polymers for Nonviral Gene Delivery. *Bioconjugate Chemistry* 10:589-597.
16. Forrest ML, Meister GE, Koerber JT, Pack DW 2004. Partial Acetylation of Polyethylenimine Enhances In Vitro Gene Delivery. *Pharmaceutical Research* 21(2):365-371.
17. Forrest ML, Gabrielson N, Pack DW 2005. Cyclodextrin-polyethylenimine conjugates for targeted in vitro gene delivery. *Biotechnology and Bioengineering* 89(4):416-423.
18. Mao HQ, Roy K, Troung-Le VL, Janes KA, Lin KY, Wang Y, August JT, Leong KW 2001. Chitosan-DNA nanoparticles as gene carriers: synthesis, characterization and transfection efficiency. *Journal of Controlled Release* 70(3):399-421.
19. Köping-Höggård M, Tubulekas I, Guan H, Edwards K, Nilsson M, Vårum KM, Artursson P 2001. Chitosan as a nonviral gene delivery system. Structure-property relationships and characteristics compared with polyethylenimine in vitro and after lung administration in vivo. *Gene Therapy* 8(14):1108-1121.
20. Kean T, Roth S, Thanou M 2005. Trimethylated chitosans as non-viral gene delivery vectors: Cytotoxicity and transfection efficiency. *Journal of Controlled Release* 103(3):643-653.
21. Jeong JH, Park TG 2002. Poly (l-lysine)-g-poly (d, l-lactic-co-glycolic acid) micelles for low cytotoxic biodegradable gene delivery carriers. *Journal of Controlled Release* 82(1):159-166.
22. Kim YH, Park JH, Lee M, Kim YH, Park TG, Kim SW 2005. Polyethylenimine with acid-labile linkages as a biodegradable gene carrier. *Journal of Controlled Release* 103(1):209-219.
23. Forrest ML, Koerber JT, Pack DW 2003. A Degradable Polyethylenimine Derivative with Low Toxicity for Highly Efficient Gene Delivery. *Bioconjugate Chemistry* 14(5):934-940.
24. Knorr V, Ogris M, Wagner E 2008. An Acid Sensitive Ketal-Based Polyethylene Glycol-Oligoethylenimine Copolymer Mediates Improved Transfection Efficiency at Reduced Toxicity. *Pharm Res* 25(12):2937-2945.
25. Jain R, Standley SM, Frechet JMJ 2007. Synthesis and degradation of pH-sensitive linear poly (amidoamine) s. *Macromolecules* 40(3):452-457.
26. Lin C, Zhong Z, Lok MC, Jiang X, Hennink WE, Feijen J, Engbersen JFJ 2006. Linear poly (amido amine) s with secondary and tertiary amino groups and variable amounts of disulfide linkages: Synthesis and in vitro gene transfer properties. *Journal of Controlled Release* 116(2):130-137.
27. Thomas M, Lu JJ, Ge Q, Zhang C, Chen J, Klivanov AM 2005. Full deacylation of polyethylenimine dramatically boosts its gene delivery efficiency and specificity to mouse lung. *Proceedings of the National Academy of Sciences* 102(16):5679-5684.
28. Lee CC, Liu Y, Reineke TM 2008. General Structure-Activity Relationship for Poly (glycoamidoamine) s: The Effect of Amine Density on Cytotoxicity and DNA Delivery Efficiency. *Bioconjugate Chem* 19(2):428-440.
29. Congiu A, Pozzi D, Esposito C, Castellano C, Mossa G 2004. Correlation between structure and transfection efficiency: a study of DC-Chol- DOPE/DNA complexes. *Colloids and Surfaces B: Biointerfaces* 36(1):43-48.

30. Chen DJ, Majors BS, Zelikin A, Putnam D 2005. Structure–function relationships of gene delivery vectors in a limited polycation library. *Journal of Controlled Release* 103(1):273-283.
31. Zugates GT, Peng W, Zumbuehl A, Jhunjhunwala S, Huang YH, Langer R, Sawicki JA, Anderson DG 2007. Rapid Optimization of Gene Delivery by Parallel End-modification of Poly (β -amino ester) s. *Molecular Therapy* 15(7):1306.
32. Anderson DG, Akinc A, Hossain N, Langer R 2005. Structure/property studies of polymeric gene delivery using a library of poly (β -amino esters). *Molecular Therapy* 11:426-434.
33. Kim B, Peppas NA 2003. In vitro release behavior and stability of insulin in complexation hydrogels as oral drug delivery carriers. *International Journal of Pharmaceutics* 266(1-2):29-37.
34. Toussaint JF, Dubois A, Dispas M, Paquet D, Letellier C, Kerkhofs P 2007. Delivery of DNA vaccines by agarose hydrogel implants facilitates genetic immunization in cattle. *Vaccine* 25(7):1167-1174.
35. Ishii Y, Nakae T, Sakamoto F, Matsuo K, Quan YS, Kamiyama F, Fujita T, Yamamoto A, Nakagawa S 2008. A transcutaneous vaccination system using a hydrogel patch for viral and bacterial infection. *Journal of Controlled Release* 131(2):113-120.
36. Shi L, Khondee S, Linz TH, Berkland C 2008. Poly (N-vinylformamide) Nanogels Capable of pH-Sensitive Protein Release. *Macromolecules* 41(17):6546-6554.
37. Murthy N, Campbell J, Fausto N, Hoffman AS, Stayton PS 2003. Design and synthesis of pH-responsive polymeric carriers that target uptake and enhance the intracellular delivery of oligonucleotides. *Journal of Controlled Release* 89(3):365-374.
38. Shi L, Berkland C 2007. Acid-Labile Polyvinylamine Micro-and Nanogel Capsules. *Macromolecules* 40(13):4635-4643.
39. Shi L, Berkland C 2006. pH-triggered dispersion of nanoparticle clusters. *Advanced materials(Weinheim)* 18(17):2315-2319.
40. Forster S, Hermsdorf N, Bottcher C, Lindner P 2002. Structure of polyelectrolyte block copolymer micelles. *Macromolecules* 35(10):4096-4105.
41. Gebhardt K, Ahn S, Venkatachalam G, Savin D 2007. Rod-Sphere Transition in Polybutadiene- Poly (l-lysine) Block Copolymer Assemblies. *Langmuir* 23(5):2851-2856.
42. Putnam D, Gentry CA, Pack DW, Langer R 2001. Polymer-based gene delivery with low cytotoxicity by a unique balance of side-chain termini. *Proceedings of the National Academy of Sciences* 98(3):1200.
43. Xu P, Li SY, Li Q, Ren J, Van Kirk EA, Murdoch WJ, Radosz M, Shen Y 2006. Biodegradable cationic polyester as an efficient carrier for gene delivery to neonatal cardiomyocytes. *Biotechnology and Bioengineering* 95(5):893.
44. Dash PR, Read ML, Barrett LB, Wolfert MA, Seymour LW 1999. Factors affecting blood clearance and in vivo distribution of polyelectrolyte complexes for gene delivery. *Gene Therapy* 6:643-650.
45. Suh J, Wirtz D, Hanes J 2003. Efficient active transport of gene nanocarriers to the cell nucleus. *Proceedings of the National Academy of Sciences* 100(7):3878-3882.
46. Singh AK, Kasinath BS, Lewis EJ 1992. Interaction of polycations with cell-surface negative charges of epithelial cells. *Biochimica et biophysica acta Protein structure and molecular enzymology* 1120(3):337-342.

47. Wiethoff CM, Smith JG, Koe GS, Middaugh CR 2001. The Potential Role of Proteoglycans in Cationic Lipid-mediated Gene Delivery Studies of the interaction of cationic lipid-DNA complexes with model glycosaminoglycans *Journal of Biological Chemistry* 276(35):32806-32813.
48. Zaric V WD, Erbacher P, Remy JS, Behr JP, D. S 2004. Effective polyethylenimine-mediated gene transfer into human endothelial cells. *J Gene Med* 6:176-184.
49. Rémy-Kristensen A, Clamme JP, Vuilleumier C, Kuhry JG, Mély Y 2001. Role of endocytosis in the transfection of L929 fibroblasts by polyethylenimine/DNA complexes. *BBA-Biomembranes* 1514(1):21-32.
50. James MB, Giorgio TD 2000. Nuclear-Associated Plasmid, but Not Cell-Associated Plasmid, Is Correlated with Transgene Expression in Cultured Mammalian Cells. *Molecular Therapy* 1(4):339-346.
51. Banks GA, Roselli RJ, Chen R, Giorgio TD 2003. A model for the analysis of nonviral gene therapy. *Gene Therapy* 10:1766-1775.
52. Rejman J, Conese M, Hoekstra D 2006. Gene transfer by means of lipo- and polyplexes: role of clathrin and caveolae-mediated endocytosis. *Journal of Liposome Research* 16(3):237-247.
53. Rejman J, Bragonzi A, Conese M 2005. Role of clathrin- and caveolae-mediated endocytosis in gene transfer mediated by lipo- and polyplexes. *Molecular Therapy* 12(3):468-474.
54. Rejman J, Oberle V, Zuhorn IS, Hoekstra D 2004. Size-dependent internalization of particles via the pathways of clathrin- and caveolae-mediated endocytosis. *Biochemical Journal* 377(1):159-170.
55. Ahmad A, Evans HM, Ewert K, George CX, Samuel CE, Safinya CR 2005. New multivalent cationic lipids reveal bell curve for transfection efficiency versus membrane charge density: lipid-DNA complexes for gene delivery. *J Gene Med* 7:739-748.
56. Park MR, Han KO, Han IK, Cho MH, Nah JW, Choi YJ, Cho CS 2005. Degradable polyethylenimine-alt-poly (ethylene glycol) copolymers as novel gene carriers. *Journal of Controlled Release* 105(3):367-380.
57. Sellins K, Fradkin L, Liggitt D, Dow S 2005. Type I Interferons Potently Suppress Gene Expression Following Gene Delivery Using Liposome-DNA Complexes. *Molecular Therapy* 12:451-459.
58. Eliyahu H, Joseph A, Azzam T, Barenholz Y, Domb AJ 2006. Dextran-spermine-based polyplexes—Evaluation of transgene expression and of local and systemic toxicity in mice. *Biomaterials* 27(8):1636-1645.
59. Mansouri S, Lavigne P, Corsi K, Benderdour M, Beaumont E, Fernandes J 2004. Chitosan-DNA nanoparticles as non-viral vectors in gene therapy: strategies to improve transfection efficacy. *European journal of pharmaceutics and biopharmaceutics* 57(1):1-8.
60. Miyata K, Oba M, Nakanishi M, Fukushima S, Yamasaki Y, Koyama H, Nishiyama N, Kataoka K 2008. Polyplexes from poly (aspartamide) bearing 1, 2-diaminoethane side chains induce pH-selective, endosomal membrane destabilization with amplified transfection and negligible cytotoxicity. *Journal of the American Chemical Society* 130:48.
61. Jang J, Kim S, Lee S, Kim K, Han J, Lee Y 2006. Poly (ethylene glycol)/poly (-caprolactone) diblock copolymeric nanoparticles for non-viral gene delivery: The role of charge group and molecular weight in particle formation, cytotoxicity and transfection. *Journal of Controlled Release* 113(2):173-182.

62. Nagasaki T, Hojo M, Uno A, Satoh T, Koumoto K, Mizu M, Sakurai K, Shinkai S 2004. Long-Term Expression with a Cationic Polymer Derived from a Natural Polysaccharide: Schizophyllan. *Bioconjugate Chem* 15(2):249-259.
63. Miyata K, Kakizawa Y, Nishiyama N, Harada A, Yamasaki Y, Koyama H, Kataoka K 2004. Block cationic polyplexes with regulated densities of charge and disulfide cross-linking directed to enhance gene expression. *J Am Chem Soc* 126(8):2355-2361.

Chapter 3

**Calcium-crosslinked LABL-TAT complexes effectively
target gene delivery to ICAM-1 expressing cells**

3.1 Introduction

The efficient delivery of therapeutic genes to a target site is a key to success in gene therapy. The basic principle of gene therapy has now been established with human using viral vectors. Viruses are very efficient gene vectors, but safety concerns such as immunogenicity of viral proteins and risk of oncogenesis still remain.¹ Both viral and non-viral vectors are continually under development.² Cell penetrating peptides (CPPs), also called protein transduction domains (PTD), have emerged as a valuable component of non-viral vehicles facilitating the delivery of various molecules such as small molecule drugs³⁻⁴, imaging agents⁵⁻⁶, peptides⁷⁻⁸, proteins⁹⁻¹⁰, nucleic acids¹¹⁻¹², and nanoparticles¹³⁻¹⁴ across biological barriers. CPPs are relatively short (<30 amino acids) and usually contain multiple basic amino acids. The cationic properties of many CPPs allows complexation with nucleic acids, which can be further condensed into small nanoparticles by the addition of calcium chloride.¹⁵⁻¹⁶ When translating these cationic complexes to in vivo studies, shielding with polyethylene glycol (PEG) and adding a peptide ligand to enable cell targeting may improve performance.

The HIV-1 trans-activating transcription factor (TAT) protein was among the first found to be capable of translocating cell membranes and gaining intracellular access. Specific peptide domains were identified from this protein that maintained translocation ability. One specific domain, TAT₄₉₋₅₇ (RKKRRQRRR), is one of the most widely studied CPPs for intracellular therapeutic delivery. TAT has been extensively utilized to deliver a multitude of cargo in liposomes, polyplexes, solid lipid nanoparticles or other nanoparticle types or by direct conjugation to molecules of interest.¹⁷⁻²² TAT peptide has also been used to form electrostatic complexes with DNA and siRNA to facilitate intracellular delivery. Unfortunately, the transfection

efficiency of TAT complexes with DNA has been relatively poor, possibly due to an inability to form small complexes or deactivation of this CPP when bound to nucleic acids.²³⁻²⁴ It has been suggested that high molecular weight cationic polymers offer stable complexes, while small polymers give rise to large, unstable complexes.²⁴ As a result, many groups have attempted to improve transfection efficiency by using a reducible TAT polymer²³ or by stringing together multiple TAT copies (e.g. TAT₂, TAT₃, and TAT₄).²⁵⁻²⁶ Recent work showed that TAT/DNA complexes have comparable transfection efficiency to polyethylenimine (PEI) when condensed using calcium.¹⁵ Calcium was reported to bind both DNA phosphate groups and/or TAT amine groups resulting in compact complexes with optimal DNA release.¹⁵ Translation of these complexes may require charge shielding to avoid clearance or targeting to promote accumulation at diseased tissue.

Cell adhesion molecules play an essential role in cell trafficking in the immune system. Intercellular cell-adhesion molecule-1 (ICAM-1), a member of the immunoglobulin superfamily, promotes cell adhesion in immunological and inflammatory reactions. It is constitutively expressed on some tissues and upregulated by inflammatory cytokines such as interleukin-1 (IL-1), tumor necrosis factor- α (TNF- α) or interferon- γ (INF- γ).²⁷⁻²⁸ ICAM-1 can be expressed on vascular endothelial cells, epithelial cells, fibroblasts, tissue macrophages, and antigen presenting cells.²⁹ The upregulation of ICAM-1 is associated with diverse diseases such as atherosclerosis, ischemia and reperfusion, asthma, arthritis, graft rejection, and cancer metastasis.³⁰⁻³¹ As a result, elevated ICAM-1 has been used as a target to deliver enzymes, nanoparticles, contrast agents, and antisense oligonucleotides in an effort to improve health of patients.³²⁻³⁸

LABL peptide (ITDGEATDSG) is derived from the I-domain of the α_L -subunit of leukocyte function associated antigen-1 (LFA-1). LABL inhibits LFA-1/ICAM-1 interaction by binding to the D1 domain of ICAM-1 through its active region, ITDGEA.³⁹ Blocking ICAM-1/LFA-1 interactions with antibodies and LABL-antigenic peptide conjugate have been shown to modulate disease severity and progression of psoriasis and experimental autoimmune encephalomyelitis (EAE), a model for multiple sclerosis.^{29,40-42} In addition to receptor binding, LABL can be internalized by ICAM-1 suggesting an alternative mechanism to deliver therapeutics into cells having elevated ICAM-1 expression.⁴³ Recent work showed that cLABL-conjugated nanoparticles could be successfully delivered to lung carcinoma epithelial cells.³²

The aim of this study was to target TAT/DNA complexes as a means to transfect ICAM-1 expressing cells. TAT peptide was conjugated with LABL peptide using a polyethylene glycol (PEG) spacer. This block peptide was then complexed with plasmid DNA encoding luciferase. Calcium chloride was used to condense the complexes, thus yielding a small size with optimized DNA release.¹⁵ At optimal calcium concentration, the TAT-PEG-LABL was able to target DNA to ICAM-1 expressing cells and enhance transfection in comparison to untargeted complexes (e.g. TAT-PEG) offering an effective gene carrier to ICAM-1 expressing cells.

3.2 Materials and methods

3.2.1 Materials

Branched polyethylenimine (PEI, 25 kDa) was purchased from Aldrich. Peptide conjugates were synthesized in house via solid phase peptide synthesis using an automated Pioneer Peptide Synthesizer (PerSeptive Biosystems, Foster City, CA). Resins were purchased from Applied Biosystems (Foster City, CA). Fmoc-

(CH₂CH₂O)₁₂ (MW 840, 46.5 Å spacer) and Fmoc amino acids were purchased from Peptide International Inc (Louisville, KY) and Advanced ChemTech (Louisville, KY), respectively. All peptide conjugates were purified by semi-preparative HPLC on a C18 column, and the purity was determined by analytical HPLC with detection at a wavelength of 220 nm (Shimadzu scientific instruments, Columbia, MD). The mobile phase was 0.1 % trifluoroacetic acid, with gradient elution using acetonitrile (15-40 % over 45 min). The molecular weight was confirmed by electron spray mass spectrometry (LCT premier mass spectrometer, Water, Milford, MA). Carcinoma human alveolar basal epithelial cells (A549) were purchased from the American Type Culture Collection (ATCC) and cultured according to ATCC protocol. Plasmid DNA encoding firefly luciferase (pGL3, 4.8 kbp) was obtained from Promega (Madison, WI). Plasmids were grown in *Escherichia coli* cells in Lubris Bertani (LB) broth supplemented with 60 µg/mL ampicillin and purified using QIAGEN plasmid Giga Kits (Valencia, CA) according to the manufacturer's instructions. The DNA purity level was determined using a UV/VIS spectrometer. DNA with an A₂₆₀/A₂₈₀ ratio of 1.8 or greater was used. F-12K medium was purchased from Mediatech, Inc (Manassas, VA). Agarose was purchased from Fisher Scientific (Fair Lawn, NJ). Heparin sodium was obtained from Spectrum Chemical Mfg. Corp. (Gardena, CA). Recombinant, human, tumor necrosis factor-α (TNF-α), luciferase assay kit and CellTiter 96[®] Aqueous non-radioactive cell proliferation assay (MTS) were purchased from Promega (Madison, WI). Bicinchoninic acid assay (BCA) was purchased from Thermo Fisher Scientific Inc (Rockford, IL). Monoclonal anti-human CD54 (ICAM-1) domain D1 and monoclonal anti-human CD54 (ICAM-1) domain D1/FITC were purchased from Ansell (Bayport, MN). Lipofectamine 2000, 4',6-diamidino-2-

phenylindole, dilactate (DAPI, dilactate), TOTO-3 and SYBR green I were purchased from Invitrogen Molecular Probes Inc. (Carlsbad, CA).

3.2.2 Complex formation

Complex formation was conducted as described earlier.¹⁵ Briefly, complexes were prepared by adding 10 μL (0.1 $\mu\text{g}/\mu\text{L}$) of DNA to 15 μL of PEI (polymer nitrogen to DNA phosphate (N/P) ratio of 10) or to 15 μL of TAT conjugates (at desired N/P ratios) followed by intensive mixing. Fifteen microliters of DNase free water or known concentrations (e.g. 150 mM) of CaCl_2 solution was then added to PEI and TAT complexes respectively, and the solution was vigorously pipetted again. Complexes were allowed to incubate at 4 $^{\circ}\text{C}$ for 30 min before use. Lipofectamine/DNA complex was prepared according to the manufacturer's protocol.

3.2.3 Size and morphology

Complexes were prepared as described earlier. Hydrodynamic diameters of complex solutions were determined at 20 $^{\circ}\text{C}$ by dynamic light scattering (DLS) using a DynaPro plate reader (Wyatt Technology, Santa Barbara, CA). Complexes were analyzed in Corning 384-well UV-transparent plates using 30s data acquisitions and auto-attenuation laser power. The mean diameter of the sample was obtained from the Stoke-Einstein equation using the method of cumulants. The Dynamics Software package version 6.12 was used to analyze the data.

Complex size was also examined over time in serum-free F12K medium. Complexes were prepared and diluted with the medium in the same manner as in transfection study, using 1 part of complex solution: 4 parts of medium. Complex size was monitored at 0, 1, 2 and 4 hrs using the DLS plate reader.

Complexes intended for transmission electron microscopy (TEM) were air-dried on copper grids coated with carbon film. TEM images of complexes were

obtained using A JEOL 1200 EXII transmission electron microscope operating at an accelerating voltage of 80 kV.

3.2.4 Agarose gel electrophoresis

Complexes were prepared as described earlier. Four μL of Tris-acetate-EDTA (TAE) buffer and 4 μL of SYBR Green I were then added into the mixture. The mixture was incubated at room temperature for 30 min, and 7 μL of DNA loading buffer was added. Then, 6 μL of the mixture was loaded onto a 1 % agarose gel, and electrophoresed at 110 V for 30 min. A 1 kb DNA ladder was used as a marker. DNA migration bands were visualized and photographed with an Alpha Imager (Alpha Innotech Corp., San Leandro, CA).

For heparin displacement studies, complexes were challenged with 0.05 to 0.35 U heparin for 30 min at room temperature. Complex solutions were treated with TAE buffer and SYBR Green I, followed by the addition of DNA loading buffer and electrophoresis as described above. Uncomplexed and untreated DNA diluted with identical electrophoresis solutions were used as a control.

3.2.5 Cytotoxicity assay

Cytotoxicity of TAT conjugates and PEI was determined using a CellTiter 96 AQueous Cell Proliferation assay kit. A549 cells were seeded in 96-well plates (8,000 cells/well) for 24 h prior to use. The growth medium was replaced with serum-free medium containing TAT conjugates and PEI at various concentrations and incubated for 24 h. After incubation, the medium containing sample was replaced with 100 μL of serum-free medium. Then, 20 μL of solution mixture of MTS ([3-(4,5-dimethylthiazol-2-yl)-5-(3-carboxymethoxyphenyl)-2-(4-sulfophenyl)-2H-tetrazolium]) and PMS (phenazine methosulfate) were added to each well, and the plates were then incubated at 37 °C, 5% CO₂ for 2 h. The absorbance of the formazan

product was measured at 490 nm using a microplate reader (SpectraMax M5; Molecular Devices Corp., CA).

3.2.6 Relative ICAM-1 expression on A549 cells

Cells were incubated with TNF- α (1000 U/mL) for 24 and 48 h to activate ICAM-1 expression on the cell surface.⁴⁴ Cells were then trypsinized, centrifuged, and washed three times with ice-cold PBS. Cells were divided into microcentrifuge tubes (5×10^5 cells/ 50 μ L). AB serum was added to block non-specific binding (25 μ L) and incubated on ice for 10 min at room temperature. Cells were washed with ice-cold PBS and monoclonal anti-human CD54 (ICAM-1) domain D1/FITC (80 μ L) was added and incubated on ice for 45 min. Cells were washed three times with ice-cold PBS and fixed with 4 % paraformaldehyde. The fluorescent intensity of cells was measured using a FACscan flow cytometer. Data analysis was performed using Cell Quest software (BD).

3.2.7 Transfection studies

A549 cells were seeded in 96-well plate (8,000 cells/well) for 24 h prior to transfection or activation of ICAM-1. Cells were incubated with TNF- α (1,000 U/mL) for an additional 48 h for transfection studies on cells with up-regulated ICAM-1. Complexes were prepared as described earlier. Prior to transfection, growth medium was removed and cells were washed with PBS (100 μ L) twice. Complexes (20 μ L) were diluted with serum-free medium (80 μ L) and then were added to each well. After 5 h of transfection, transfection medium was replaced with growth medium and cells were incubated for another 48 h. The luciferase assay kit was used to determine gene expression. Cells were harvested and luciferase expression was measured according to the manufacturer's protocol. Luciferase activity was quantified in relative light units (RLUs) using a microplate reader (SpectraMax M5; Molecular

Devices Corp., CA), and normalized by total cellular protein which was determined using a bicinchoninic acid (BCA) assay.

Transfection parameters such as CaCl_2 concentrations (0-300 mM) and N/P ratios (5–30) were optimized using TAT and TAT-PEG complexes in normal A549 cells. For targeting, studies in cells activated using $\text{TNF-}\alpha$, 25 and 50% of the TAT-PEG-LABL were selected to be incorporated into complexes (the remainder was TAT-PEG). Previous work demonstrated that increasing ligand density (e.g. from 25% to 50%) increased the binding and uptake of particles targeting ICAM-1 receptors.⁴⁵ Particles with 50% targeting ligand showed the highest interaction compared to other formulations. Increasing ligand density (e.g. 75% and 100%) resulted in decreased binding and uptake of the particles.

The effect of ICAM-1 receptor blocking on transfection efficiencies of targeted complexes was also examined. Activated cells were incubated with various concentrations of free LABL peptide or anti-ICAM-1 mAb for 30 min. Cells were then washed three times with serum-free medium and incubated with 50% TAT-PEG-LABL/DNA and TAT/DNA complexes for 5 h. Luciferase expression was measured as described above.

3.2.8 Confocal microscopy of internalization

DNA was fluorescently labeled with the intercalating nucleic acid stain TOTO-3 using a molar ratio of 1 dye molecule per 300 base pairs for 30 min at room temperature in the dark. Then, complexes were prepared as described earlier with the labeled DNA. A549 cells were mounted onto glass slides and activated with $\text{TNF-}\alpha$. Cells were then incubated with complexes for 4 h. Cells were then washed three times with ice-cold PBS and fixed with 4 % paraformaldehyde. Nuclei were labeled with DAPI dilactate (300 nM, ex: 358 nm, em: 461 nm) for 5 min at 37 °C, 5 % CO_2 . Cells

were observed using an Olympus Spinning Disk Confocal Microscope and TIRF-M inverted fluorescence microscope using 20X or 60X objectives (DAPI, ex: 387 nm, em: 415-470 nm, TOTO-3, ex: 628 nm, em: 669-726 nm). Bright field transmission images were obtained at the same time.

3.2.9 *Statistic analysis*

GraphPad Prism 4 software was used for statistical analysis. Statistical significance for differences between two data sets was determined by unpaired Student's *t*-test (95% confidential interval). One-way ANOVA, Tukey post test was used to analyze the differences when more than two data sets were compared.

3.3 Results

3.3.1 *Purification and characterization of TAT, TAT-PEG, and TAT-PEG-LABL*

All TAT peptide conjugates were synthesized according to a standard Fmoc protocol. The crude peptide and conjugates were purified by semi-preparative HPLC on a C18 column, and the purity was determined by analytical RP-HPLC (purity >95 %) (Figure 3.1). The expected molecular weight was confirmed by electrospray ionization mass spectrometry; TAT MW 1338.9 Da, TAT-PEG MW 1939.2 Da, TAT-PEG-LABL MW 2885.6 Da (Figure 3.2).

3.3.2 *Physicochemical characterization of complexes*

An important characteristic for efficient gene delivery using cationic polymers is the formation of small and stable complexes with DNA.⁴⁶ The ability of TAT and TAT conjugates to form complexes with DNA was studied using agarose gel electrophoresis at N/P ratios of 0, 1, 2, 3, 4, 5, 10, 20, and 30. The immobilization of DNA suggested that TAT and TAT-PEG conjugates were able to form complexes with DNA and completely immobilize DNA starting at an N/P ratio of 1 and 2, respectively (Figure 3.3). Targeting ligands (TAT-PEG-LABL) were included at

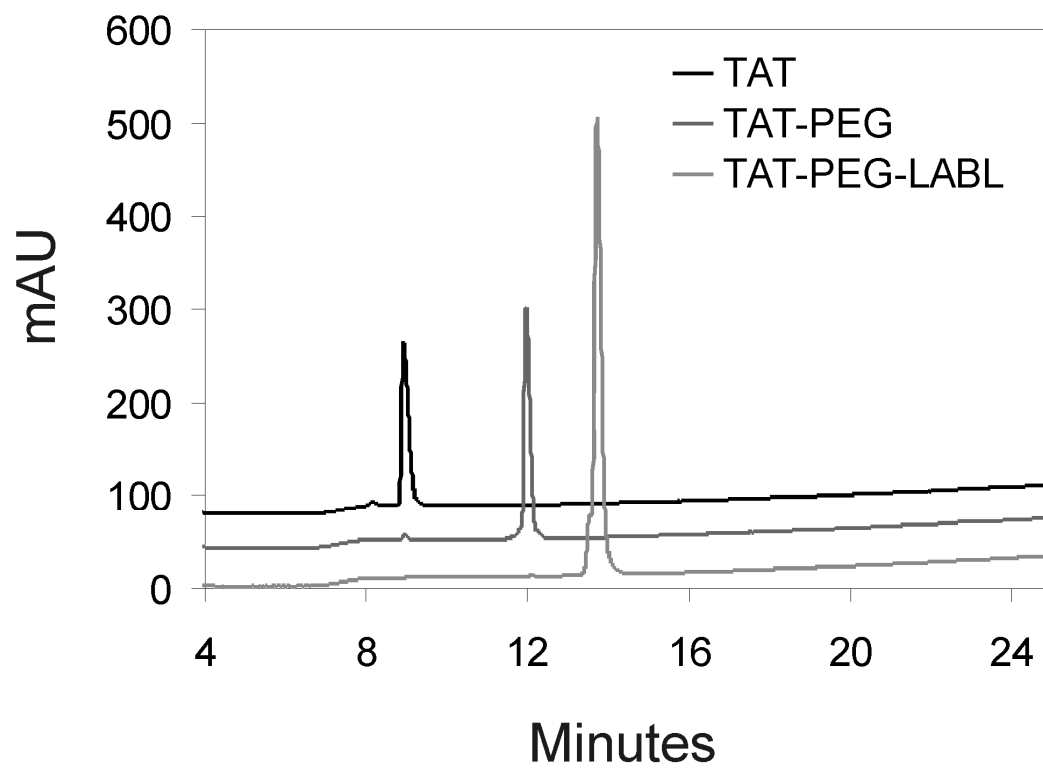


Figure 3.1. HPLC chromatograms for TAT, TAT-PEG, and TAT-PEG-LABL confirmed purity > 95%.

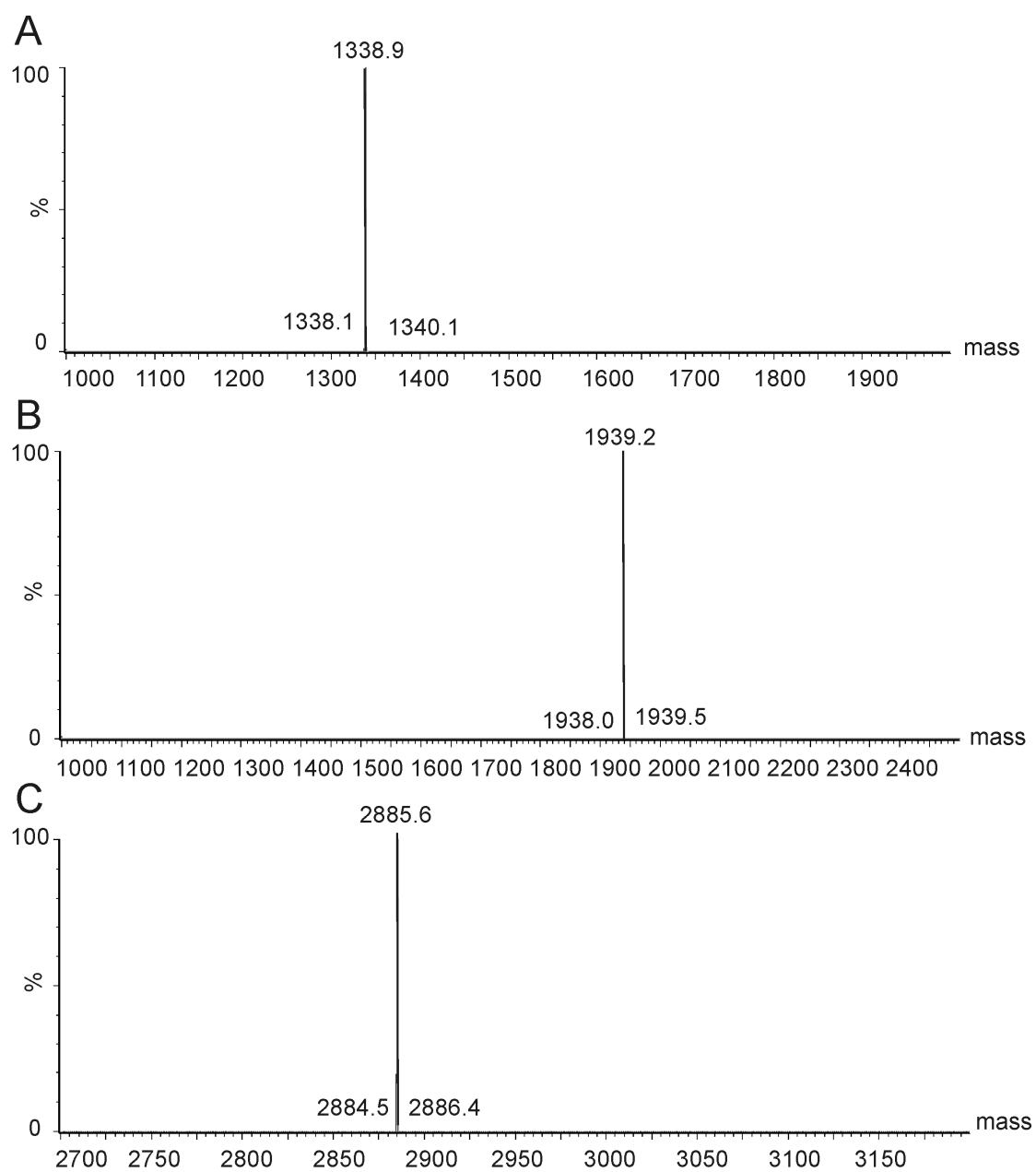


Figure 3.2. Electrospray ionization (ESI) mass spectra of (A) TAT, (B) TAT-PEG, and (C) TAT-PEG-LABL were in agreement with calculated masses.

various ratios with TAT-PEG and DNA mobility was assessed at an N/P ratio of 30. Targeted TAT conjugates in all formulations (e.g. 25, 50, and 75 % TAT-PEG-LABL) were able to immobilize DNA. The data also suggested that PEGylation did not negatively affect the ability of TAT to complex with DNA at N/P ratios ≥ 2 .

The hydrodynamic diameters and morphology of the complexes were evaluated by DLS and TEM, respectively. TAT, TAT-PEG, 25 % TAT-PEG-LABL, and 50 % TAT-PEG-LABL complexes were prepared at an N/P ratio of 30 and in the presence of various concentrations of CaCl₂. Complexes with discrete percentages of targeting ligands were prepared by varying the relative amounts of TAT-PEG and TAT-PEG-LABL (e.g. 25% or 50% TAT-PEG-LABL). The complex size in deionized water varied with CaCl₂ concentration (Figure 3.4A). TAT and TAT-PEG complexes were generally smaller than 25 % and 50 % TAT-PEG-LABL complexes. Without CaCl₂, most complexes were quite large (>400 nm) as determined by DLS. When adding 30 mM CaCl₂, the complexes were larger than the initial size suggesting that a low concentration of CaCl₂ may induce aggregation. Adding 150 mM CaCl₂ yielded a minimum diameter for most complexes (110, 190, 290 nm for TAT, TAT-PEG, and 50 % TAT-PEG-LABL complexes, respectively). The data suggested that the TAT peptide could not condense DNA well without calcium chloride and that an optimal amount of calcium chloride is essential to form compact particles. Comparing the size of TAT and TAT-PEG complexes suggested that PEGylation increased the hydrodynamic diameter as observed by others.⁴⁷

Complex size in serum-free F12K media was also determined over time. TAT, TAT-PEG, 25 % TAT-PEG-LABL, and 50 % TAT-PEG-LABL complexes were prepared as described earlier at an N/P ratio of 30 and in the presence of various

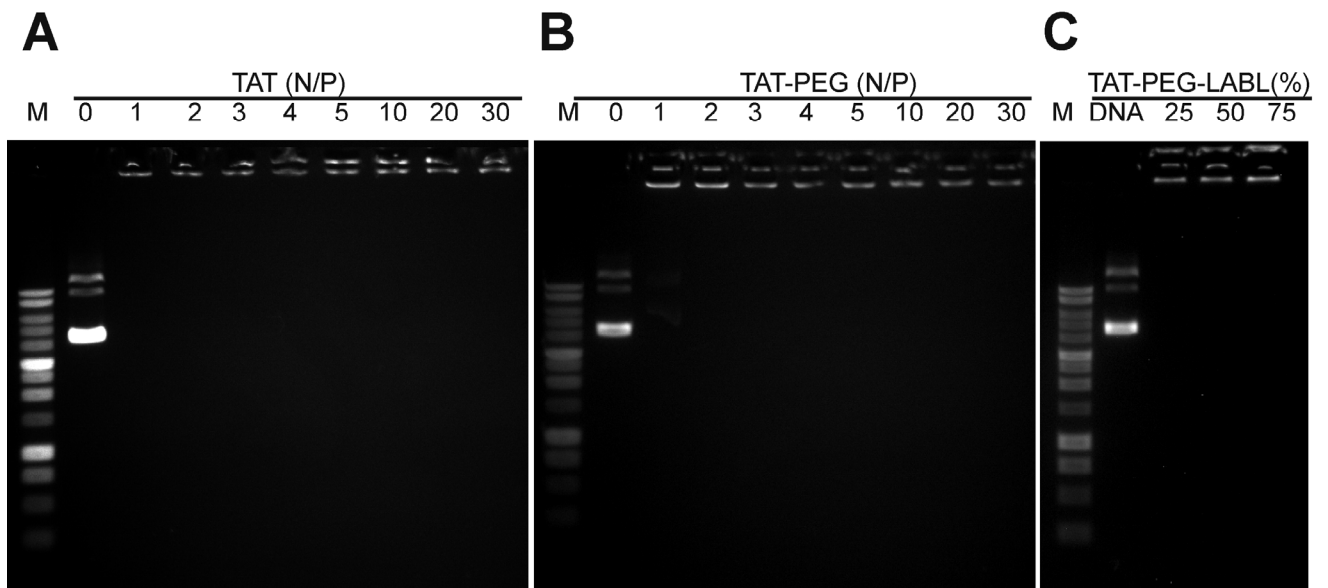


Figure 3.3. Gel electrophoresis of (A) TAT/DNA and (B) TAT-PEG/DNA complexes at different N/P ratios. (C) TAT-PEG-LABL/DNA complexes at an N/P ratio of 30 with different amounts of TAT-PEG-LABL combined with TAT-PEG. All complexes at all N/P ratios limited the mobility of DNA.

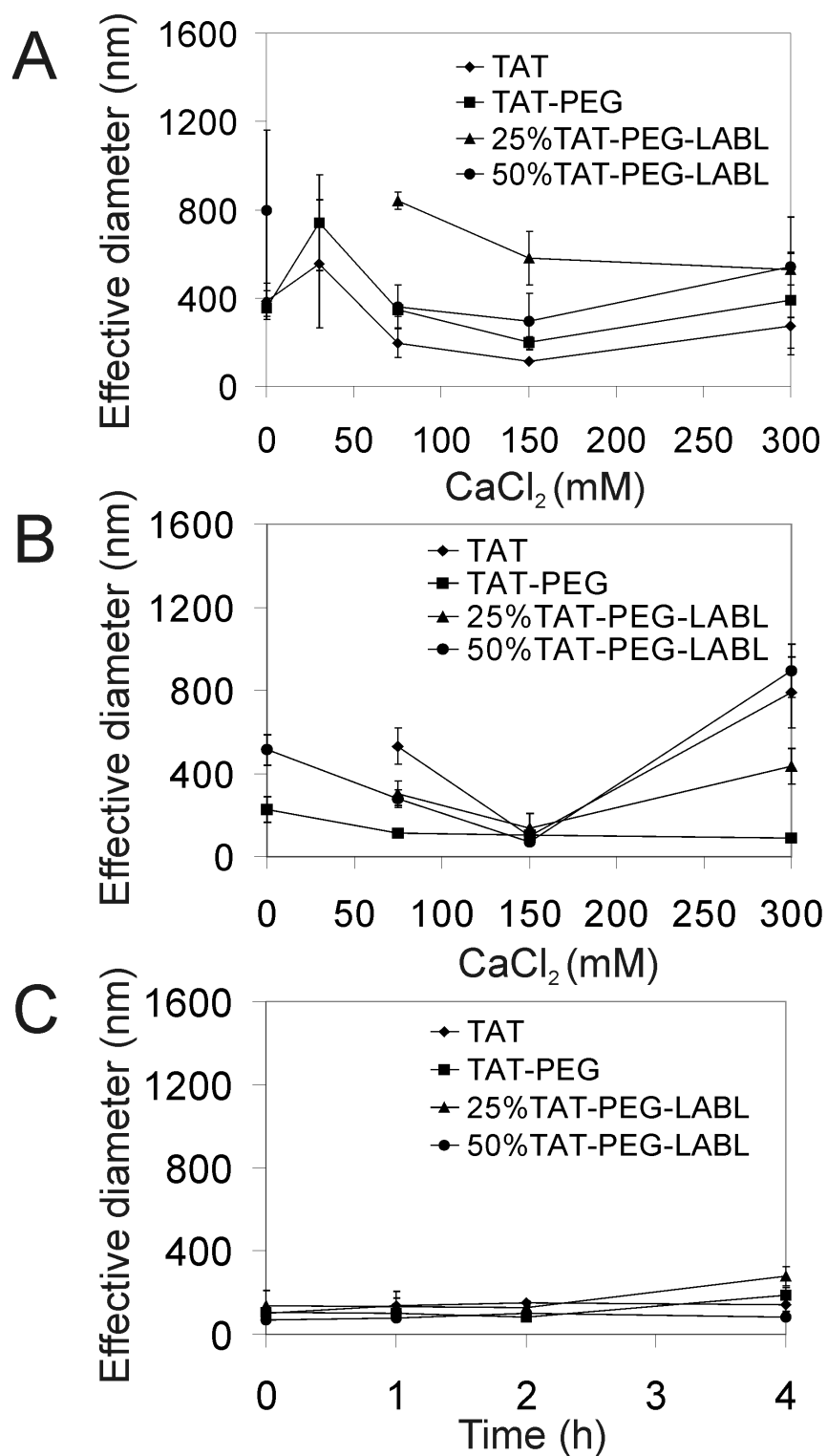


Figure 3.4. DLS was used to determine the size of TAT/DNA, TAT-PEG/DNA, 25% TAT-PEG-LABL/DNA, and 50% TAT-PEG-LABL/DNA complexes at an N/P ratio of 30 with different concentration of CaCl₂. (A) The hydrodynamic diameters of complexes were determined in deionized water and (B) in serum-free F12K media. (C) The hydrodynamic diameter of complexes (formed with 150 mM CaCl₂) in F12K media were stable over time. For missing data points, diameter was >1 μ m.

concentrations of CaCl_2 . Complexes were handled similarly to transfection studies. Generally, most complexes in media (Figure 3.4B) were substantially smaller than in deionized water (Figure 3.4A). At lower or higher CaCl_2 concentration (75 and 300 mM), particle size was initially larger than at CaCl_2 150 mM, but no precipitation was observed (Figure 3.4B). The hydrodynamic diameter was also monitored for complexes with 150 mM of added CaCl_2 for 4 h. Complexes were small and stable over time (Figure 3.4C).

The morphology of complexes was characterized using transmission electron microscopy (TEM). TAT, TAT-PEG, 25 % TAT-PEG-LABL, and 50 % TAT-PEG-LABL complexes were prepared as described earlier at an N/P ratio of 30. Formulations without CaCl_2 were compared to those including 75 mM CaCl_2 . TEM images indicated that most complexes had a globular shape and were substantially smaller than 300 nm (Figure 3.5), but images reflect the dry state. Agglomerates were occasionally visible in these samples and may account for the larger diameters observed by DLS or may be attributable to sample drying. This difference between the DLS data and TEM data could be due to small amount of flocculates observed from DLS experiments. The flocculates ($\sim 1 \mu\text{m}$, $<5\%$ of population) have greatly shifted the mean diameter, which is a major disadvantage of DLS.

Forming complexes with polycations can protect DNA from degradation and often effectively condenses DNA, but DNA release is also crucial for enhancing transfection efficiency.⁴⁸ Complex stability was evaluated by displacing DNA using heparin. TAT, TAT-PEG, 25 % TAT-PEG-LABL and 50 % TAT-PEG-LABL complexes were tested in this experiment. The complexes were formed at an N/P ratio of 30 using various concentrations of CaCl_2 and challenged with free heparin (Figure 3.6). TAT complexes yielded the most stable DNA complexes, whereas TAT-PEG

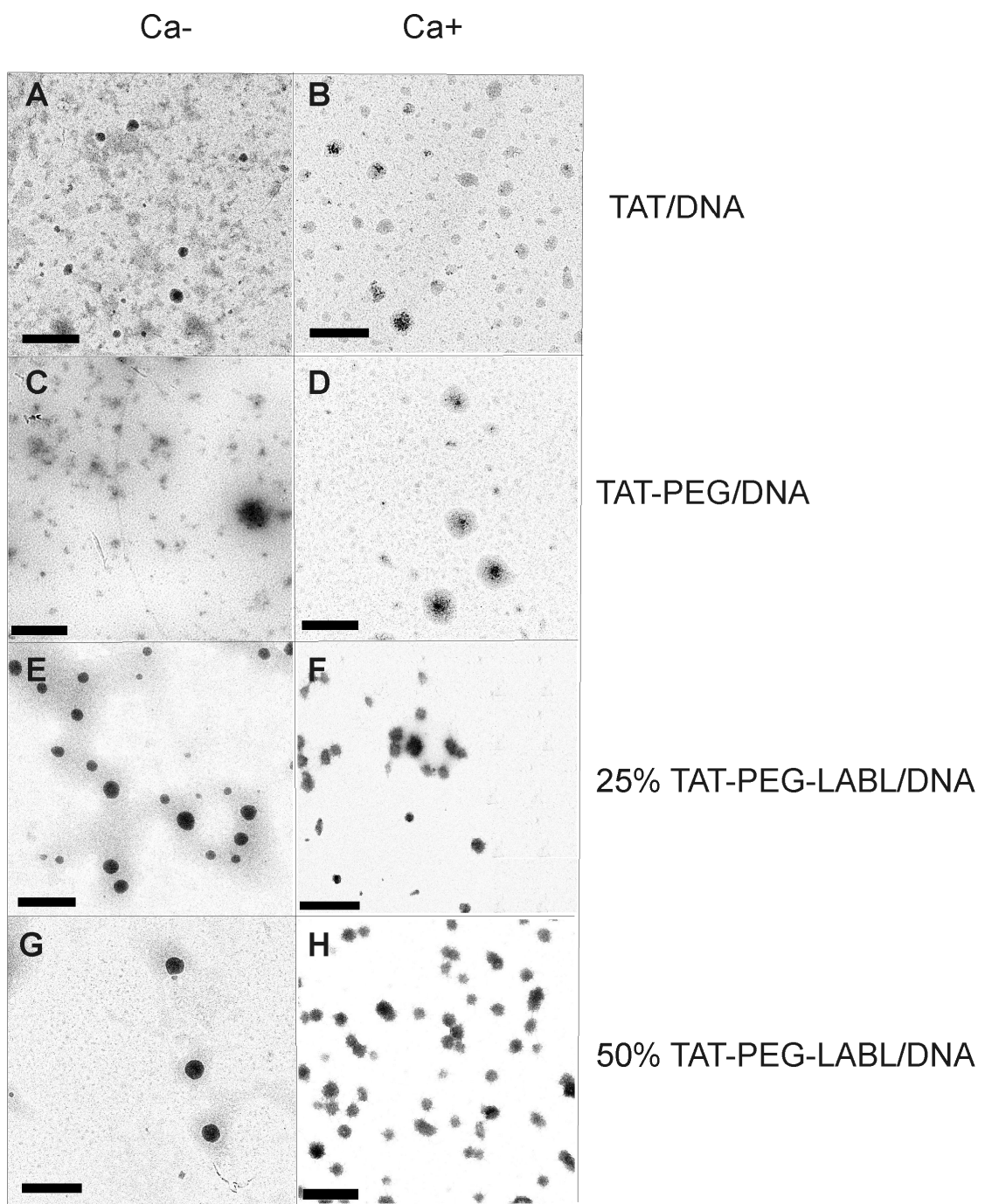


Figure 3.5. Transmission electron micrographs of (A) TAT/DNA, (B) TAT/DNA-Ca, (C) TAT-PEG/DNA, (D) TAT-PEG/DNA-Ca, (E) 25% TAT-PEG-LABL/DNA, (F) 25% TAT-PEG-LABL/DNA-Ca (G) 50% TAT-PEG-LABL/DNA, and (H) 50% TAT-PEG-LABL/DNA-Ca complexes. Complexes were formed at an N/P ratio of 30 without CaCl_2 (left panel) or with 75 mM of CaCl_2 (right panel). Scale bars are 500 nm.

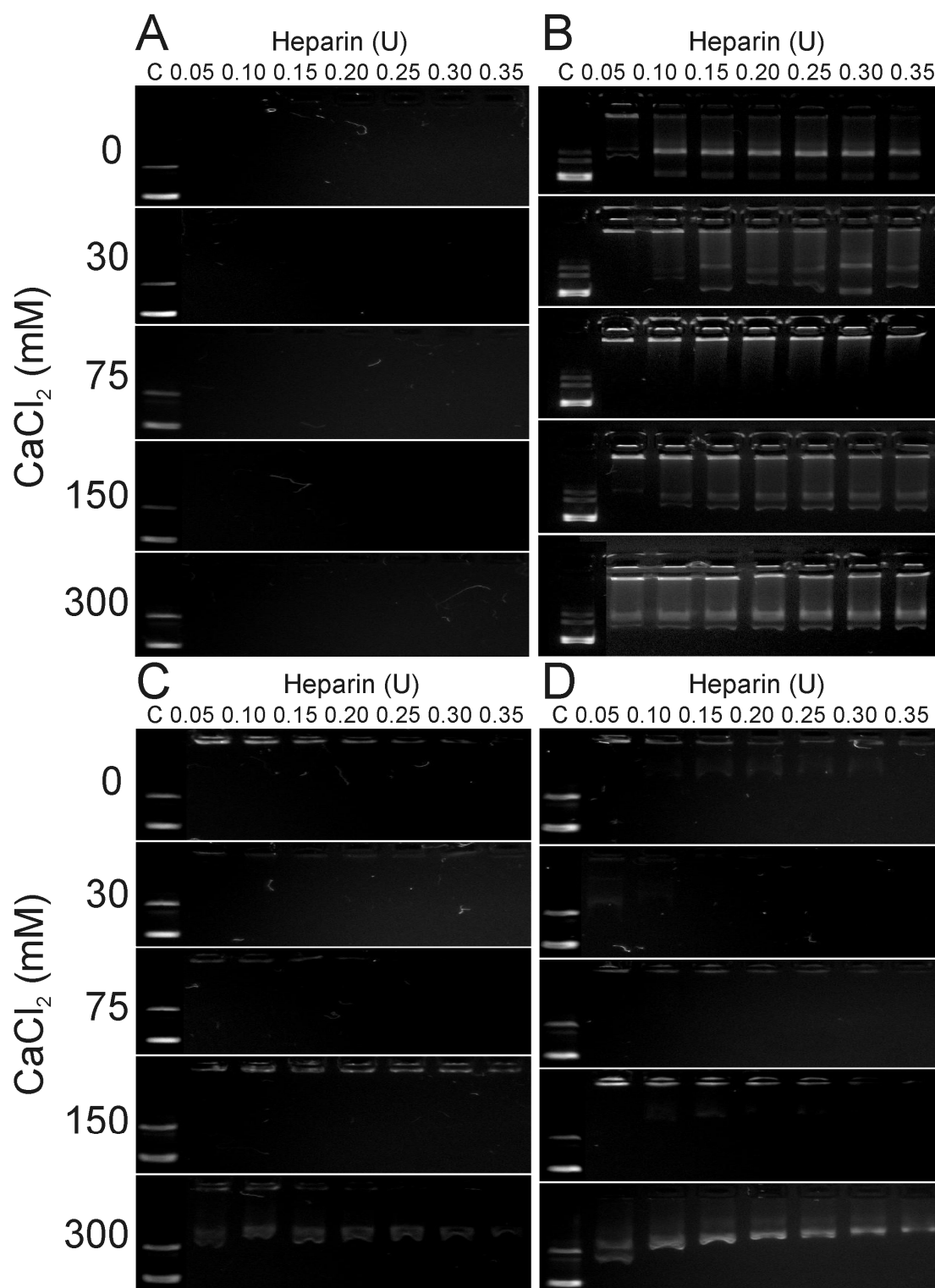


Figure 3.6. A heparin displacement assay for (A) TAT/DNA, (B) TAT-PEG/DNA, (C) 25% TAT-PEG-LABL/DNA, and (D) 50% TAT-PEG-LABL/DNA complexes was used to assess the effect of calcium chloride concentration (0, 30, 75, 150, 300 mM) on complex stability. Complexes were formed at an N/P of 30 and incubated for 30 min with increasing heparin concentrations (0.05-0.35 U). Free DNA is shown as a control (C) to the left.

complexes had the lowest stability. The 25 % TAT-PEG-LABL and 50 % TAT-PEG-LABL complexes showed intermediate stability between TAT and TAT-PEG complexes. At all CaCl_2 concentrations, TAT complexes were very stable and did not release DNA even at high heparin concentration (Figure 3.6A). TAT-PEG complexes were most stable at a CaCl_2 concentration of 75 mM; however, some DNA mobility was observed at most all CaCl_2 concentrations (Figure 3.6B). The stability of 25 % TAT-PEG-LABL and 50 % TAT-PEG-LABL complexes also depended on CaCl_2 concentration. Fifty percent TAT-PEG-LABL complexes started to release DNA at a CaCl_2 concentration of 150 mM and DNA was substantially displaced by heparin at a CaCl_2 concentration of 300 mM (Figure 3.6D).

3.3.3 Cytotoxicity, transfection efficiency, and intracellular accumulation of complexes

Toxicity is a major issue with many non-viral vectors and a correlation between high toxicity and improved transfection efficiency is often reported.⁴⁹ The cytotoxicity of TAT, TAT-PEG, and TAT-PEG-LABL in unactivated and activated A549 cells overexpressing ICAM-1 was evaluated and compared to PEI. After 24 hrs of incubation, TAT, TAT-PEG, and TAT-PEG-LABL revealed negligible cytotoxicity, whereas PEI showed extreme cytotoxicity with an IC_{50} value of ~ 50 and ~ 10 $\mu\text{g/mL}$ in normal and activated cells, respectively (Figure 3.7). At high concentration, TAT-PEG had slightly less cytotoxicity than TAT in unactivated cells (Figure 3.7A).

Transfection efficiency was determined in A549 cells. This cell line may be activated by proinflammatory cytokines to overexpress ICAM-1. In order to optimize transfection parameters such as CaCl_2 concentration and N/P ratios, transfection studies of TAT/DNA and TAT-PEG/DNA complexes were evaluated in unactivated

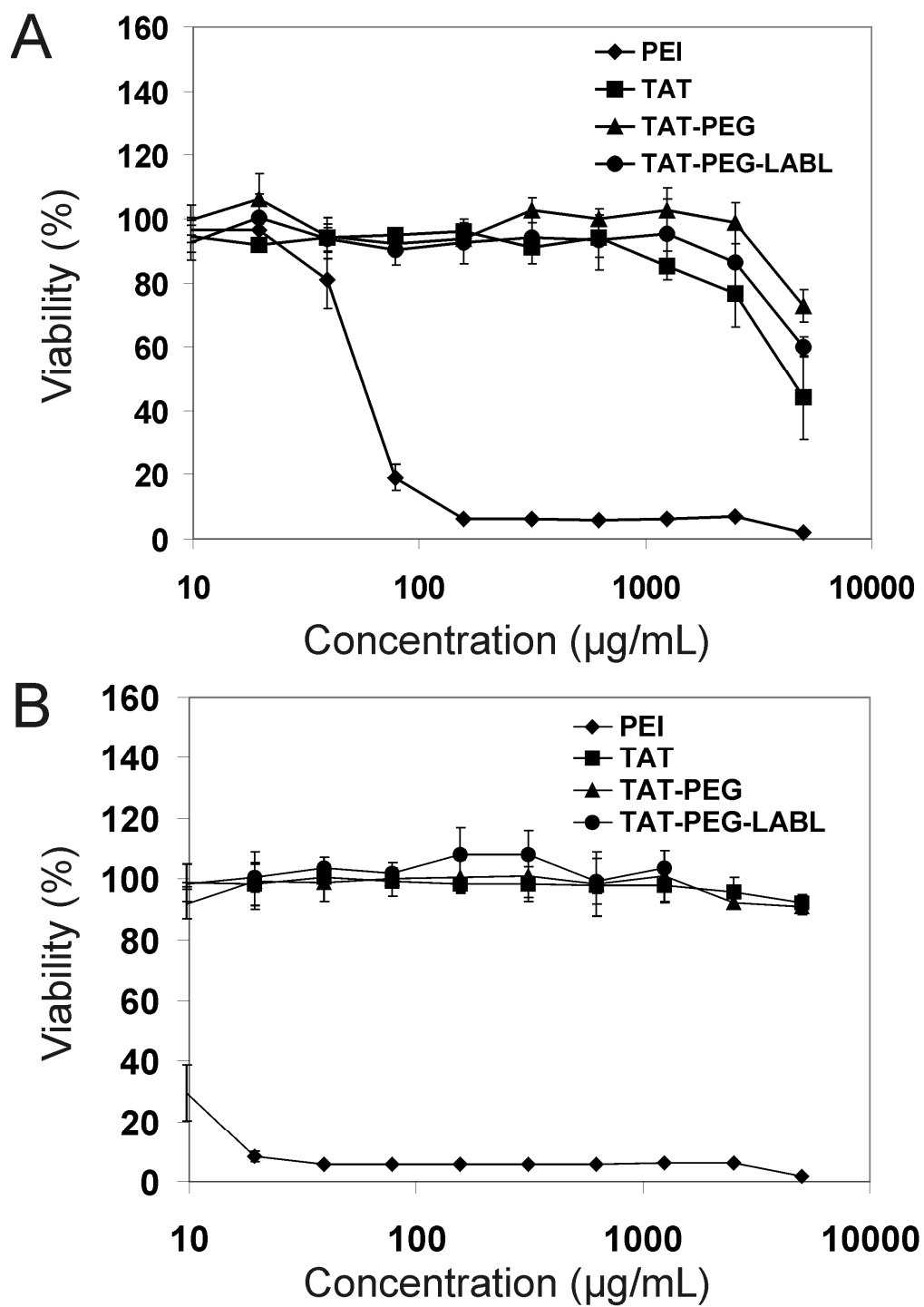


Figure 3.7. TAT peptide and derivatives showed low cytotoxicity in comparison to PEI (A) in unactivated and (B) in activated A549 cells, which overexpress ICAM-1.

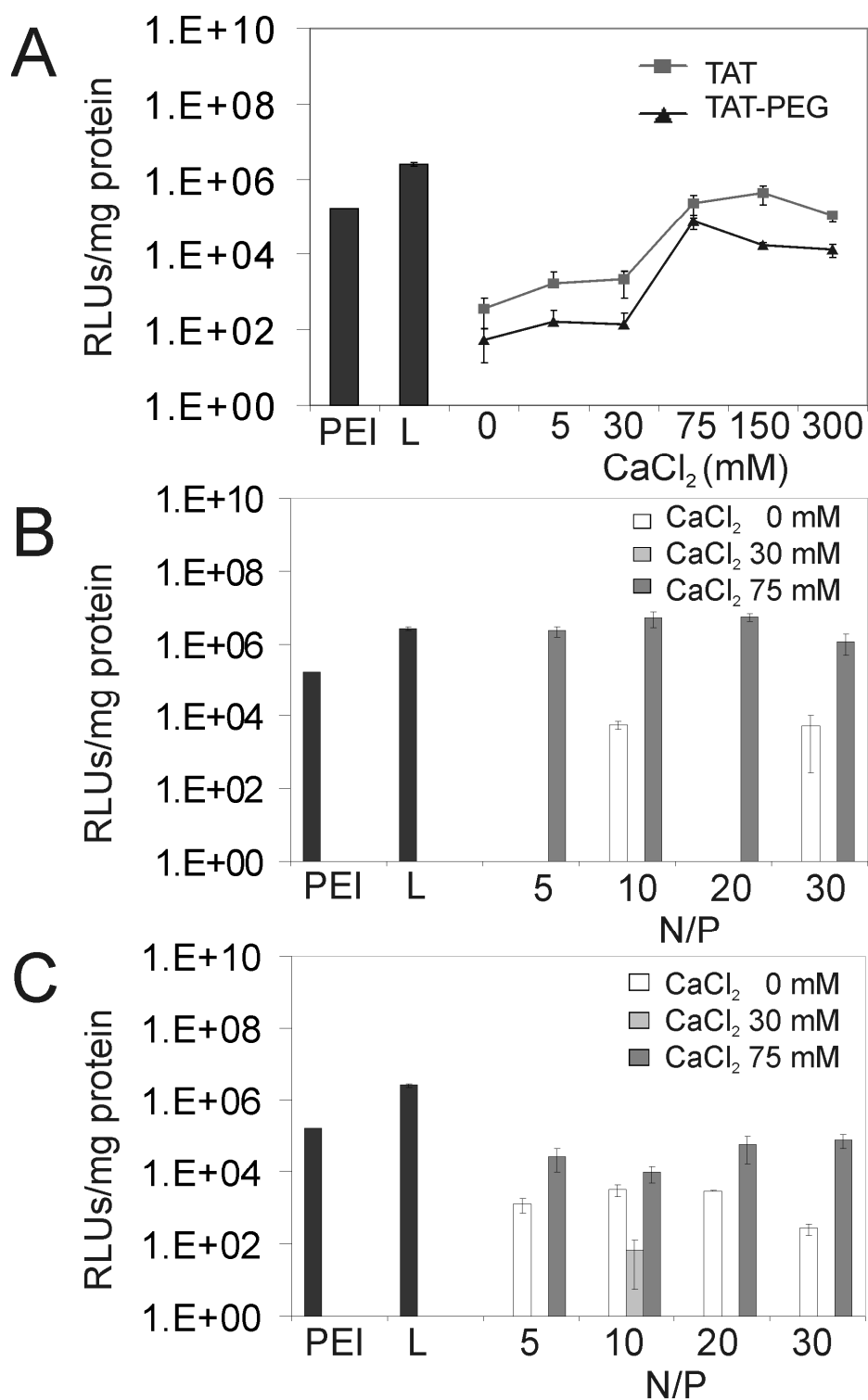


Figure 3.8. Transfection efficiencies of TAT peptide derivative/DNA complexes in A549 cells. (A) TAT/DNA and TAT-PEG/DNA complexes at an N/P ratio of 30 with different concentrations of calcium chloride (B) TAT/DNA complexes at different N/P ratios (C) TAT-PEG/DNA complexes at different N/P ratios. L= Lipofectamine.

A549 cells (Figure 3.8). Luciferase gene expression was measured 48 hrs post-transfection and compared to PEI and Lipofectamine 2000. Generally, TAT and TAT-PEG complexes showed relatively low transfection efficiencies in the absence of CaCl_2 and at low CaCl_2 concentrations (e.g. 5 and 30 mM). TAT complexes showed the highest transfection efficiency at 150 mM added CaCl_2 (Figure 3.8A). TAT-PEG complexes showed slightly lower and a similar trend of transfection efficiency compared to TAT complexes. The data suggested that CaCl_2 concentrations around 150 mM provided optimal transfection, perhaps due to the small complex size, DNA protection, and/or efficient DNA release.

Next, the transfection efficiencies of TAT and TAT-PEG complexes at different N/P ratios were examined at CaCl_2 concentrations of 0, 30, and 75 mM. Using 75 mM of added CaCl_2 , N/P ratios between 10 and 20 yielded high transfection levels for TAT complexes, exceeding the performance of PEI and Lipofectamine 2000 (Figure 3.8B). TAT-PEG complexes showed a somewhat similar trend, reaching the maximum transfection level at N/P \sim 30 and at the highest calcium concentration of 75 mM (Figure 3.8C). Transfection levels of TAT-PEG complexes were substantially lower than TAT complexes, as expected. The reduced transfection level of TAT-PEG was in agreement with complex stability data since TAT-PEG was less effective at packaging DNA (Figure 3.6B).

Relative ICAM-1 receptor expression levels in A549 cells after activation with $\text{TNF-}\alpha$ for 24 and 48 h was quantified using FITC-labeled monoclonal anti-human CD54 (anti-ICAM-1) and a FACscan flow cytometer. The fluorescence intensity representing the relative ICAM-1 expression level showed 22-fold and 41-fold increases in A549 cells after 24 and 48 h of activation compared to normal cells, respectively (Figure 3.9).

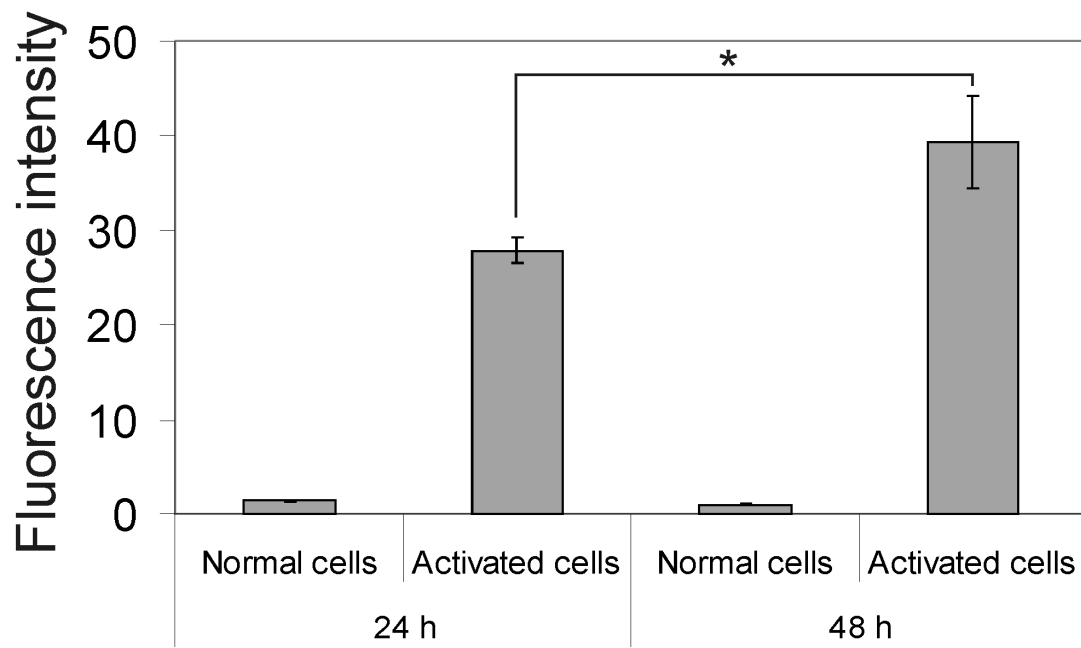


Figure 3.9. Relative ICAM-1 expression level in A549 cells after activation with TNF- α for 24 h and 48 h (* = $p < 0.05$, t -test).

Transfection efficiencies of TAT derivative complexes (e.g. TAT, TAT-PEG, 25 % and 50 % TAT-PEG-LABL + TAT-PEG) in A549 cells with upregulated ICAM-1 at different concentrations of calcium chloride were examined. Cells were activated with TNF- α for 48 h prior to transfection. Complexes were formed at an N/P ratio of 30 and luciferase gene expression was measured 48 hrs post-transfection. Overall, complexes formed with 150 mM of added CaCl₂ showed superior transfection efficiency compared to complexes formed with other CaCl₂ concentrations (Figure 3.10). Data were consistent with transfection data in normal cells, which showed maximum transfection levels at 75 and 150 mM CaCl₂ (Figure 3.8A). In both normal and activated cells, TAT complexes showed transfection efficiencies (150 mM CaCl₂) that were comparable to PEI and Lipofectamine 2000.

As anticipated, TAT-PEG complexes showed the lowest gene expression level; however, transfection efficiency was regained by including targeting ligands (TAT-PEG-LABL) in the formulations. Including twenty five percent TAT-PEG-LABL with TAT-PEG gave improved transfection efficiency compared to TAT-PEG, and 50% TAT-PEG-LABL complexes achieved the highest transfection level for targeted complexes (75 and 150 mM CaCl₂). The observed transfection efficiency was consistent with complex size. According to DLS data, complex sizes at 150 mM CaCl₂ were small (100-200 nm) and stable in the medium.

A blocking study was performed to determine the effect of ICAM-1 receptor blocking on transfection efficiency of targeted complexes. TAT/DNA and 50% TAT-PEG-LABL/DNA complexes were formed as described earlier at an N/P ratio of 30 using 150 mM CaCl₂. Activated cells were incubated with various concentrations of free LABL peptide or anti-ICAM-1 mAb prior to exposure to TAT complexes. The reduced transfection levels of targeted complexes (Figure 3.11) suggested that the

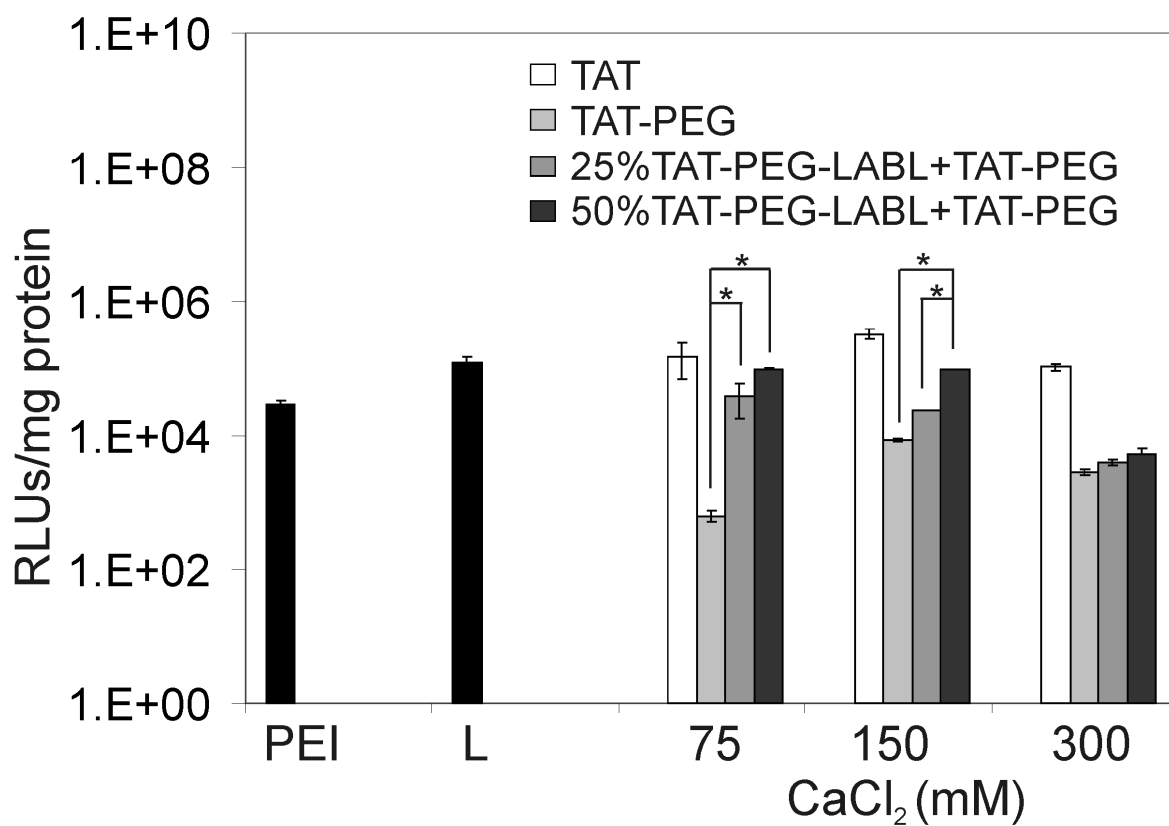


Figure 3.10. Transfection efficiencies of TAT peptide derivative/DNA complexes in activated A549 cells (overexpressing ICAM-1) at different concentrations of calcium chloride. Complexes were formed at an N/P ratio of 30. L= Lipofectamine (* = $p < 0.05$, one-way ANOVA, Tukey post test).

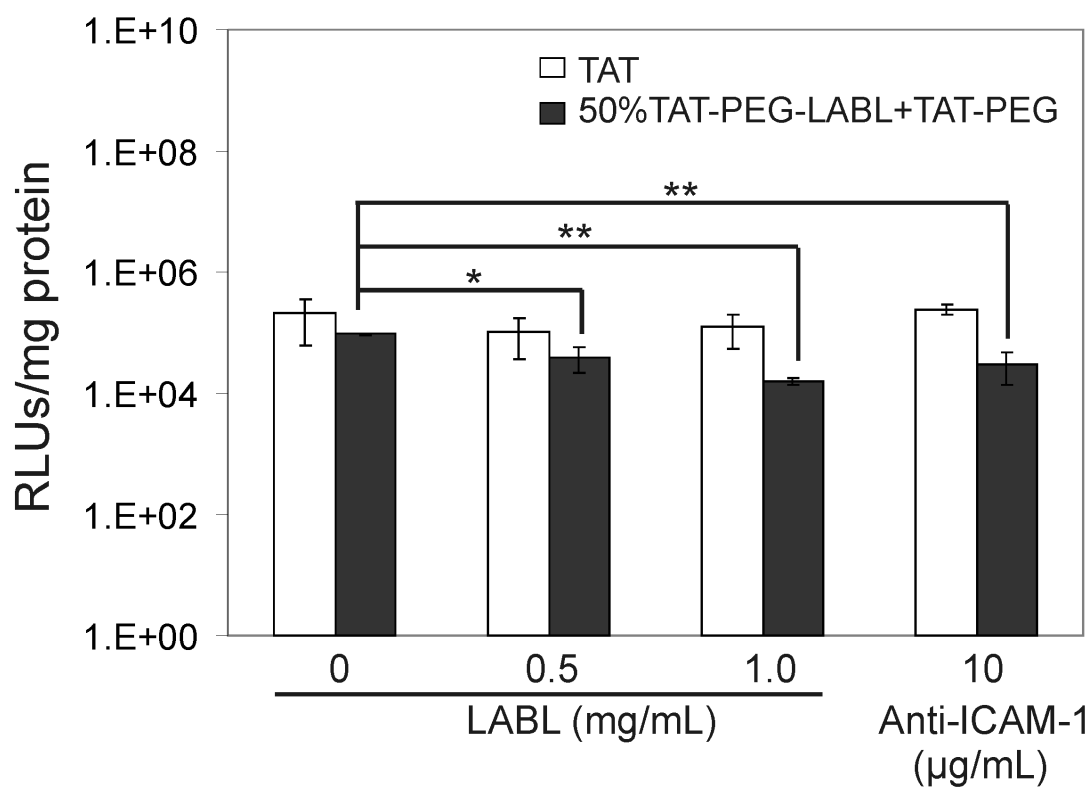


Figure 3.11. Transfection efficiencies of TAT/DNA and 50% TAT-PEG-LABL/DNA complexes in activated A549 cells (overexpressing ICAM-1) after incubation with free LABL peptide or anti-ICAM-1 mAb prior to exposure to TAT complexes. Complexes were formed at an N/P ratio of 30 and 150 mM CaCl₂. (* = p<0.05, ** = p<0.01, one-way ANOVA, Tukey post test).

binding of targeted complexes to ICAM-1 on activated A549 cells was hindered when free LABL peptide or anti-ICAM-1 mAb was added. Inhibition was dose dependent with higher LABL concentrations leading to lower transfection. It is worth noting that activated A549 cells exhibited substantially lower transfection when compared to normal cells. Transfection efficiencies of PEI and Lipofectamine 2000 in activated cells were significantly reduced compared to normal cells. Interestingly, 25% and 50% TAT-PEG-LABL complexes were able to maintain transfection levels in both normal and activated cells (Figure 3.12).

Targeted complexes were expected to enhance binding and internalization compared to untargeted complexes in activated ICAM-1 expressing cells. Untargeted (TAT-PEG) and targeted complexes (50 % TAT-PEG-LABL) were imaged by confocal microscopy. DNA was fluorescently labeled using TOTO-3. Both complexes were formed with labeled DNA under the same conditions (CaCl_2 150 mM, N/P = 30) and incubated with activated cells for 4 h. DNA in TAT-PEG complexes was difficult to detect in culture. Conversely, DNA from 50 % TAT-PEG-LABL complexes were observed in the vast majority of the cells and overlaid both the cell bodies and nuclei (Figure 3.13).

3.4 Discussion

Despite its low molecular weight, TAT was confirmed as a powerful transfection agent when condensed with an optimal concentration of CaCl_2 . Targeting ligands are expected to improve the performance of these types of vectors when translated to *in vivo* studies. Therefore, TAT was modified with PEG and the peptide LABL, a well-characterized ligand for ICAM-1. TAT, TAT-PEG, and TAT-PEG-LABL block peptides were carefully synthesized and the structure validated. In general, all forms of TAT showed minimal cytotoxicity. TAT-PEG had less

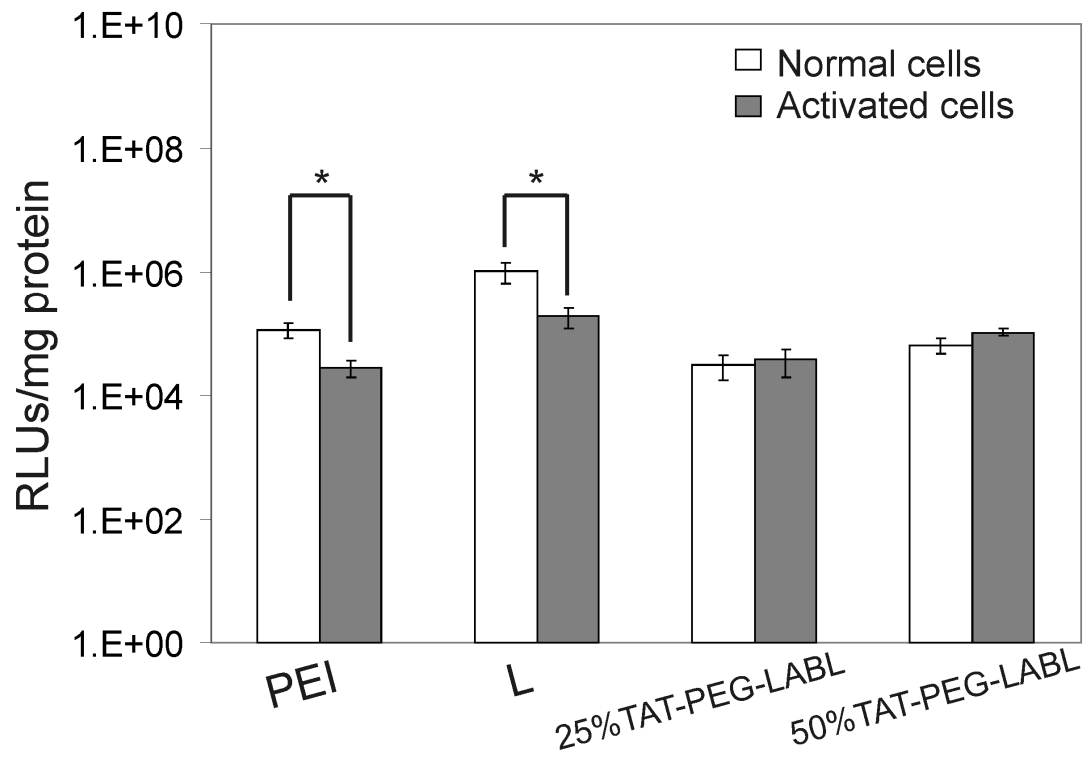


Figure 3.12. Transfection efficiencies of 25% and 50% TAT-PEG-LABL/DNA complexes in normal and activated A549 cells. Complexes were formed at an N/P ratio of 30 and 150 mM CaCl₂. (* = p<0.05, *t*-test)

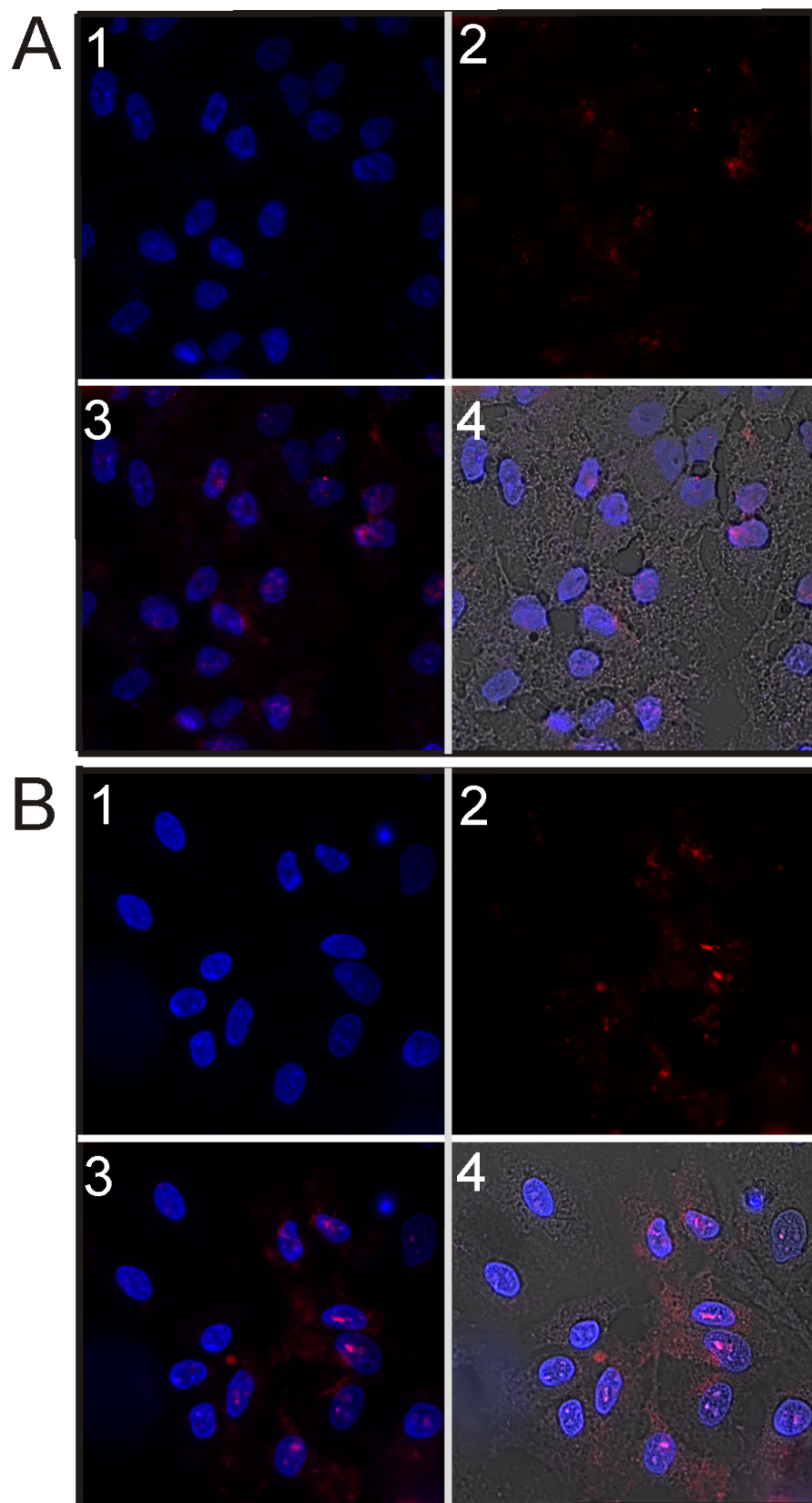


Figure 3.13. Micrographs of (A) TAT-PEG/DNA complexes and (B) 50% TAT-PEG-LABL/DNA complexes in A549 cells (activated with TNF- α) after 4 h of incubation at 37 °C. Complexes were formed at an N/P ratio of 30 and a CaCl₂ of 150 mM. (1 = DAPI fluorescence (cell nuclei), 2 = TOTO-3 fluorescence (DNA), 3 = Merged DAPI and TOTO-3 fluorescence, 4 = Merged DAPI, TOTO-3 fluorescence, and bright field transmission.)

cytotoxicity than TAT in unactivated A549 cells. Earlier reports suggest PEGylation often reduces cytotoxicity of cationic polymers.⁵⁰⁻⁵¹ The CaCl₂ concentration range used in this study was relatively safe. The IC₅₀ value of CaCl₂ was ~210 mM for A549 cells.¹⁵ Final concentrations of CaCl₂ used with cells in transfection studies ranged from 1-60 mM (corresponding to the reported starting concentrations of 5-300 mM) which were far below this IC₅₀ value.

TAT and TAT-PEG were able to immobilize DNA starting from N/P ratios 1 and 2, respectively. The data were consistent with previous reports that indicated TAT can immobilize DNA at an N/P ratio as low as ~2.^{15,25} The data also suggested that PEGylation and incorporation of targeting ligand did not interfere with DNA complexation.

Size and morphology of block peptide/DNA complexes were then characterized. Complex stability was also examined using heparin displacement. The data suggested that CaCl₂ played a critical role on complex size and DNA release. At optimal CaCl₂ concentration (150 mM CaCl₂), complexes were small and stable in the medium. It is probable that calcium bridges between DNA phosphate groups and/or TAT amine groups helped condense complexes into compact particles.¹⁵ Ionic strength is known to affect the size of nanoparticle formulations, especially for charged particles. It was reported that adding calcium and magnesium (>30 mM) reduced aggregation and yielded more monodisperse plasmid-lipid nanoparticles.⁵²

In addition to controlling particle size, calcium concentration also affected DNA release. For example, 50% TAT-PEG-LABL complexes started to release DNA at a CaCl₂ concentration of 150 mM and DNA was substantially displaced by heparin at a CaCl₂ concentration of 300 mM (Figure 3.6D). A previous study suggested that TAT complexes may be “loosened” at high calcium concentration as evidenced by

fluorescent DNA probes.¹⁵ Ionic strength may also contribute to the observed destabilization. It has been reported that, at low salt concentration (≤ 50 mM NaCl), polymer-DNA binding is not strongly dependent on ionic strength. High salt concentration, however, can alter polymer-DNA binding and may cause dissociation of complexes due to electrostatic shielding.⁵³ The stability of polycation/ DNA complexes has been identified as a rate limiting step for intracellular release of DNA, which can impair transfection efficiency. Previous reports showed 'weak' chitosan polyplexes offered a faster onset of transfection and higher gene expression both *in vitro* and *in vivo*.⁵⁴ Therefore, a fine balance between complex stability and DNA release is essential for efficient transfection. Tuning calcium concentration provides a simple formulation approach for optimizing TAT complex size and DNA release.

Transfection efficiencies of TAT and TAT-PEG in A549 cells were enhanced by optimizing calcium concentration. The data suggested that small complex size, optimal complex stability and DNA release may contribute to the improved gene expression. Calcium has been shown to enhance transfection efficiency for lipid gene delivery systems.^{52,55-57} The detailed mechanism of calcium enhancement for these systems has not been clear and several mechanisms have been proposed.^{52,56-57} It was suggested that calcium may increase membrane association or cellular uptake of complexes or particles. More importantly, calcium may act as a lysosomotropic agent and destabilize endosomal and/or lysosomal membranes thus increasing endo-lysosomal release. Interestingly, Fujita and others reported that calcium did not improve the performance of arginine-PEG-lipid-coated DNA/ protamine complexes.⁵⁵ Generally, substantially higher calcium concentrations were used to condense and control DNA release from modified TAT complexes reported here.

Several groups have used TAT peptides at high N/P ratios possibly because TAT peptides have also been shown to lose membrane translocation ability upon binding to DNA.^{25,58} It was reported that excess free TAT peptides enhanced transfection efficiency of TAT/DNA complexes by preventing complex disruption by proteoglycans.⁵⁹ Interestingly, it was also previously reported that large amounts of free PEI remained in PEI/DNA mixtures. The presence of free PEI was suggested to improve membrane permeability, thus enhancing DNA release into the cytoplasm.⁶⁰

Adding the PEG block served as a hydrophilic arm for attaching targeting ligands with the goal of recovering transfection efficiency and adding specificity. LABL, a peptide ligand for ICAM-1 was linked to TAT-PEG using solid phase synthesis. The resulting TAT-PEG-LABL was confirmed using mass spectrometry (Fig. 3.2), and used in studies with activated A549 cells, which overexpress ICAM-1. TAT-PEG-LABL and TAT-PEG were mixed at different ratios resulting in a different percentage of targeting ligands when forming complexes with DNA. This targeted gene delivery system was then explored their ability to transfect A549 cells overexpressing ICAM-1. PEGylation significantly reduced transfection efficiency when compared to unmodified TAT as expected. The low transfection observed for TAT-PEG complexes was consistent with poor complex stability and with previous reports that indicated PEG-based polymers or liposomes had reduced transfection levels, possibly due to steric hindrance.^{18,53} Transfection efficiency was recovered by incorporating the LABL targeting ligand.

Complexes containing 50% TAT-PEG-LABL 75 and 150 mM showed high transfection levels when 75 and 150 mM CaCl_2 was added. The relatively low transfection efficiencies of 25% and 50% TAT-PEG-LABL complexes at 300 mM CaCl_2 may be due to their large sizes (430 and ~900 nm, respectively) in the medium

and inadequate ability to protect DNA as suggested by heparin displacement data. It was previously reported that particles smaller than ~200 nm were internalized mainly by endocytosis, whereas particles larger than ~200 nm were taken up primarily by phagocytosis.⁶¹ It was also reported that when phagocytosis occurs, transfection efficiency can be reduced.¹⁶ The blocking data strongly supported a specific, ICAM-1 receptor mediated interaction.

PEI and Lipofectamine 2000 showed significantly reduced transfection levels in activated cells compared to normal cells. Exposure to TNF- α , a pro-inflammatory cytokine, can alter cellular functions. Previous reports showed that TNF- α decreased cell viability in primary and immortalized cell lines.⁶²⁻⁶³ Some studies have also shown that, under inflammatory conditions, cells often have decreased endocytic activity and different endocytic pathways may be favored.⁶⁴ This is important evidence that certain cell types may be more difficult to transfect due to abnormal cellular functions under pathological conditions.

3.5 Conclusions

The observed transfection efficiency of targeted complexes resulted from a combination of optimal complex size, complex stability, DNA release, and the presence of targeting ligands. These characteristics are well known to effect internalization and DNA release, and the resulting transfection efficiency. The performance of targeted TAT-PEG-LABL suggested that these complexes may be a promising vector for targeted gene transfection to sites of inflammation *in vivo*. Although accurate targeting of TAT-PEG-LABL complexes was demonstrated here, it may be necessary to investigate other epithelial, endothelial, or inflammatory cell lines.

3.6 Bibliography

1. Russ V, Wagner E 2007. Cell and tissue targeting of nucleic acids for cancer gene therapy. *Pharmaceutical research* 24(6):1047-1057.
2. Li SD, Huang L 2006. Gene therapy progress and prospects: non-viral gene therapy by systemic delivery. *Gene therapy* 13(18):1313-1319.
3. Kirschberg TA, VanDeusen CL, Rothbard JB, Yang M, Wender PA 2003. Arginine-based molecular transporters: the synthesis and chemical evaluation of releasable taxol-transporter conjugates. *Org Lett* 5(19):3459-3462.
4. Rothbard JB, Garlington S, Lin Q, Kirschberg T, Kreider E, McGrane PL, Wender PA, Khavari PA 2000. Conjugation of arginine oligomers to cyclosporin A facilitates topical delivery and inhibition of inflammation. *Nature Medicine* 6(11):1253-1257.
5. Bhorade R, Weissleder R, Nakakoshi T, Moore A, Tung CH 2000. Macrocyclic chelators with paramagnetic cations are internalized into mammalian cells via a HIV-tat derived membrane translocation peptide. *Bioconjugate Chem* 11(3):301-305.
6. Kersemans V, Kersemans K, Cornelissen B 2008. Cell penetrating peptides for in vivo molecular imaging applications. *Current pharmaceutical design* 14(24):2415-2427.
7. Corradin S, Ransijn A, Corradin G, Bouvier J, Delgado MB, Fernandez-Carneado J, Mottram JC, Vergères G, Mauël J 2002. Novel peptide inhibitors of Leishmania gp63 based on the cleavage site of MARCKS (myristoylated alanine-rich C kinase substrate)-related protein. *Biochemical Journal* 367(Pt 3):761.
8. Datta K, Sundberg C, Karumanchi SA, Mukhopadhyay D 2001. The 104-123 Amino Acid Sequence of the β -domain of von Hippel-Lindau Gene Product Is Sufficient to Inhibit Renal Tumor Growth and Invasion. *Cancer research* 61(5):1768.
9. Fawell S, Seery J, Daikh Y, Moore C, Chen LL, Pepinsky B, Barsoum J 1994. Tat-mediated delivery of heterologous proteins into cells. *Proceedings of the National Academy of Sciences* 91(2):664.
10. Wadia J, Dowdy S 2005. Transmembrane delivery of protein and peptide drugs by TAT-mediated transduction in the treatment of cancer. *Advanced drug delivery reviews* 57(4):579-596.
11. Eguchi A, Akuta T, Okuyama H, Senda T, Yokoi H, Inokuchi H, Fujita S, Hayakawa T, Takeda K, Hasegawa M 2001. Protein transduction domain of HIV-1 Tat protein promotes efficient delivery of DNA into mammalian cells. *Journal of Biological Chemistry* 276(28):26204.
12. Snyder EL, Dowdy SF 2001. Protein/peptide transduction domains: potential to deliver large DNA molecules into cells. *Current opinion in molecular therapeutics* 3(2):147.
13. Jesus M, Berry CC 2005. Tat peptide as an efficient molecule to translocate gold nanoparticles into the cell nucleus. *Bioconjugate Chem* 16(5):1176-1180.
14. Sethuraman VA, Bae YH 2007. TAT peptide-based micelle system for potential active targeting of anti-cancer agents to acidic solid tumors. *Journal of Controlled Release* 118(2):216-224.
15. Baoum A, Xie S, Fakhari A, Berkland C 2009. "Soft" Calcium Crosslinks Enable Highly Efficient Gene Transfection Using TAT Peptide. *Pharmaceutical research* 26(12):2619-2629.

16. Pedraza CE, Bassett DC, McKee MD, Nelea V, Gbureck U, Barralet JE 2008. The importance of particle size and DNA condensation salt for calcium phosphate nanoparticle transfection. *Biomaterials* 29(23):3384.
17. Josephson L, Tung C, Moore A, Weissleder R 1999. High-efficiency intracellular magnetic labeling with novel superparamagnetic-Tat peptide conjugates. *Bioconjugate Chem* 10(2):186-191.
18. Kale A, Torchilin V 2007. Enhanced transfection of tumor cells in vivo using "Smart" pH-sensitive TAT-modified pegylated liposomes. *Journal of drug targeting* 15(7):538-545.
19. MacKay J, Li W, Huang Z, Dy E, Huynh G, Tihan T, Collins R, Deen D, Szoka Jr F 2008. HIV TAT peptide modifies the distribution of DNA nanolipoparticles following convection-enhanced delivery. *Molecular therapy* 16(5):893-900.
20. Moschos S, Williams A, Lindsay M 2007. Cell-penetrating-peptide-mediated siRNA lung delivery. *Biochemical Society Transactions* 35:807-810.
21. Pappalardo J, Quattrocchi V, Langellotti C, Di Giacomo S, Gnazzo V, Olivera V, Calamante G, Zamorano P, Levchenko T, Torchilin V 2009. Improved transfection of spleen-derived antigen-presenting cells in culture using TATp-liposomes. *Journal of Controlled Release* 134(1):41-46.
22. Suk J, Suh J, Choy K, Lai S, Fu J, Hanes J 2006. Gene delivery to differentiated neurotypic cells with RGD and HIV Tat peptide functionalized polymeric nanoparticles. *Biomaterials* 27(29):5143-5150.
23. Manickam S 2005. Influence of TAT-peptide polymerization on properties and transfection activity of TAT/DNA polyplexes. *Journal of Controlled Release* 102(1):293-306.
24. Reschel T 2002. Physical properties and in vitro transfection efficiency of gene delivery vectors based on complexes of DNA with synthetic polycations. *Journal of Controlled Release* 81(1-2):201-217.
25. Rudolph C, Plank C, Lausier J, Schillinger U, M ller R, Rosenecker J 2003. Oligomers of the arginine-rich motif of the HIV-1 TAT protein are capable of transferring plasmid DNA into cells. *Journal of Biological Chemistry* 278(13):11411.
26. Rudolph C, Schillinger U, Ortiz A, Tabatt K, Plank C, M ller R, Rosenecker J 2004. Application of novel solid lipid nanoparticle (SLN)-gene vector formulations based on a dimeric HIV-1 TAT-peptide in vitro and in vivo. *Pharmaceutical research* 21(9):1662-1669.
27. Hersmann GHW, Kriegsmann J, Simon J, Hüttich C, Bräuer R 1998. Expression of cell adhesion molecules and cytokines in murine antigen-induced arthritis. *Cell Communication and Adhesion* 6(1):69-82.
28. Swerlick RA, Garcia-Gonzalez E, Kubota Y, Xu Y, Lawley TJ 1991. Studies of the Modulation of MHC Antigen and Cell Adhesion Molecule Expression on Human Dermal Microvascular Endotheliam Cells. *Journal of Investigative Dermatology* 97(2):190-196.
29. Zecchinon L, Fett T, Vanden Bergh P, Desmecht D 2006. Bind another day: The LFA-1/ICAM-1 interaction as therapeutic target. *Clinical and Applied Immunology Reviews* 6(3-4):173-189.
30. Bevilacqua MDPDMP, Nelson PDRM, Mannori MDPDG, Cecconi MO 1994. Endothelial-leukocyte adhesion molecules in human disease. *Annual review of medicine* 45(1):361-378.
31. Melis M, Spatafora M, Melodia A, Pace E, Gjomarkaj M, Merendino AM, Bonsignore G 1996. ICAM-1 expression by lung cancer cell lines: effects of

upregulation by cytokines on the interaction with LAK cells. *European Respiratory Journal* 9(9):1831.

32. Chittasupho C, Xie SX, Baoum A, Yakovleva T, Siahaan TJ, Berkland CJ 2009. ICAM-1 targeting of doxorubicin-loaded PLGA nanoparticles to lung epithelial cells. *European journal of pharmaceutical sciences* 37(2):141-150.

33. Yacyshyn BR, Chey WY, Goff J, Salzberg B, Baerg R, Buchman AL, Tami J, Yu R, Gibiansky E, Shanahan WR 2002. Double blind, placebo controlled trial of the remission inducing and steroid sparing properties of an ICAM-1 antisense oligodeoxynucleotide, alicaforsen (ISIS 2302), in active steroid dependent Crohn's disease. *Gut* 51(1):30.

34. Weller GER, Villanueva FS, Tom EM, Wagner WR 2005. Targeted ultrasound contrast agents: in vitro assessment of endothelial dysfunction and multi-targeting to ICAM-1 and sialyl Lewisx. *Biotechnology and Bioengineering* 92(6):780-788.

35. Demos SM, Alkan-Onyuksel H, Kane BJ, Ramani K, Nagaraj A, Greene R, Klegerman M, McPherson DD 1999. In vivo targeting of acoustically reflective liposomes for intravascular and transvascular ultrasonic enhancement* 1. *Journal of the American College of Cardiology* 33(3):867-875.

36. Muro S, Cui X, Gajewski C, Murciano JC, Muzykantov VR, Koval M 2003. Slow intracellular trafficking of catalase nanoparticles targeted to ICAM-1 protects endothelial cells from oxidative stress. *American Journal of Physiology- Cell Physiology* 285(5):C1339.

37. Murciano JC, Muro S, Koniaris L, Christofidou-Solomidou M, Harshaw DW, Albelda SM, Granger DN, Cines DB, Muzykantov VR 2003. ICAM-directed vascular immunotargeting of antithrombotic agents to the endothelial luminal surface. *Blood* 101(10):3977.

38. Scherpereel A, Wiewrodt R, Christofidou-Solomidou M, Gervais R, Murciano JC, Albelda SM, Muzykantov VR 2001. Cell-selective intracellular delivery of a foreign enzyme to endothelium in vivo using vascular immunotargeting. *The FASEB Journal* 15(2):416.

39. Yusuf-Makagiansar H, Yakovleva TV, Tejo BA, Jones K, Hu Y, Verkhivker GM, Audus KL, Siahaan TJ 2007. Sequence Recognition of -LFA-1-derived Peptides by ICAM-1 Cell Receptors: Inhibitors of T-cell Adhesion. *Chemical Biology & Drug Design* 70(3):237-246.

40. Anderson ME, Siahaan TJ 2003. Targeting ICAM-1/LFA-1 interaction for controlling autoimmune diseases: designing peptide and small molecule inhibitors. *Peptides* 24(3):487.

41. Zhao H, Kiptoo P, Williams T, Siahaan T, Topp E 2009. Immune response to controlled release of immunomodulating peptides in a murine experimental autoimmune encephalomyelitis (EAE) model. *Journal of Controlled Release*.

42. Yonekawa K, Harlan J 2005. Targeting leukocyte integrins in human diseases. *Journal of leukocyte biology* 77(2):129.

43. Yusuf-Makagiansar H, Siahaan T 2001. Binding and internalization of an LFA-1-derived cyclic peptide by ICAM receptors on activated lymphocyte: a potential ligand for drug targeting to ICAM-1-expressing cells. *Pharmaceutical research* 18(3):329-335.

44. Konno S, Grindle K, Lee W, Schroth M, Mosser A, Brockman-Schneider R, Busse W, Gern J 2002. Interferon-gamma enhances rhinovirus-induced RANTES secretion by airway epithelial cells. *American journal of respiratory cell and molecular biology* 26(5):594.

45. Fakhari A, Baoum A, Siahaan TJ, Le KB, Berkland C 2010. Controlling Ligand Surface Density Optimizes Nanoparticle Binding to ICAM-1. *Journal of pharmaceutical sciences* 100(3):1045-1056.
46. Mansouri S, Lavigne P, Corsi K, Benderdour M, Beaumont E, Fernandes J 2004. Chitosan-DNA nanoparticles as non-viral vectors in gene therapy: strategies to improve transfection efficacy. *European journal of pharmaceutics and biopharmaceutics* 57(1):1-8.
47. Veronese F, Pasut G 2005. PEGylation, successful approach to drug delivery. *Drug Discovery Today* 10(21):1451-1458.
48. Won Y, Sharma R, Konieczny S 2009. Missing pieces in understanding the intracellular trafficking of polycation/DNA complexes. *J Control Release* 139:88–93.
49. Godbey W, Wu K, Mikos A 2001. Poly (ethylenimine)-mediated gene delivery affects endothelial cell function and viability. *Biomaterials* 22(5):471-480.
50. Beyerle A, Merkel O, Stoeger T, Kissel T 2010. PEGylation affects cytotoxicity and cell-compatibility of poly (ethylene imine) for lung application: Structure-function relationships. *Toxicology and applied pharmacology* 242(2):146-154.
51. Zhang X, Pan S, Hu H, Wu G, Feng M, Zhang W, Luo X 2007. Poly (ethylene glycol)-block-polyethylenimine copolymers as carriers for gene delivery: Effects of PEG molecular weight and PEGylation degree. *Journal of Biomedical Materials Research Part A* 84(3):795-804.
52. Palmer L, Chen T, Lam A, Fenske D, Wong K, MacLachlan I, Cullis P 2003. Transfection properties of stabilized plasmid-lipid particles containing cationic PEG lipids. *Biochimica et Biophysica Acta (BBA)-Biomembranes* 1611(1-2):204-216.
53. Rungsardthong U, Deshpande M, Bailey L, Vamvakaki M, Armes SP, Garnett MC, Stolnik S 2001. Copolymers of amine methacrylate with poly (ethylene glycol) as vectors for gene therapy. *Journal of Controlled Release* 73(2-3):359-380.
54. Köping-Höggård M, Vårum KM, Issa M, Danielsen S, Christensen BE, Stokke BT, Artursson P 2004. Improved chitosan-mediated gene delivery based on easily dissociated chitosan polyplexes of highly defined chitosan oligomers. *Gene therapy* 11(19):1441-1452.
55. Fujita T, Furuhashi M, Hattori Y, Kawakami H, Toma K, Maitani Y 2009. Calcium enhanced delivery of tetraarginine-PEG-lipid-coated DNA/protamine complexes. *International Journal of Pharmaceutics* 368(1-2):186-192.
56. Sandhu A, Lam A, Fenske D, Palmer L, Johnston M, Cullis P 2005. Calcium enhances the transfection potency of stabilized plasmid-lipid particles. *Analytical biochemistry* 341(1):156-164.
57. Shiraishi T, Pankratova S, Nielsen P 2005. Calcium ions effectively enhance the effect of antisense peptide nucleic acids conjugated to cationic tat and oligoarginine peptides. *Chemistry & biology* 12(8):923-929.
58. Liu Z, Li M, Cui D, Fei J 2005. Macro-branched cell-penetrating peptide design for gene delivery. *Journal of Controlled Release* 102(3):699-710.
59. Ignatovich I, Dizhe E, Pavlotskaya A, Akifiev B, Burov S, Orlov S, Perevozchikov A 2003. Complexes of plasmid DNA with basic domain 47-57 of the HIV-1 Tat protein are transferred to mammalian cells by endocytosis-mediated pathways. *Journal of Biological Chemistry* 278(43):42625.
60. Moghimi S, Symonds P, Murray J, Hunter A, Debska G, Szewczyk A 2005. A two-stage poly (ethylenimine)-mediated cytotoxicity: implications for gene transfer/therapy. *Molecular therapy* 11(6):990-995.

61. Xiang SD, Scholzen A, Minigo G, David C, Apostolopoulos V, Mottram PL, Plebanski M 2006. Pathogen recognition and development of particulate vaccines: does size matter? *Methods* 40(1):1-9.
62. Beg A, Baltimore D 1996. An essential role for NF-kappa B in preventing TNF-alpha-induced cell death. *Science* 274(5288):782.
63. Li L, Thomas R, Suzuki H, De Brabander J, Wang X, Harran P 2004. A small molecule Smac mimic potentiates TRAIL-and TNF {alpha}-mediated cell death. *Science* 305(5689):1471.
64. Foerg C, Merkle HP 2007. On the biomedical promise of cell penetrating peptides: limits versus prospects. *Journal of pharmaceutical sciences* 97(1):144-162.

Chapter 4

**Non-covalent PEGylation by polyanion complexation as a
novel means to stabilize Keratinocyte Growth Factor-2
(KGF-2)**

4.1 Introduction

Therapeutic proteins such as antibodies, cytokines, growth factors and enzymes are increasingly important in the treatment of difficult to treat diseases such as viral infections, malignant cancers, and autoimmune disorders. The use of protein therapeutics has grown dramatically and is predicted to expand 15-20 % annually.¹ The development of therapeutic proteins can be impeded by several problems such as insufficient stability, short biological half-life, immunogenicity, and costly production.²

Approaches to improve the stability and pharmacokinetic properties of therapeutic proteins include structural modification and covalent conjugation of polyethylene glycol (PEGylation). PEGylation can provide multiple benefits. Some proteins exhibit a short half-life because of fast renal clearance, often a result of their small size and hydrophilicity.² PEGylation increases protein molecular weight, which can prolong plasma half-life allowing less frequent administration. Additionally, PEG can physically mask the protein, which can improve stability and decrease immunogenicity. A common consequence of PEGylation is a reduction in biological activity, but a significant increase in biological half-life may outweigh this disadvantage.³ Several PEGylated protein products have received approval including PEGylated asparaginase (Onspar®), PEGylated adenosine deamidase (Adagen®) and PEGylated interferon (PEG-Intron™ and PEG-Asys®).⁴

Fibroblast growth factors (FGFs) are small polypeptide growth factors sharing common structural characteristics. They bind to glycosaminoglycans as well as polyanions such as heparin. The binding of FGFs to proteoglycans such as heparan sulfate serves to protect FGFs from degradation and to create local reservoirs of growth factors.⁵ Proteoglycans also present FGFs to their cell surface receptors in a

biologically active form.⁶⁻⁷ The heparin-binding domains of FGFs constitute clusters of basic amino acid residues brought together by the secondary and tertiary structure of the folded polypeptide.⁸⁻¹⁰ Heparin, heparan and chondroitin sulfate proteoglycans are also reported to protect HBGFs from proteolytic degradation and potentiate their biological effects.¹¹⁻¹³

Fibroblast growth factor-10 (FGF-10) also known as keratinocyte growth factor-2 (KGF-2) is a 208 amino acid glycoprotein expressed in stromal cells.¹⁴ KGF-2 has a sequence similar to FGF-7 (KGF-1) and both are highly mitogenic for keratinocytes.¹⁵ Repifermin® is a truncated form of recombinant FGF-10 containing 140 amino acids. Repifermin® was reported to promote angiogenesis and accelerate wound healing and was a potential candidate for the treatment of mucositis, ulcerative colitis and cutaneous wound healing.¹⁶⁻¹⁹ Repifermin® development has been impeded, however, by poor stability and a relatively short half-life *in vivo*.²⁰⁻²¹ The protein unfolds around body temperature (~37 °C) and the unfolded protein aggregates rapidly.²² Thus, an improved thermal stability and an extended biological half-life are highly desirable. In this work, the non-covalent PEGylation of KGF-2 is explored by electrostatically complexing the PEGylated polyanions pentosan polysulfate (PPS) and dextran sulfate (DS). PPS and DS are sulfated polysaccharides (Figure 4.1). DS has been reported to protect many fibroblast growth factors from heat, acid, and proteolytic degradation at low ionic strength.²³⁻²⁵ PPS has been used to treat interstitial cystitis, transmissible spongiform encephalopathies (TSEs) and various forms of cancer and is currently being evaluated as an antiviral agent and anti-tumor agent as well.²⁶⁻²⁸ PPS is capable of stabilizing FGF-1 against heat-induced aggregation.²⁹ The aim of this work is to test the ability of these PEGylated

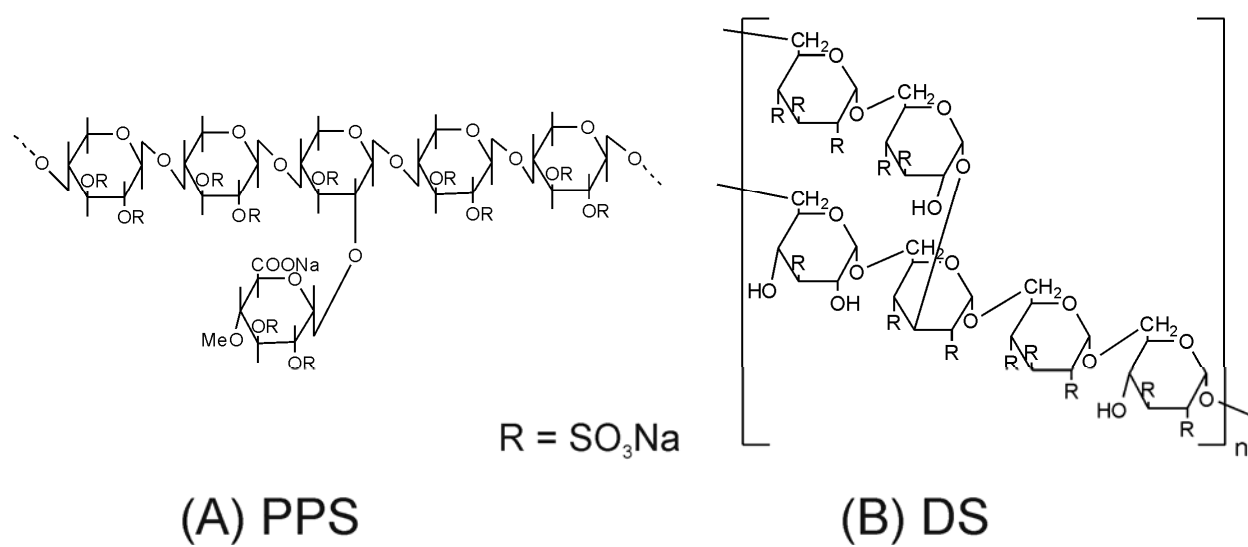


Figure 4.1. Representative structures of (A) pentosan polysulfate (PPS) and (B) dextran sulfate (DS).

polyanions to increase the thermal stability of KGF-2 and provide general reagents to favorably alter the properties of these potential therapeutic proteins.

4.2 Materials and methods

4.2.1 Materials

Repifermin®, a truncated form of KFG-2, was obtained from Human Genome Sciences (HGS). DS sodium (MW 5 kDa), branched polyethylenimine (PEI, MW 25 kDa), phosphate buffered saline (PBS), and 2-mercaptoethanol were purchased from Sigma (St. Louis, MO). PPS sodium (MW 4-6 kDa) was purchased as solution for injection from the Wedgewood Pharmacy (Swedesboro, NJ). Methoxy-PEG-amine (MW 5 kDa) and methoxy-PEG-ethylamine (MW 20 kDa) were purchased from Jenkem Technology (Allen, TX) and NOF Corporation (Tokyo, Japan), respectively. 1-Ethyl-3-(3-dimethylaminopropyl) carbodiimide HCl (EDC), N-hydroxysuccinimide (NSH), 2-(N-morpholino) ethanesulfonic acid (MES) buffer, and side-A-lyzer dialysis cassettes were purchased from Thermo Fisher Scientific Inc. (Rockford, IL). Aqueous non-radioactive cell proliferation assay kit (MTS) was purchased from Promega (Madison, WI). Human umbilical vein endothelial cells (HUVEC) were purchased from the American Type Culture Collection (ATCC) and cultured according to ATCC protocols. F-12K medium was purchased from Mediatech Inc (Manassas, VA). Dialysis membranes were purchased from Spectrum laboratories Inc. (Rancho Dominguez, CA) All other chemicals are reagent grade and were used as received.

4.2.2 Synthesis of carboxymethyl dextran sulfate (CMDS)

CMDS was synthesized as described elsewhere.³⁰⁻³¹ Briefly, DS (0.072 mmole) was dissolved in ultrapure water. NaOH (2.5 mmole) was added to the solution, isopropanol (IPA) was then added followed by monochloroacetic acid (20

mmole). The reaction solution was stirred at 240 rpm and 60 °C for 3 h and then dialyzed against ultrapure water for 3 days (molecular weight cut off (MWCO) 1000 Da). The dialyzing water was changed periodically. The product in the retentate was lyophilized.

4.2.3 Synthesis of dextran sulfate-PEG 5 kDa and 20 kDa

Methoxy-PEG-amine (MW 5 kDa) was conjugated to CMDS via carbodiimide chemistry. Briefly, methoxy-PEG-amine (2.5 μ mole) was dissolved in PBS (pH 7.4). CMDS (10 μ mole) was dissolved in MES buffer (pH 6). EDC (50 μ mole) was added to the solution, followed by NHS (60 μ mole), and the solution was stirred for 15 min. 2-Mercaptoethanol was added to produce a final concentration of 20 mM. Methoxy-PEG-amine in PBS was then added to the solution. The reaction solution was stirred for 20 h at room temperature and subsequently dialyzed against ultrapure water for 3 days (MWCO 6-8 kDa) and 1 day (MWCO 12-14 kDa). The product in the retentate was lyophilized and characterized. $^1\text{H-NMR}$ (500 MHz, D_2O): 3.30 ppm PEG $\text{CH}_3\text{-O-}$, 3.4-3.63 ppm dextran methylene, 3.54 ppm PEG $\text{O-CH}_2\text{-CH}_2\text{-}$. $^{13}\text{C-NMR}$ (500 MHz, D_2O): 42.64 ppm PEG $\text{-NH-CH}_2\text{-}$, 56-58 ppm dextran tetrahydropyran -CH- , 69.53-70.93 ppm dextran methylene and PEG $\text{O-CH}_2\text{-CH}_2\text{-}$. FTIR: 3450, 2875, 1750 cm^{-1} .

Methoxy-PEG-ethylamine (MW 20 kDa) was conjugated to CMDS using the same procedure except for the MWCO of the dialysis membrane used (12-14 kDa). $^1\text{H-NMR}$ (500 MHz, D_2O): 3.30 ppm PEG $\text{CH}_3\text{-O-}$, 3.4-3.63 ppm dextran methylene, 3.54 ppm PEG $\text{O-CH}_2\text{-CH}_2\text{-}$. $^{13}\text{C-NMR}$ (500 MHz, D_2O): 42.64 ppm PEG $\text{-NH-CH}_2\text{-}$, 56-58 ppm dextran tetrahydropyran -CH- , 69.53-70.93 ppm dextran methylene and PEG $\text{O-CH}_2\text{-CH}_2\text{-}$. FTIR: 3450, 2875, 1750 cm^{-1} .

4.2.4 Synthesis of pentosan sulfate-PEG 5 kDa and 20 kDa

PPS solution for injection was dialyzed against ultrapure water for 3 days (MWCO 1000 Da) followed by lyophilization. Methoxy-PEG-amine (MW 5 kDa) and methoxy-PEG-ethylamine (MW 20 kDa) were conjugated to PPS using the carbodiimide reaction as described above. The reaction solution was then dialyzed against ultrapure water for 3 days (MWCO 6-8 kDa) and 1 day (MWCO 12-14 kDa) for PEG5 conjugates. PEG20 conjugates were dialyzed for 3 days (MWCO 12-14 kDa). The product in the retentate was lyophilized and characterized.

PPS-PEG 5 kDa $^1\text{H-NMR}$ (500 MHz, D_2O): 3.30 ppm PPS $-\text{CH}_3$, 3.35, 3.60 ppm PPS $-\text{CH}_2-$ and PEG $\text{O-CH}_2\text{-CH}_2$, 5.68, 5.92 ppm PPS $-\text{CH}_2-$. $^{13}\text{C-NMR}$ (500 MHz, D_2O): 14.4 ppm PPS $-\text{CH}_3$, 42.73 ppm, PEG $-\text{NH-CH}_2-$, 58.8 ppm PPS $-\text{CH}_3$, 72.3-72.6 ppm PPS $-\text{C-}$ tetrahydropyran, 74.4 ppm PPS $-\text{CH}_2-$ and PEG $\text{O-CH}_2\text{-CH}_2-$, 99.48 ppm PPS $-\text{C-}$ tetrahydropyran. FTIR: 3450, 2875, 1750 cm^{-1} .

PPS-PEG 20 kDa $^1\text{H-NMR}$ (500 MHz, D_2O): 3.30 ppm PPS $-\text{CH}_3$, 3.35, 3.60 ppm, PPS $-\text{CH}_2-$ and PEG $\text{O-CH}_2\text{-CH}_2$, 5.68, 5.92 ppm PPS $-\text{CH}_2-$. $^{13}\text{C-NMR}$ (500 MHz, D_2O): 14.4 ppm PPS $-\text{CH}_3$, 42.73 ppm PEG $-\text{NH-CH}_2-$, 58.8 ppm PPS $-\text{CH}_3$, 72.3-72.6 ppm PPS $-\text{C-}$ tetrahydropyran, 74.4 ppm PPS $-\text{CH}_2-$ and PEG $\text{O-CH}_2\text{-CH}_2-$, 99.48 ppm PPS $-\text{C-}$ tetrahydropyran. FTIR: 3450, 2875, 1750 cm^{-1} .

4.2.5 Characterization of polyanion conjugates

^1H nuclear magnetic resonance (NMR) and ^{13}C NMR spectra were recorded on a Bruker Avance AV-III 500 spectrometer. Fourier transform infrared (FTIR) spectra were obtained with a Perkin Elmer 100 FTIR spectrometer employing a universal ATR sampling accessory in the range of 4000-650 cm^{-1} .

Size exclusion chromatography (SEC) was carried out with a Shimadzu LC-2010C HT equipped with a low temperature-evaporative light scattering detector

(ELSD-LT II) (Columbia, MD). The detector temperature was set at 50 °C. A Shodex OH pak SB 806 HQ column was used with ammonium acetate buffer pH 5 as eluent at a flow rate of 0.8 mL/min. The column temperature was kept constant at 40 °C. Various PEG standards, hyaluronic acid (HA), dextran, and DS were used as controls. The purity of the conjugates was determined by peak area percent.

Sodium dodecyl sulfate-polyacrylamide gel electrophoresis (SDS-PAGE) was used as a second method to determine the electrophoretic mobility of conjugates. SDS-PAGE was performed using NuPAGE 4-12 % Bis-Tris Gels and NuPAGE Tris-acetate SDS running buffer (Invitrogen, Carlsbad, CA). PEG standard and sample solutions were mixed with sample loading buffer and loaded onto the gel. The gel was electrophoresed at 130 mV for 40 min. After electrophoresis, the gel was fixed and stained at room temperature as described previously.³²⁻³⁴ Briefly, the gel was soaked in a 5 % glutaraldehyde solution for 15 min and immersed in 0.1 M perchloric acid for 15 min. The gel was then stained with barium iodine (a mixture of 5 % barium chloride and 0.1 M iodine solution at a ratio of 5:2 (v/v)). The gel was photographed using a densitometer (AlphaImager 2000, San Leonardo, CA).

UV-VIS spectroscopy was used as a means to indirectly determine the numbers of PEG chains on conjugates by quantifying the amount of associated polyanion. Electrostatic interactions between sulfated polysaccharides and methylene blue molecules modified the visible spectrum of methylene blue. Therefore, these spectral changes could be used to quantify the amount of sulfated polysaccharides in unknown samples or to study the interactions of the two molecules. This method is described elsewhere.³⁵⁻³⁷ Briefly, polyanion conjugates were dissolved and diluted to optimal concentrations (1-21 µg/mL). Methylene blue solution (0.07 mg/mL, 150 µL) was added to polyanion conjugate solution (100 µL) and mixed. After 5-15 min of

mixing, water (1.5 mL) was added. The depletion of methylene blue absorbance at 664 nm was used to quantify the amount of polyanion on conjugates. PPS and DS were used as standards. The amount of conjugated PEG was obtained by subtracting the amount of polyanion from the total conjugate weight.

4.2.6 Cytotoxicity assay

The cytotoxicity of polyanions and PEGylated polyanions was determined using a CellTiter 96 AQueous Cell Proliferation assay kit. HUVEC were seeded in 96-well plates (8,000 cells/well) for 24 h prior to use. The growth medium was replaced with serum-free medium containing polyanions and PEGylated polyanions at various concentrations and incubated for 24 h. After incubation, the medium containing sample was replaced with 100 μ L of serum-free medium. Then, 20 μ L of the mixture of MTS ([3-(4,5-dimethylthiazol-2-yl)-5-(3-carboxymethoxyphenyl)-2-(4-sulfophenyl)-2H-tetrazolium]) and PMS (phenazine methosulfate) was added to each well, and the plates were incubated at 37 °C, 5 % CO₂ for 2 h. The absorbance of the formazan product was measured at 490 nm using a microplate reader (SpectraMax M5; Molecular Devices Corp., CA).

4.2.7 Formulation of KGF-2:polyanion complexes

KGF-2 was aliquoted and stored at -80 °C. Prior to use, KGF-2 was thawed and dialyzed in PBS buffer overnight using a dialysis cassette (MWCO 10 kDa). The concentration of KGF-2 was determined by UV spectroscopy using extinction coefficient. The extinction coefficient of the protein is 35360 M⁻¹ cm⁻¹. PEGylated polyanions tested included PPS-PEG5, PPS-PEG20, DS-PEG5, and DS-PEG20. PPS and DS were used as controls. To prepare KGF-2:polyanion complexes, KGF-2 and polyanions were diluted with citrate phosphate buffer (20 mM, pH 6.2, 100 mM NaCl) to desired concentrations to produce the molar ratios and proper final protein

concentrations needed for each instrument. KGF-2 was mixed with polyanions or conjugates at 4 different molar ratios (e.g. KGF-2:polyanions or conjugates = 1:2, 1:1, 2.4:1, and 6:1) throughout the studies unless otherwise noted. The protein solution was added into the polyanion solution slowly while stirring at 800 rpm. The mixture was stirred for 30 minutes prior to analysis.

4.2.8 Physical characterization of KGF-2 complexes

All experiments were conducted in 20 mM citrate phosphate buffer (pH 6.2, 100 mM NaCl). This system was chosen because it was reported to provide sufficient solubility and stability of the protein.²⁰ KGF-2 alone was used as a control in all studies.

Far-UV Circular dichroism (CD) spectra were obtained with a Jasco-810 spectropolarimeter equipped with a peltier temperature controller (Tokyo, Japan). The samples contained a final KGF-2 concentration of 0.2 mg/mL in a 0.1 cm path length cell. Spectra over a wavelength range of 200-250 nm were collected at 10 °C. The spectra were collected at a scan rate of 10 nm/min, a resolution of 0.5 nm, a response time of 4 s, and a bandwidth of 1 nm. In temperature-dependent studies, the thermal unfolding of KGF-2 and KGF-2 complexes were monitored at 229 nm over a temperature range of 10-85 °C in increments of 0.5 °C at a temperature ramp rate of 1.5 °C/min and an incubation time of 120 s.

Intrinsic tryptophan fluorescence experiments were performed with a PTI QM-1 spectrofluorometer equipped with a four position peltier thermostated cuvette holder (Brunswick, NJ). An excitation wavelength of 295 nm (> 95% Trp emission) was used for simultaneously measuring both static light scattering and intrinsic tryptophan fluorescence. The emission spectra over a range of 300 to 400 nm were recorded at a 1 nm/s collection rate. A second photomultiplier placed at 180° to the

emission detector was used to record light scattering. Data were collected every 2.5 °C from 10 to 85 °C with 180 seconds of thermal equilibrium at each temperature. A final KGF-2 concentration of 0.2 mg/mL was used. Fluorescence intensity and peak positions were obtained by a mean spectral center of mass method, after buffer subtraction. This method results in peak positions shifted by about 10 nm, but yields a better signal to noise ratio and increased reproducibility. Data analysis was performed using Felix™ (PTI) and Microcal Origin (V 7.0) software.

Differential scanning calorimetry (DSC) was performed with a VP-capillary DSC system (MicroCal Inc, Northampton, MA) equipped with an autosampler. Samples at a final KGF-2 concentration of 0.4 mg/mL were loaded in a 96-well plate and stored at 4 °C in a temperature controlled chamber prior to examination. Thermograms were obtained by increasing temperature from 5 to 80 °C with a ramping rate of 1 °C/min, a pre-scan equilibration time of 10 min and a filtering period of 16 s. Data were analyzed using Origin software after buffer subtraction. T_m values were selected using a multiple-state model in Microcal Origin software provided with the instrument.

Heat induced aggregation was monitored by changes in optical density at 350 nm using a Varian® UV-Visible spectrophotometer (Walnut creek, CA) over a temperature range of 20-90 °C. Changes in hydrodynamic diameters were obtained using dynamic light scattering (DLS) (DynaPro plate reader, Wyatt Technology, Santa Barbara, CA) over a temperature range of 10-65 °C. The observed hydrodynamic diameter was obtained using multi-component analysis function (based on mass). Final concentrations of KGF-2 used in both experiments were 0.05 mg/mL.

Isothermal titration calorimetry (ITC) was used to monitor enthalpy changes resulting from the binding of KGF-2 to polyanions or conjugates (Microcal VP-ITC

calorimeter, MicroCal Inc, Northampton, MA) with a reaction cell volume of 1.45 mL. KGF-2 (15-20 μM) in the cell was titrated with polyanions or conjugates (170-500 μM) every 3-4 min at 25 $^{\circ}\text{C}$ with $\sim 8 \mu\text{L}$ injection volumes and ~ 25 -30 total injections with stirring at 300 rpm. All solutions were degassed prior to use. Control titrations were performed to obtain heats of dilution which were subtracted from the corresponding heats of binding.

4.3 Results

DSC was initially used to screen for the ability of several polyanions to increase the thermal stability of KGF-2. Polyanions tested include chromotropic acid (320 Da), acid fuchsin (585 Da), pyridoxal-phosphate-6-azophenyl-2',4'-disulfonate (PPADS, 599 Da), congo red (699 Da), trypan blue (873 Da), PPS (5,000 Da), and DS (5,000 Da) (Figure 4.2). PPS and DS were chosen because of their superior performance in enhancing the thermal stability of KGF-2 (see below). DS was modified to CMDS to make it amenable to PEG conjugation. PPS and CMDS were then covalently attached to two different amine-PEGs (5 and 20 kDa) via the carbodiimide reaction. A solution mixture of methoxy PEG (mPEG) (6 kDa) and KGF-2 was also tested using DSC, CD and fluoresce spectroscopy. Data showed that mPEG alone did not alter KGF-2 structure or increase the thermal stability of KGF-2 (data not shown).

4.3.1 Synthesis and characterization of polyanion-PEGs

Different polyanion-PEGs were synthesized and extensively purified by dialysis. The conjugates were characterized by ^1H NMR, ^{13}C NMR, FTIR, and UV-VIS spectroscopy. ^1H NMR, ^{13}C NMR, and FTIR showed characteristic peaks from both the polyanions and PEG. The yield of different polyanion conjugates ranged from ~ 54 -88 % (Table 4.1). The yield of PPS-PEG5 and DS-PEG5 conjugates (~ 54 -

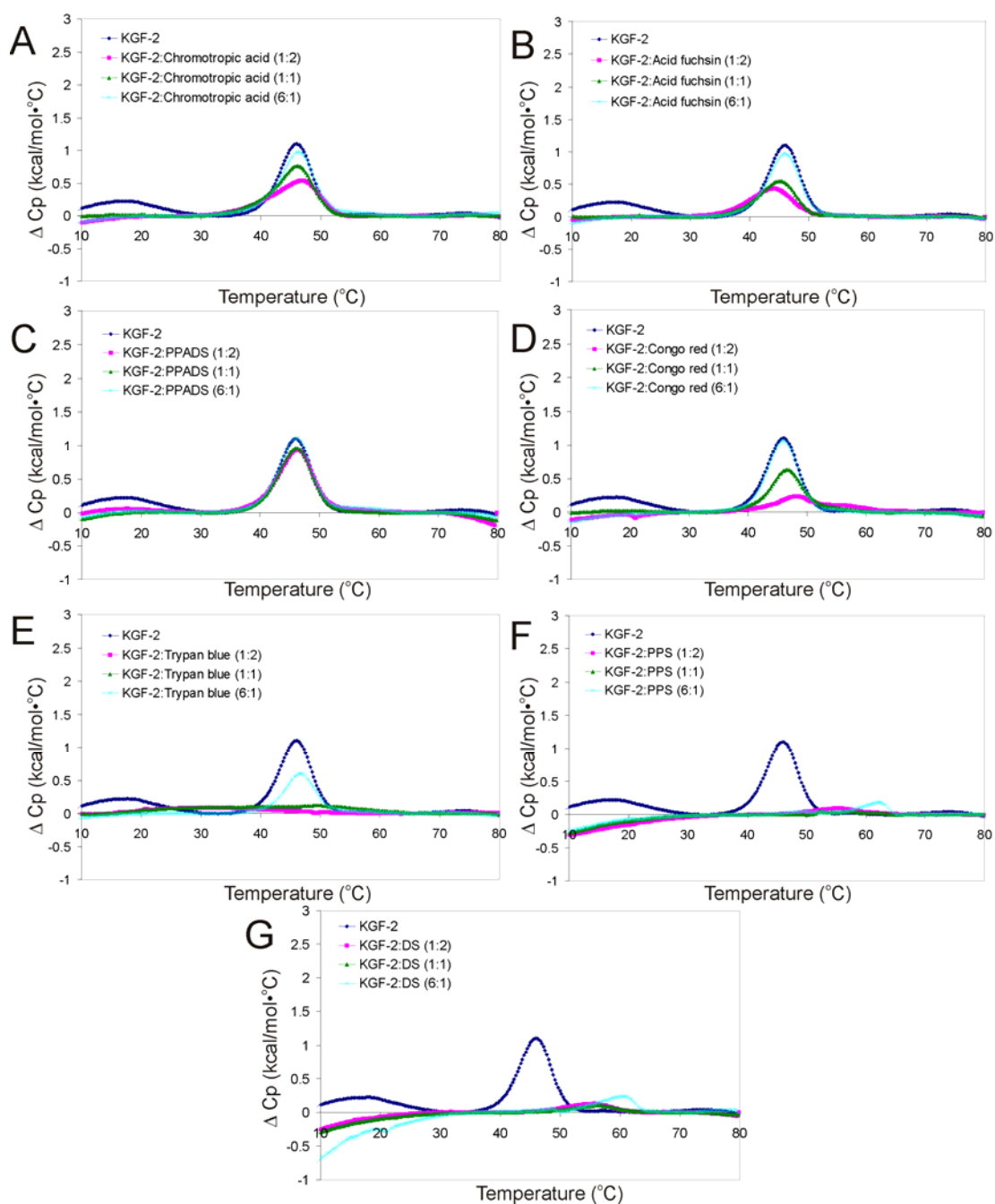


Figure 4.2. DSC thermograms of KGF-2 and KGF-2:polyanion complexes at different molar ratios for (A) chromotropic acid (B) acid fuchsin (C) pyridoxal-phosphate-6-azophenyl-2',4'-disulfonate (PPADS) (D) congo red (E) trypan blue (F) PPS and (G) DS (upward = endothermic).

Table 4.1. Characteristics of polyanion conjugates

Compound	Actual yield (%)	Purity (%)*	PEG/ polyanion (molar ratio)**	Estimated MW (Da) ***
PPS-PEG5	65.4	~ 92	1.0 ± 0.5	10,000
PPS-PEG20	88.7	~ 92	0.8 ± 0.1	25,000
DS-PEG5	53.8	~ 97	5.0 ± 0.8	30,000
DS-PEG20	84.5	~ 95	2.3 ± 0.5	45,000

* Calculated from SEC peak areas.

** Average ± SD from two different syntheses.

** and *** Obtained from methylene blue experiments.

65 %) was generally lower than that of PPS-PEG20 and DS-PEG20 conjugates (~84-89 %).

Conjugates were analyzed using SEC to assess product purity and relative size. PEG standards and HA polymers exhibited a linear relationship between MW and retention time (Figure 4.3 A). HA polymers, bearing carboxylate, hydroxyl, and acetyl groups, were eluted earlier than PEG standards possibly due to self-association.³⁸ Highly sulfated PPS and DS appear to interact with the column and were eluted much later (~17 min) regardless of their MW. Dextran bearing mainly hydroxyl groups was eluted sooner than DS. The apparent MW of PPS-PEG5 and DS-PEG5 appeared to be < 3 kDa, while the MW of PPS-PEG20 and DS-PEG20 appeared to be between 12-21 kDa when calculated using a linear regression equation for the PEG standard curve (Figure 4.3 A). These apparent MWs were inaccurate due to polyanion interaction with the column. The data indicated high purity (~92-97 %) of the conjugates as calculated from peak areas (Table 4.1 and Figure 4.3 B and C). The retention profile also suggested that the PPS and DS conjugates were primarily a single species with the exception of DS-PEG5 which manifested two populations.

SDS-PAGE was employed as a second means to estimate the relative MW of the conjugates. Different PEG standards (7, 12, 21, and 66 kDa) were used as references. The electrophoretic mobility of conjugates through polyacrylamide was strongly influenced by the electrical field (Figure 4.4). The negatively charged conjugates migrated much faster than the PEG standards due to the high charge density of the polyanion moieties.

The number of PEG chains in the conjugates was quantified indirectly using the reduction of methylene blue absorbance at 664 nm upon binding to polyanions

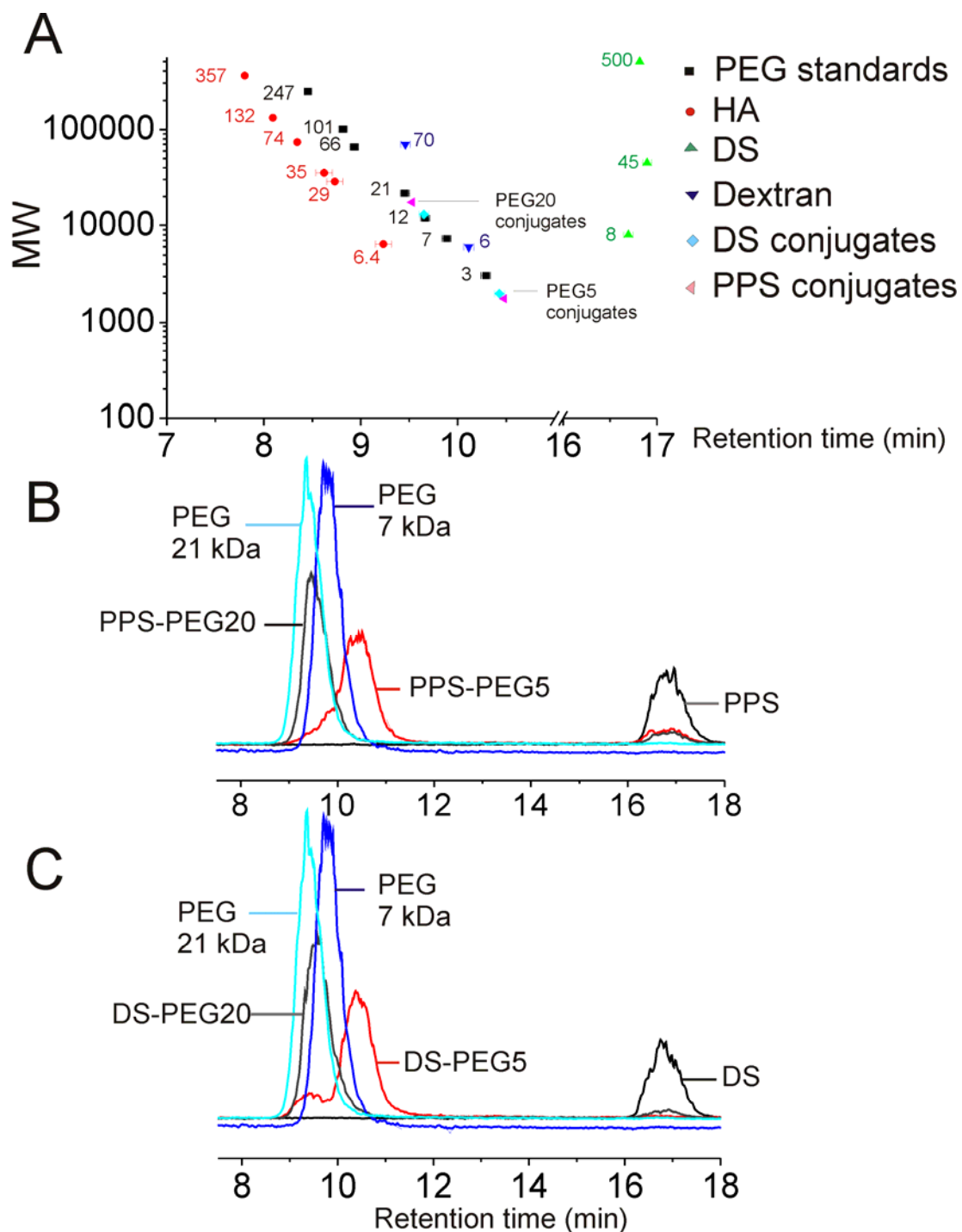


Figure 4.3. Size exclusion chromatography showed (A) polymers with different MW, structure, and charge exhibiting different retention times (numbers indicate MW (kDa)) (B) Chromatograms of PPS and PPS-conjugates and (C) chromatograms of DS and DS-conjugates.

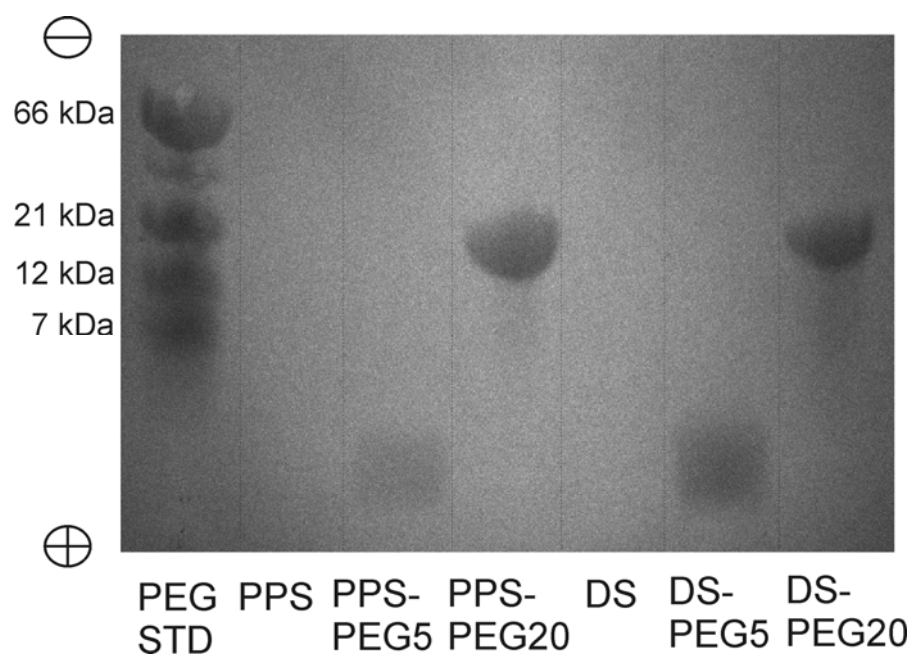


Figure 4.4. SDS-PAGE analysis of polyanions and conjugates compared to PEG standards.

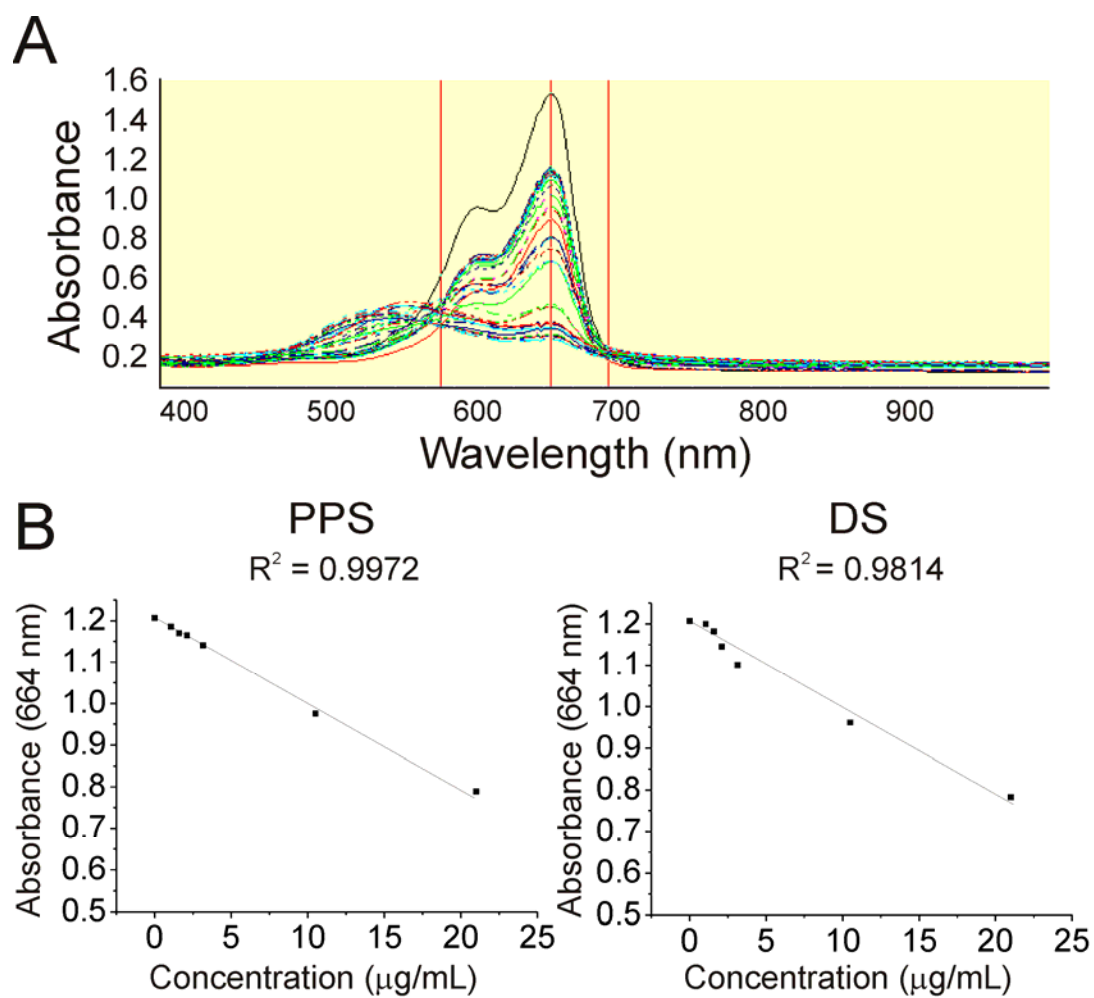


Figure 4.5. (A) The depletion of methylene blue absorbance (664 nm) upon binding with increasing amount of polyanions and (B) standard curves of PPS and DS.

(Figure 4.5 A). Standard curves were fit by linear regression with $r^2 = 0.9972$ and 0.9814 for PPS and DS, respectively (Figure 4.5 B). The number of polyanions in the conjugates was calculated from these linear regression equations. The amount of PEG was calculated by subtracting the amount of PPS or CMDS from the total conjugate weight. These experiments were carried out twice using materials from two different syntheses. PPS conjugates each contained one PEG chain per molecule as expected, whereas DS-PEG5 and DS-PEG20 conjugates had an average of 5 and 2 PEG chains per molecule, respectively (Table 4.1). The estimated MW of conjugates shown in Table 1 was used to estimate molar ratios throughout the remaining studies.

4.3.2 Cytotoxicity test

The cytotoxicity of polyanions and conjugates was determined with HUVEC. PPS, DS, and their conjugates showed negligible cytotoxicity, whereas PEI (highly cytotoxic agent) exhibited notably low cytotoxicity ($IC_{50} \sim 2 \mu\text{g/mL}$) (Figure 4.6).

4.3.3 Differential scanning calorimetry

DSC was employed to measure the thermal unfolding of KGF-2 and KGF-2: polyanion complexes by monitoring the heat absorbed during unfolding of the protein. KGF-2 alone showed an endothermic peak beginning at $\sim 35^\circ\text{C}$ with complete unfolding by $\sim 53^\circ\text{C}$. The transition melting temperature (T_m) was $\sim 46^\circ\text{C}$ as determined using a non two-state model. The presence of polyanions and conjugates significantly increased the transition temperature of KGF-2 suggesting they enhanced the thermal stability of the protein. For KGF-2:PPS complexes at 1:2 and 1:1 molar ratios, complexes showed a single transition peak and higher transition temperature ($\sim 60\text{--}62^\circ\text{C}$) (Figure 4.7 A1 and 2). KGF-2:PPS complexes revealed a small leading shoulder at 1:1 molar ratio and started to show two transition peaks (~ 47 and $\sim 60^\circ\text{C}$) at 2.4:1 and 6:1 molar ratios (Figure 4.7 A3 and 4). KGF-2:PPS-PEG5 and KGF-

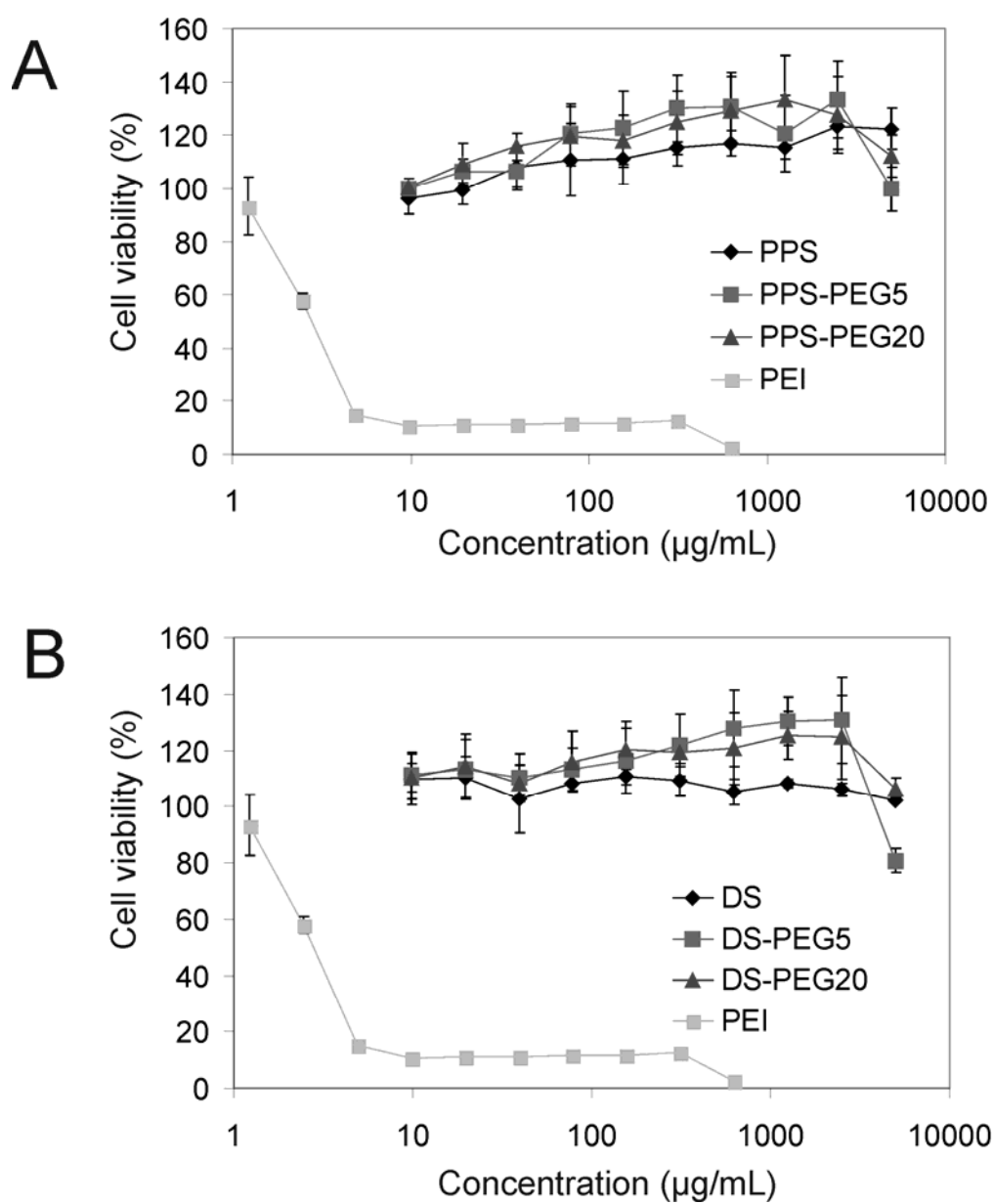


Figure 4.6. Cytotoxicity of (A) PPS and (B) DS and polyanion conjugates in HUVEC compared to PEI.

2:PPS-PEG20 complexes maintained single transition peaks at 2.4:1 molar ratios, but displayed two transition peaks (~ 47 - 53 and ~ 60 °C) at 6:1 molar ratios (Figure 4.7 A3 and 4). KGF-2:DS and KGF-2:DS-PEG5 complexes maintained single transition peaks (~ 61 - 63 °C) at 1:2, 1:1, and 2.4:1 molar ratios, but showed two transition peaks (~ 46 - 49 and ~ 58 - 61 °C) at a 6:1 molar ratio (Figure 4.7 B1 to B4). KGF-2:DS-PEG20 complexes appeared to possess single transition peaks at all molar ratios (~ 57 - 60 °C) except for the 6:1 ratio.

4.3.4 Circular dichroism

The secondary structure of KGF-2 in the presence and absence of polyanion-PEGs was examined using far-UV CD. KGF-2 alone showed a minimum around 206-208 nm and a maximum around 228-230 nm (Figure 4.8). This CD pattern is typical of proteins that share β -trefoil structure such as FGF-1 and FGF-2, interleukin-1, and hisactophillin.³⁹⁻⁴⁰ The complexes maintained similar CD spectra compared to free KGF-2 spectra at 1:2, 1:1, and 2.4:1 molar ratios, but displayed changes in intensity and positive peak wavelength position shifts (red shifts, 2-3 nm) (Figure 4.8 A1-A3 and B1-B3). This probably reflected changes in secondary structure upon binding to polyanions or conjugates or is due to absorption flattening. The complexes at the high protein ratio (6:1 molar ratio) demonstrated analogous spectra to that of free KGF-2 indicating that free KGF-2 was dominant in these systems (Figure 4.8 A4 and B4). To differentiate changes in secondary structure seen above, KGF-2 was unfolded by incubating in 4 M urea and 6 M guanidine HCl for 2 h. CD spectra of the unfolded protein showed reduction in intensity and blue shifts of positive peak wavelength positions (~ 5 nm) (Figure 4.9A).

The effect of temperature on the secondary structure of KGF-2 in the presence of various polyanions and polyanion-PEG conjugates was monitored by changes in

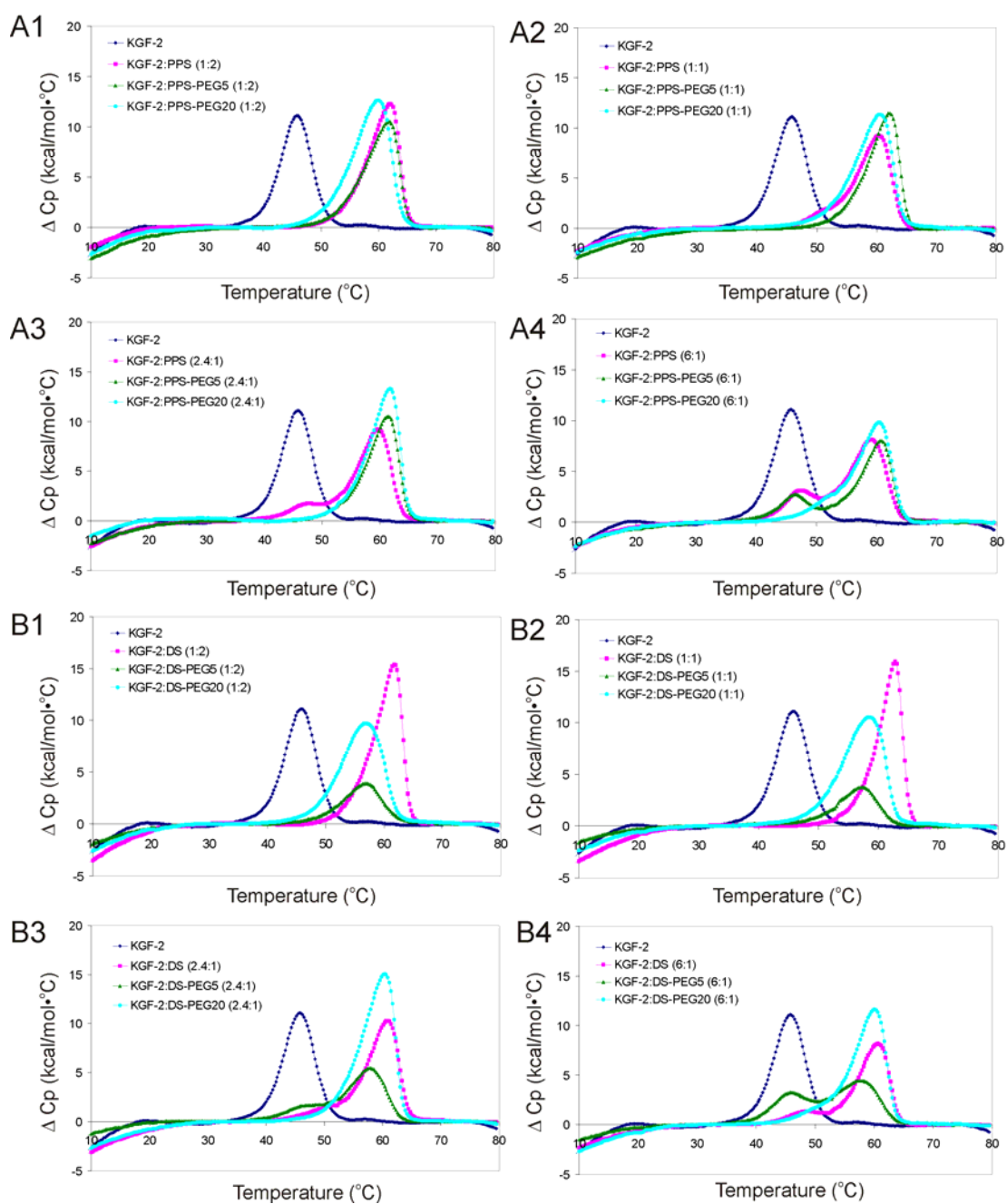


Figure 4.7. DSC thermograms of KGF-2 and KGF-2:polyanion complexes at different molar ratios for (A) PPS and (B) DS and polyanion conjugates (upward = endothermic).

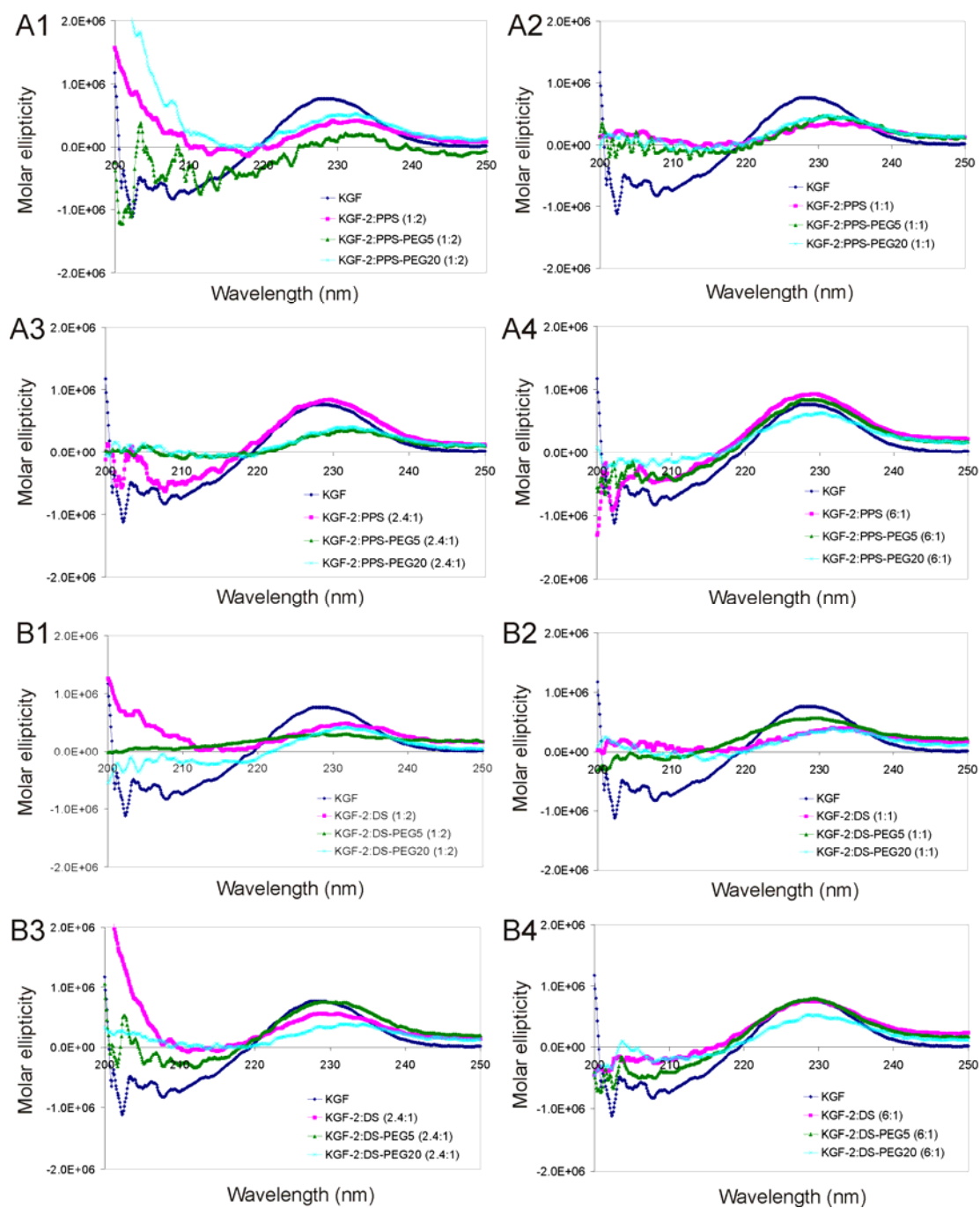


Figure 4.8. Far-UV CD spectra of KGF-2 and KGF-2:polyanion complexes at different molar ratios (scanned at 10 °C) for (A) PPS and (B) DS and polyanion conjugates.

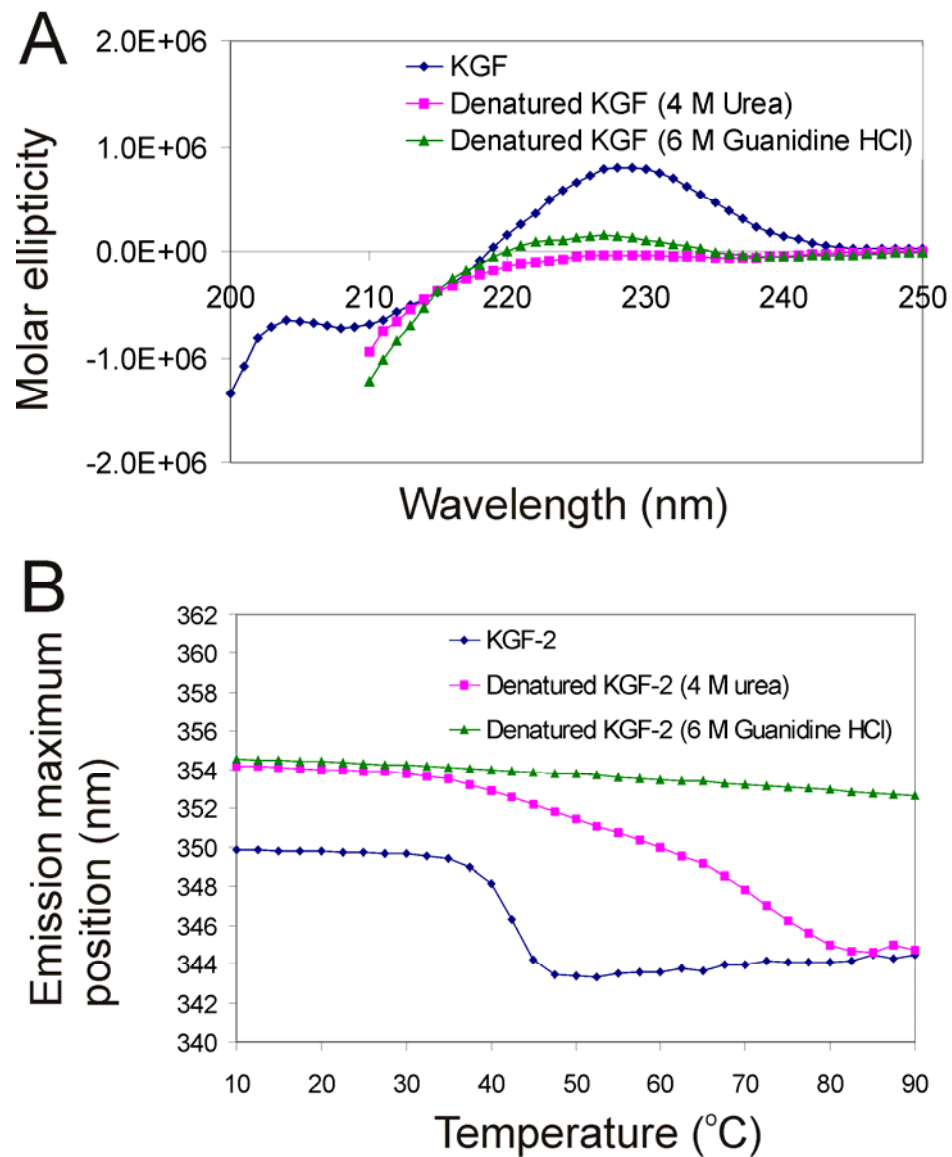


Figure 4.9. (A) Far-UV CD spectra of unfolded KGF-2 (scanned at 10 °C) (B) melting curves of unfolded KGF-2 by monitoring fluorescence emission maximum position shifts.

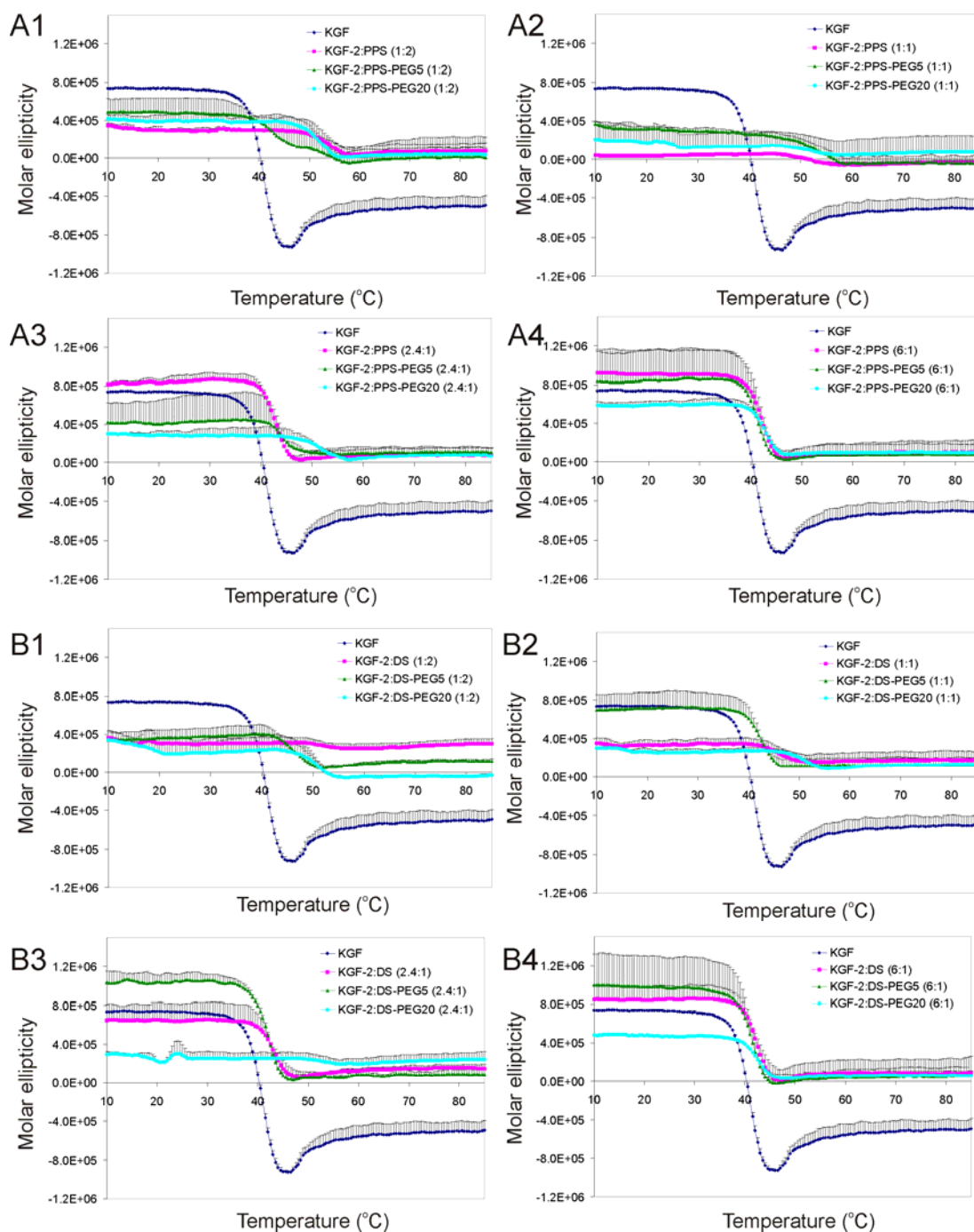


Figure 4.10. Effect of temperature on the molar ellipticity of KGF-2 and KGF-2:polyanion complexes (monitored at 229 nm) at different molar ratios for (A) PPS and (B) DS and polyanion conjugates.

CD ellipticity at 229 nm (Figure 4.10). CD measurements showed a thermal transition at ~ 39 °C for KGF-2 alone determined by a sigmoidal fit of the data. Complexes at some molar ratios showed higher melting temperatures, for example, KGF-2:PPS (1:2 and 1:1 ratios, ~ 51 - 52 °C), KGF-2:PPS-PEG5 (1:1 ratio, ~ 50 °C), KGF-2:PPS-PEG20 (1:2, 1:1 and 2.4:1 ratios, ~ 50 - 52 °C), KGF-2:DS (1:2 ratio, ~ 51 °C), KGF-2:DS-PEG20 (1:1 and 2.4:1 ratios, ~ 48 - 50 °C). Some complexes manifested low to intermediate thermal stability enhancement such as KGF-2:PPS (2.4:1 and 6:1 ratios, ~ 42 - 44 °C), KGF-2:PPS-PEG5 (2.4:1 and 6:1 ratios, ~ 41 - 44 °C), KGF-2:PPS-PEG20 (6:1 ratio, ~ 42 °C), KGF-2:DS (1:1, 2.4:1, and 6:1 ratios, ~ 42 - 45 °C). Interestingly, KGF-2:DS-PEG5 complexes showed low to intermediate stability enhancement at all molar ratios.

4.3.5 Intrinsic tryptophan fluorescence spectroscopy

The effect of polyanions and conjugates on the physical stability of KGF-2 was further explored using intrinsic tryptophan fluorescence spectroscopy. The observed emission maximum of KGF-2 was ~ 350 nm. This emission maximum was constant from 10 - 32 °C suggesting no change in the microenvironment of tryptophan residues. Upon further heating, a blue shift (7 nm) in the emission wavelength was observed suggesting that the Trp residues were less solvent-exposed. This was probably due to aggregation. After binding to polyanions or conjugates, the emission maximum positions at 10 °C were slightly shifted (blue shift, 1-4 nm) indicating subtle changes in the tertiary structure of KGF-2. In contrast, unfolded KGF-2 displayed red shifts (4 nm) of the emission maximum positions at 10 °C and no transition temperature upon further heating (Figure 4.9B). Binding to polyanions or conjugates increased the transition temperature of KGF-2 by 7 - 11 °C. Generally, more

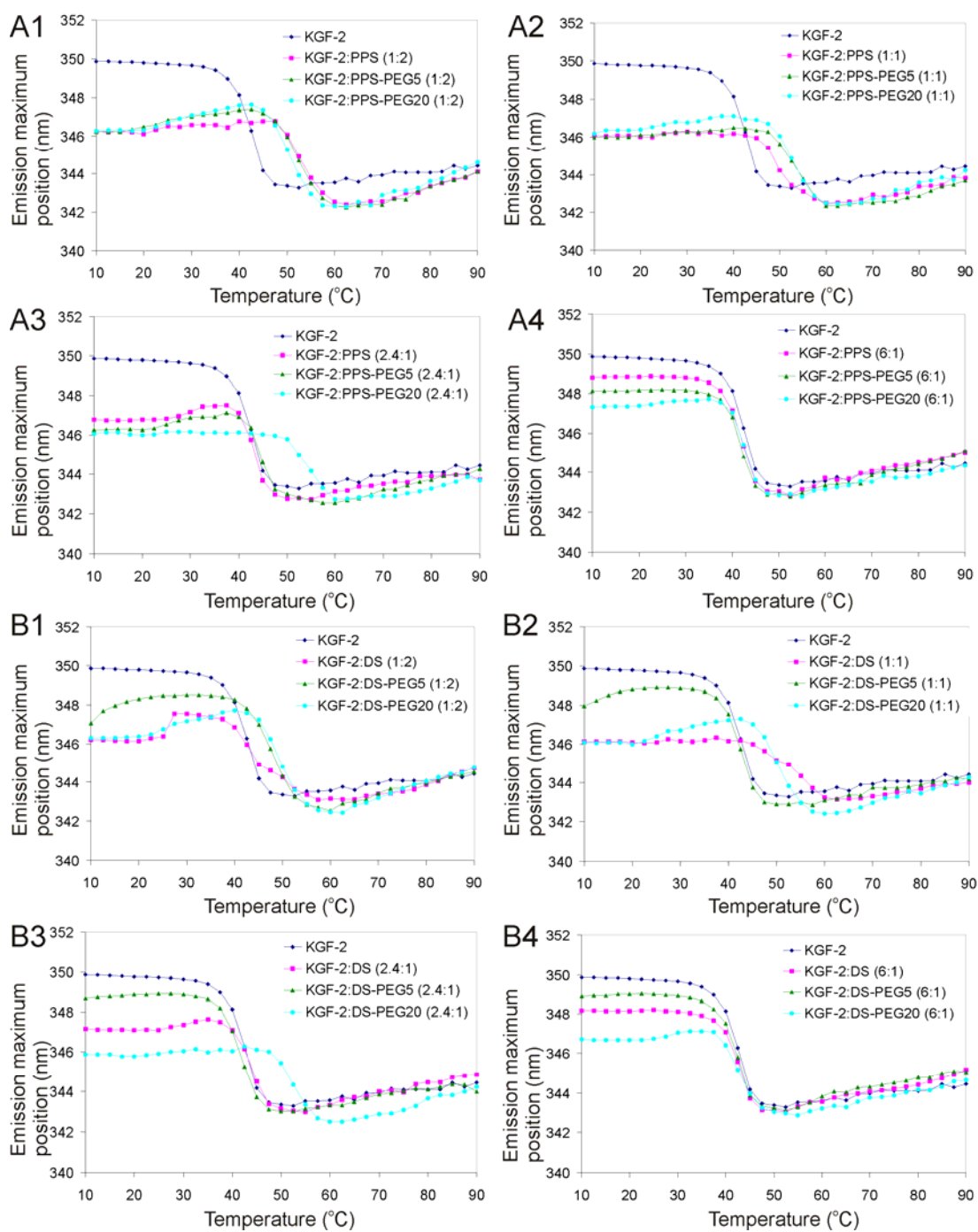


Figure 4.11. Effect of temperature on the fluorescence emission maximum positions of KGF-2 and KGF-2:polyanion complexes at different molar ratios for (A) PPS and (B) DS and polyanion conjugates.

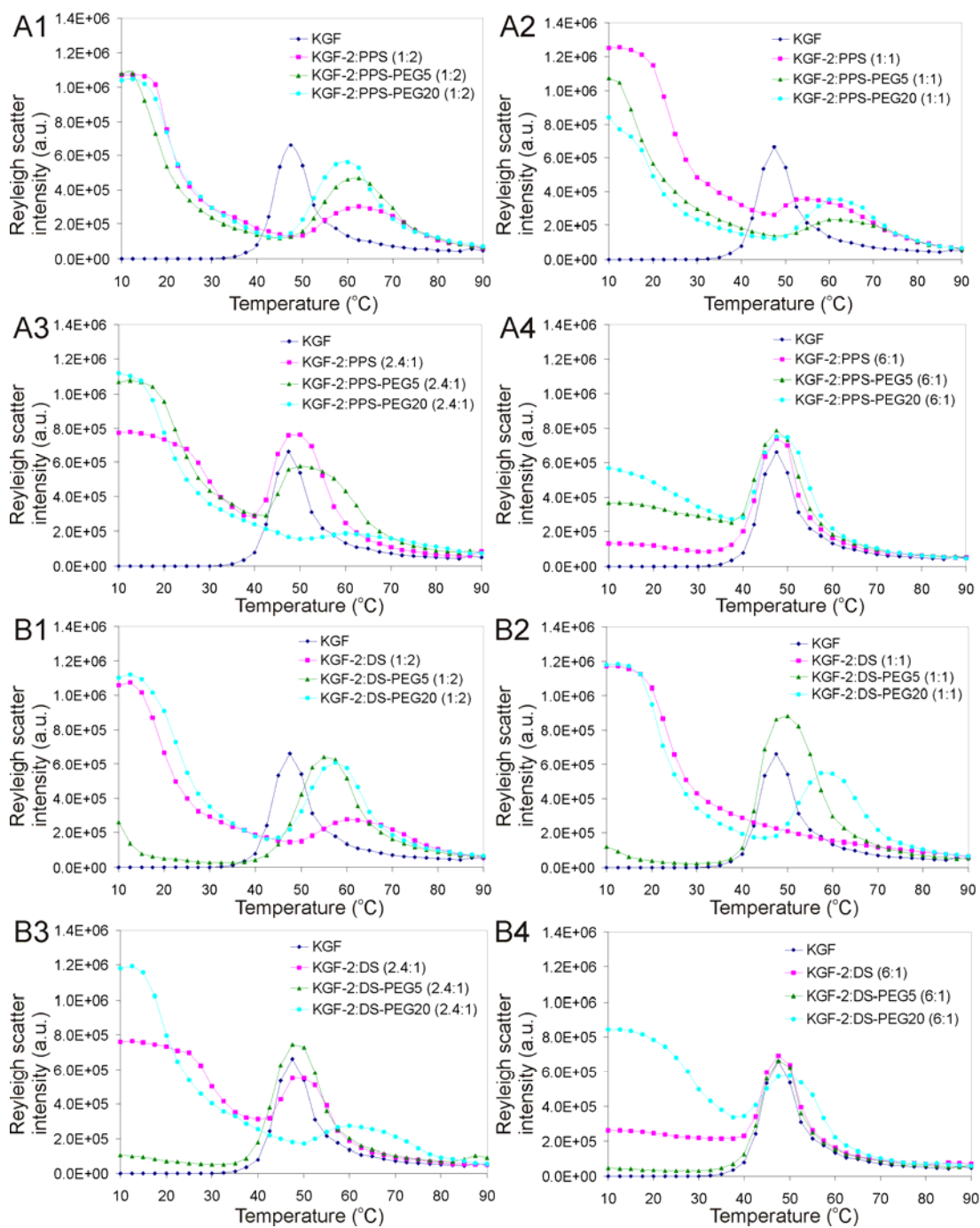


Figure 4.12. Effect of temperature on light-scattering intensity (monitored at 295 nm) of KGF-2 and KGF-2:polyanion complexes at different molar ratios for (A) PPS and (B) DS and polyanion conjugates.

polyanion (e.g. 1:2 molar ratio) yielded greater thermal stability. PPS conjugates showed superior performance compared to DS conjugates (Figure 4.11). Once again, KGF-2 complexes at the 6:1 molar ratio had transition temperatures similar to that of KGF-2 alone indicating free KGF-2 was dominant in these formulations.

Light-scattering experiments (295 nm) conducted simultaneously with intrinsic fluorescence experiments further confirmed the previously observed transition temperatures (Figure 4.12). At low temperature, most KGF-2 complexes scattered more light than free KGF-2 in solution. The scattered light from complexes decreased as temperature increased. The onset of aggregation was apparent from a dramatic increase in scattered light, which peaked and then dropped as protein ultimately precipitated out of solution.

4.3.6 Heat induced aggregation studies

Based on thermal stability studies, formulations that showed superior performance were selected for further aggregation studies. The turbidity of various formulations was monitored at 350 nm to determine the colloidal stability of the complexes. KGF-2 alone showed an onset of aggregation at ~47 °C, whereas KGF-2 complexes exhibited higher onset temperatures (5-13 °C) (Figure 4.13 A). The slight turbidity of complexes at low temperature again indicated binding of the protein and PEG-polyanion. KGF-2:DS-PEG5 (1:2) showed a higher degree of turbidity and poorer colloidal stability compared to the other formulations.

The hydrodynamic diameter of the complexes was examined using DLS at 10 °C (Table 4.2). KGF-2 complexes (17-79 nm) were larger than KGF-2 alone (~3 nm) as expected. The hydrodynamic diameter of the KGF-2 complexes with PPS:PEG20 (79 nm) were larger than that of KGF-2 complexes with PPS:PEG5 and PPS (17 and 24 nm, respectively). The hydrodynamic diameter of the KGF-2 complexes with DS,

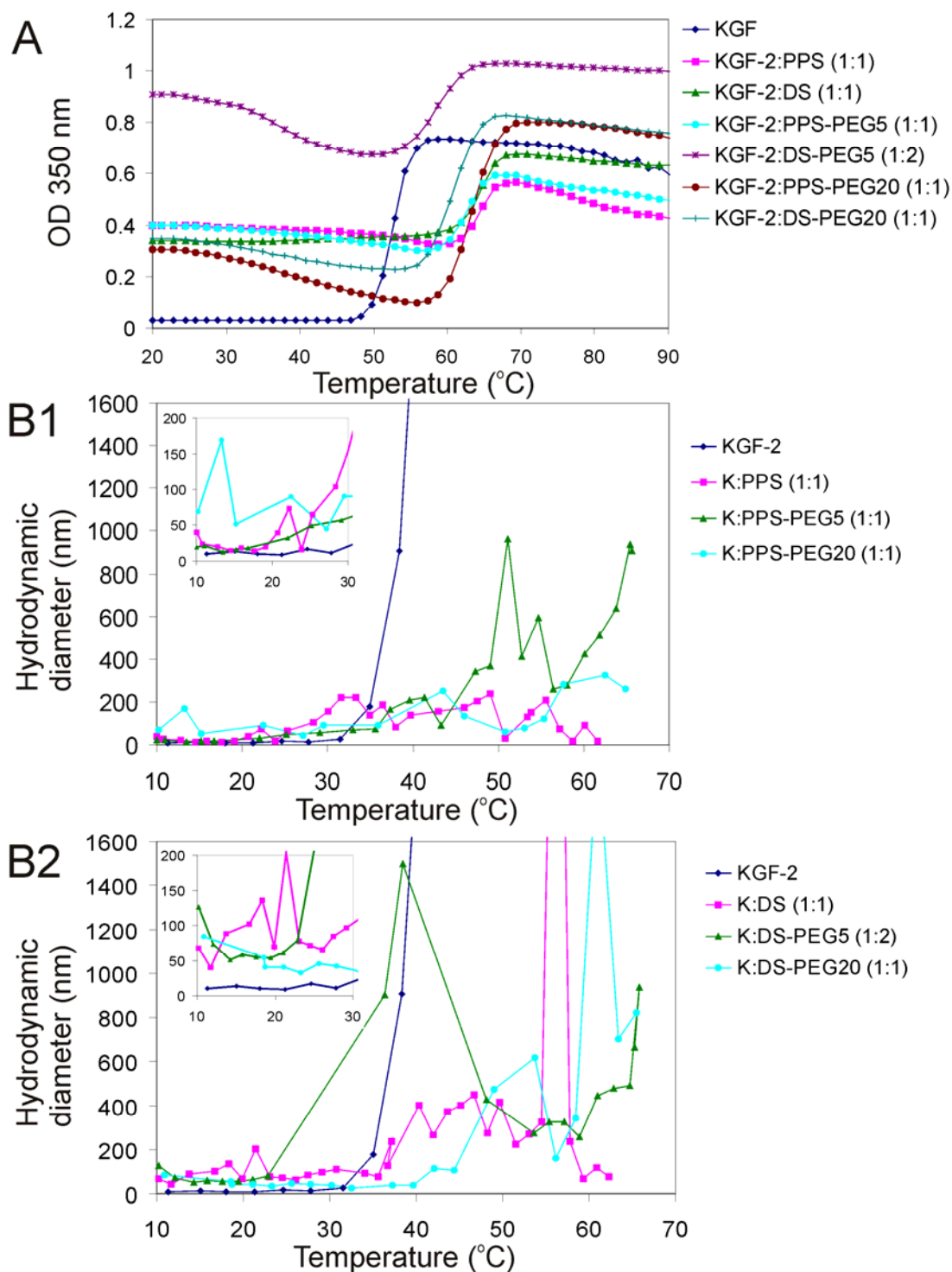


Figure 4.13. Temperature induced aggregation of KGF-2 and selected KGF-2:polyanion complexes monitored using (A) optical density (OD) at 350 nm and (B) dynamic light scattering (DLS).

Table 4.2. The hydrodynamic diameter of KGF-2 and selected KGF-2 complexes at 10 °C

Complexes	Hydrodynamic diameter (nm) \pm SD	Polydispersity
KGF-2	3.3 \pm 0.2	0.26
KGF-2:PPS (1:1)	23.6 \pm 9.9	0.20
KGF-2:PPS-PEG5 (1:1)	17.4 \pm 3.8	0.27
KGF-2:PPS-PEG20 (1:1)	79.0 \pm 23.8	0.26
KGF-2:DS (1:1)	63.3 \pm 24.0	0.34
KGF-2:DS-PEG5 (1:2)	68.8 \pm 17.9	0.37
KGF-2:DS-PEG20 (1:1)	53.9 \pm 18.1	0.43

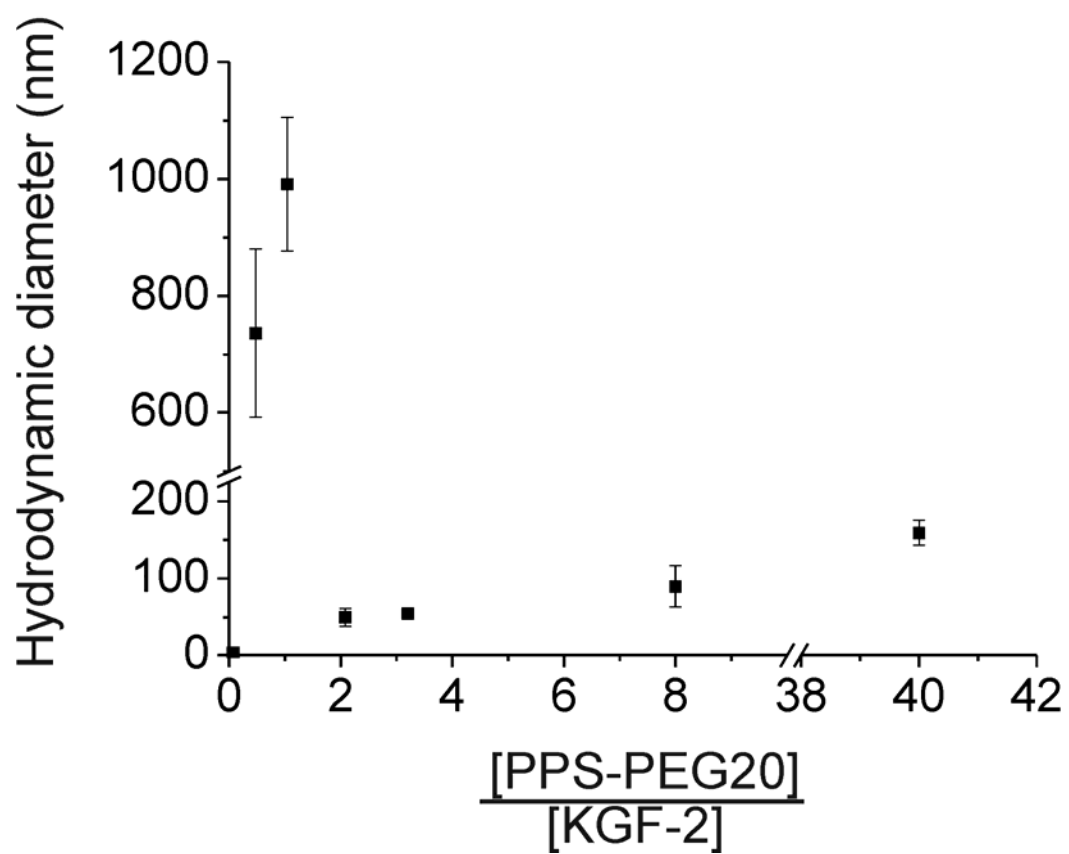


Figure 4.14. The hydrodynamic diameter of KGF-2:PPS-PEG20 complexes at 20 °C.

Table 4.3. Transition midpoint of KGF-2 alone and in the presence of polyanions and polyanion-PEGs

Samples	Molar ratios	Transition midpoint, T _m (°C)		
		Circular dichroism (CD)*	Intrinsic fluorescence*	Differential scanning calorimetry (DSC)*
KGF-2	-	39.2	42.5	45.7
KGF-2:PPS	(1:2)	51.8	52.5	62.0
	(1:1)	51.3	49.3	60.3
	(2.4:1)	44.3	43.0	47.6, 59.8
	(6:1)	42.0	42.2	47.6, 59.3
KGF-2:PPS-PEG5	(1:2)	44.1	52.1	61.7
	(1:1)	50.0	53.0	62.2
	(2.4:1)	44.3	44.7	61.4
	(6:1)	41.1	42.1	46.5, 60.9
KGF-2:PPS-PEG20	(1:2)	52.0	50.4	59.8
	(1:1)	51.1	52.4	60.6
	(2.4:1)	50.5	53.8	61.7
	(6:1)	42.5	42.2	52.8, 60.5
KGF-2:DS	(1:2)	51.0	45.0	61.7
	(1:1)	45.0	53.8	62.8
	(2.4:1)	43.0	43.2	60.9
	(6:1)	42.5	42.5	49.0, 60.61
KGF-2:DS-PEG5	(1:2)	46.1	47.1	56.8
	(1:1)	42.5	41.9	57.4
	(2.4:1)	41.0	40.0	57.9
	(6:1)	41.0	41.2	46.0, 57.6
KGF-2:DS-PEG20	(1:2)	46.5	49.4	56.8
	(1:1)	50.1	50.4	58.4
	(2.4:1)	48.2	52.0	60.3
	(6:1)	41.4	42.3	60.1

* Values are ± 0.5 °C

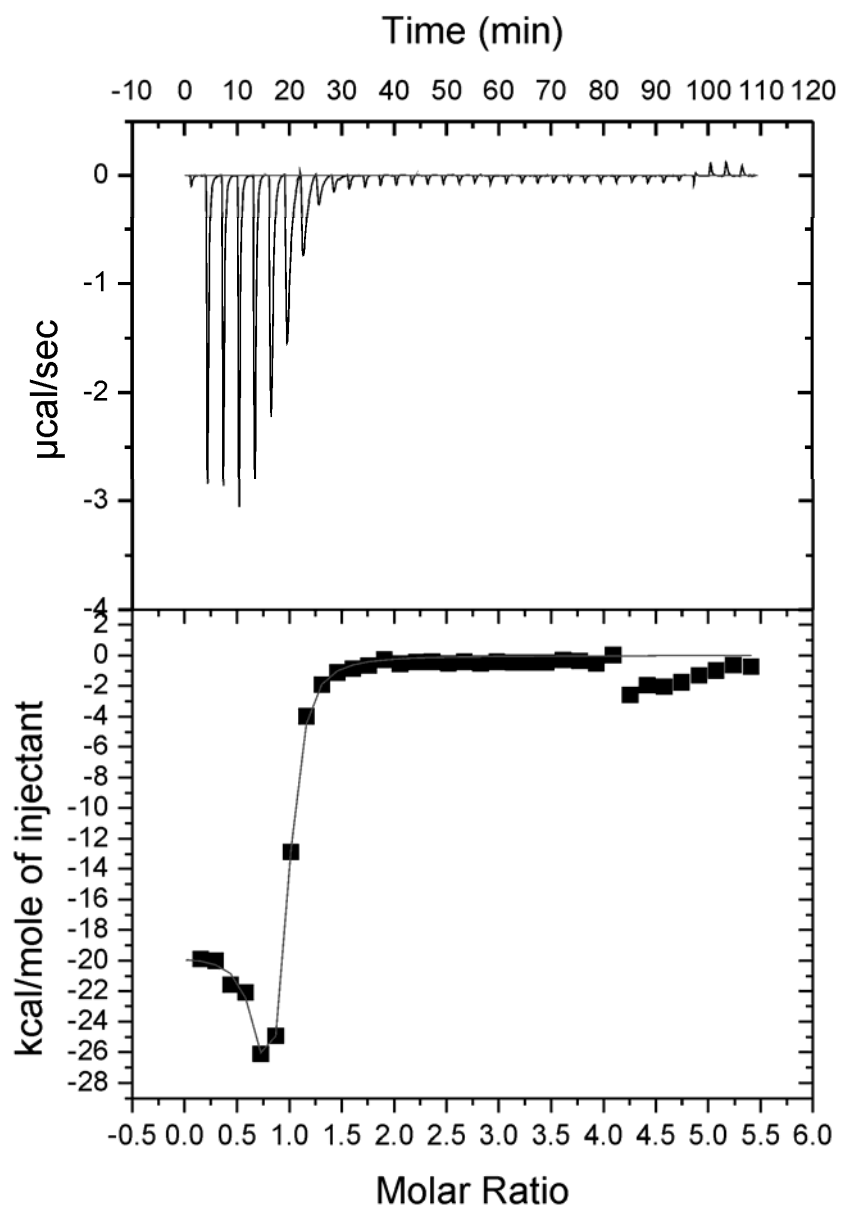


Figure 4.15. Representative ITC binding isotherm of KGF-2 (20 μM) titrated with DS (500 μM) at 25 $^{\circ}\text{C}$.

Table 4.4. Thermodynamic parameters of most KGF-2 interactions with polyanions or conjugates using a two-site model and a one-site model for KGF-2:PPS-PEG20 complexes ($*\Delta G = \Delta H - T\Delta S$, $T = 298$ K)

	PPS	PPS-PEG5	PPS-PEG20	DS	DS-PEG5	DS-PEG20
Enthalpy						
ΔH_1 (kcal/mol)	-1.41±1.8	-15.0±5.0	-4.1	-15.4±6.0	-17.0	-17.3
ΔH_2 (kcal/mol)	-73.0±34.0	-47.8±1.1		-35.9±6.9	-18.1±1.5	-29.7±17.6
Entropy						
$T\Delta S_1$ (kcal/mol)	7.6±1.9	-4.9±4.7	5.5	-5.0±5.9	3.4±16.4	-8.1
$T\Delta S_2$ (kcal/mol)	-64.7±34.1	-39.3±0.8		-26.8±7.6	-6.8±3.7	-22.2±19.6
Free energy						
$*\Delta G_1$ (kcal/mol)	-9.0±0.1	-10.0±0.2	-9.6	-10.4±0.1	-8.8	-9.2
$*\Delta G_2$ (kcal/mol)	-8.4±0.2	-8.4±0.1		-9.1±0.7	-7.5	-7.1
K_a						
K_{a1} (M ⁻¹)	3.9E6±5.4E5	2.4E7±8.5E6	1.1E7	4.3E7±7.2E6	2.6E6	6.0E5
K_{a2} (M ⁻¹)	1.5E6±5.6E5	1.6E6±2.5E5		6.2E6±5.9E6	3.3E5	1.8E5±2.4E5
Ligand/protein						
N_1	1.6±0.4	0.3±0.0	0.3	0.5±0.2	0.4±0.1	0.5±0.0
N_2	0.2±0.1	0.3±0.0		0.4±0.2	0.4±0.2	0.5±0.1
Protein/ligand						
$1/N_1$	~0.6	~3.2	~3.9	~2.0	~2.6	~2.2
$1/N_2$	~4.3	~3.1		~2.4	~2.4	~2.2

DS:PEG5 and DS:PEG20 were similar (63, 69 and 54 nm, respectively). When subjected to increasing temperature, KGF-2 alone had an onset temperature of aggregation of ~ 31 °C (Figure 4.13 B1 and 2). KGF-2:PPS-PEG20 and KGF-2:DS-PEG20 complexes had higher onset temperature of aggregation (~ 45 -50 °C) and maintained size better than other formulations. KGF-2:DS-PEG5 (1:2) showed poorer colloidal stability compared to the other formulations.

Additionally, the hydrodynamic diameters of KGF-2:PPS-PEG20 complexes were monitored over a wider molar ratio range to test whether oligomerization may be occurring (Figure 4.14). The hydrodynamic diameters of the complexes at 0.5 and 1 molar ratios (PPS-PEG20:KGF-2) increased dramatically (~ 700 -1,000 nm) suggesting high degree of oligomerization. When adding more conjugate, the complex size decreased to ~ 50 nm at 2 and 3 molar ratios. The complex size increased again to ~ 90 and 160 nm at 8 and 40 molar ratios.

4.3.7 Isothermal titration calorimetry

Thermodynamic characteristics were determined for the binding of KGF-2 to various polyanions and conjugates using ITC (Table 4.4). A representative binding isotherm of KGF-2 (20 μ M) titrated with DS (500 μ M) at 25 °C is shown in Figure 4.15. The integrated peak areas were fit to a two-site independent binding site model for most complexes (a one-site model for KGF-2:PPS-PEG20 complexes) and the resulting enthalpies of binding (ΔH), binding constant (K), entropies of binding ($T\Delta S$) and binding stoichiometries (n) were calculated. The inverse of the binding stoichiometries yielded a value for the number of proteins bound per ligand.

All interactions of KGF-2 with polyanions or conjugates revealed significant negative enthalpies of binding (Table 4.4). This may be explained by favorable electrostatic contacts between negative charges of these ligands with positive charges

on the protein. Most binding events (except KGF-2:PPS (first binding site), KGF-2:PPS-PEG20 and KGF-2:DS-PEG5) were entropically disfavored (negative ΔS values). The change in free energy was similar for all polyanions or conjugates. Moderate to strong binding constants were detected for all titrations with K_a values in the micromolar range. Observed stoichiometry values for PPS conjugates were variable, whereas the values for DS conjugates were quite consistent over duplicate runs. Approximately two to three and one to four molecules of KGF-2 were bound to DS-based and PPS-based ligands, respectively.

4.3.8 Competitive binding study

In an attempt to investigate the reversibility of the binding between polyanion conjugates and the protein, KGF-2:PPS-PEG5 and KGF-2:PPS-PEG20 complexes were challenged using heparin (14 kDa, 0.2 to 5.0 U) and were then subjected to electrophoresis (data not shown). The free protein and protein from complexes showed no differences in electrophoretic mobility. The protein may have lost the heparin-binding domain and released polyanion conjugates under these conditions.

4.4 Discussion

Heparin and other polyanionic materials have been utilized to stabilize or enhance the activity of HBGFs or other proteins such as insulin.⁴¹ Middaugh *et al.* showed that heparin enhanced the thermal stability of FGF-1 and prevented low-pH unfolding.²³ In a separate report from the same group, a variety of polyanions such as heparin, sucrose octasulfate (SOS) and inositol hexaphosphate also elevated the aggregation temperature of KGF-2.²⁰ Another report from the same group showed that heparin enhanced the thermal stability of FGF-20.²⁴ Giger *et al.* also reported that heparin was able to suppress insulin aggregation.⁴¹

Hence, the polyanions, PPS and DS, were conjugated with different molecular weight PEG polymers. The conjugation reactions exhibited moderate to high yield and the dialyzed products showed high purity. The conjugates were then characterized using variety of methods. The methylene blue experimental data indicated that there was one PEG chain on each PPS conjugate, while DS:PEG5 and DS:PEG20 conjugates had up to 5 and ~2 PEG chains, respectively (Table 4.1). PPS has a single reactive carboxyl group, while DS has multiple hydroxyl groups that can be converted to reactive carboxyl groups. Conjugation of PEG to DS agrees with previous reports indicating that the grafting density decreased as the PEG chain length increased.⁴²⁻⁴³ Higher MW PEGs have slower diffusion rates and greater excluded volume, thereby slowing transport to reaction sites and impeding tight packing compared to low MW PEGs.⁴²

In gas phase, it is difficult to ionize highly acidic compounds especially polysulfated materials or polysulfonic acids, since these compounds tend to tightly bind counterions such as Na^+ and K^+ .⁴⁴ Electrospray ionization (ESI) and matrix assisted laser desorption/ionization time-of-flight (MALDI-TOF) mass spectrometry were attempted to determine the MW of these conjugates, but the experiments were not successful even when employing special sample preparation methods.⁴⁴⁻⁴⁵ Therefore, SEC and SDS-PAGE were chosen as methods to estimate the size of these conjugates.

Based on SEC and SDS-PAGE data, the conjugates had narrow populations and exhibited characteristics of both PEG and the polyanion. Ideally, SEC systems should be calibrated with compounds having similar structures to the sample being analyzed. PEG, HA or dextran were not suitable standards for this system.

Furthermore, these sulfated polysaccharides interacted with the column of polyhydroxymethacrylate.

The effect of polyanions and conjugates on the structure and stability of KGF-2 was studied using far-UV CD and intrinsic fluorescence to track both secondary and tertiary structure changes. The observed changes in CD spectra and emission maximum positions of bound KGF-2 suggested that the binding of polyanions or conjugates altered the secondary and tertiary structures of KGF-2. Structural changes upon binding with charged compounds have been commonly observed. For example, structural alteration as seen in parathyroid hormone (PTH) in the presence of DS (40-50 kDa) or heparin (12-16 kDa) and FGF-1 upon binding with suramin.⁴⁶⁻⁴⁷

The observed changes in CD spectra may have also been due to absorption flattening from oligomerization, which has been previously reported.^{46,48} The degree of oligomerization depended on the amount of polyanion present, which is consistent with data for KGF-2:PPS-PEG20 complexes reported here (Figure 4.14). At low polyanion to protein ratio (0.1), little or no oligomerization was observed. At higher ratios (0.5 and 1), the increase in hydrodynamic diameter suggested extensive oligomerization. At even higher ratios (2 and 3), the protein was probably saturated by polyanion resulting in small complexes. As a result, high polyanion to protein ratios were used in many studies including a 50-fold excess (w/w) of SOS to KGF-2.²⁰

The apparent melting temperature of KGF-2 in the presence of polyanions and conjugates was, however, significantly increased by 11-13 °C, based on fluorescence and CD data. Polyanions probably stabilized KGF-2 by interacting with positively charged amino acid clusters on the surface of the native protein.⁴⁹

Most polyanion or conjugate interactions with KGF-2 were enthalpically driven, however, some formulations showed entropically driven binding. In many situations, electrostatic bindings usually are entropically driven. This is usually explained by the removal of water molecules from the charged compounds.⁴⁷ There are, however, examples of electrostatic interactions between proteins and charged compounds that are enthalpically driven. For example, binding between gum arabic and BSA, between heparin and PTH, and between sodium dodecyl sulphate and gelatin.^{47,50-51}

The observed negative entropy values may be indicative of different interactions occurring in this system. Negative entropy may primarily be due to oligomerization. DLS data showed a drastic increase in size of the complexes at molar ratios of 0.5:1 and 1:1 (PPS-PEG20:KGF-2). Oligomerization may interfere with interactions between KGF-2 and polyanions and constrain their motions. Also, ITC data indicated multiple molecules of KGF-2 bound to a single chain of PPS or DS conjugate. Under these conditions, microaggregates may occur in which multiple proteins bind to extended polyanion chains, which can then oligomerize.⁴⁷ In such cases, the thermodynamics of microaggregate processes may overlap with the observed thermodynamic binding parameters making interpretations difficult. Similar results have been reported by Mach and Middaugh with FGF-1 and other growth factors.^{46,48} Lastly, PEG may sterically hinder binding (e.g. DS-PEG5), which would reduce the magnitude of thermodynamic values associated with polyanion binding.

Finally, ITC data also suggested that one to four molecules of KGF-2 were bound with PPS conjugates, whereas two to three molecules of KGF-2 were bound with DS conjugates. This agreed with a previous binding study between KGF-2 and DS (8,000 Da), which revealed that 2 to 2.6 KGF-2 molecules were bound to one DS

chain.⁵³ The same study also indicated that heparin (5,000 Da):KGF-2 complexes were heterogeneous consisting of one to four KGF-2 molecules per complex.

4.5 Conclusion

Based on various spectroscopic and calorimetric methods, the polyanion conjugates appeared to increase the thermal stability of KGF-2. Conjugates with higher PEG densities (DS-PEG5) did not bind KGF-2 as well as other conjugates, thus reducing the stabilization effect. PEG MW did not have a noticeable effect. There are several important factors to consider if polyanion conjugates are used to produce more stable pharmaceutical formulation of KGF-2 including the identification of proper molar ratios to avoid oligomerization. Polyanion-PEG conjugates were validated as alternative excipients that can improve the stability of heparin-binding proteins and that may ultimately be explored to extend circulation half-life.

4.6 Bibliography

1. Dudzinski D, Kesselheim A 2008. Scientific and legal viability of follow-on protein drugs. *New England Journal of Medicine* 358(8):843.
2. Werle M, Bernkop-Schnurch A 2006. Strategies to improve plasma half life time of peptide and protein drugs. *Amino Acids* 30(4):351-367.
3. Caliceti P, Veronese F 2003. Pharmacokinetic and biodistribution properties of poly (ethylene glycol)-protein conjugates. *Advanced drug delivery reviews* 55(10):1261-1277.
4. Duncan R 2003. The dawning era of polymer therapeutics. *Nature Reviews Drug Discovery* 2(5):347-360.
5. Powers C, McLeskey S, Wellstein A 2000. Fibroblast growth factors, their receptors and signaling. *Endocrine-related cancer* 7(3):165.
6. Ledoux D, Gannoun-Zaki L, Barritault D 1992. Interactions of FGFs with target cells. *Progress in growth factor research* 4(2):107-120.
7. Rusnati M, Presta M 1996. Interaction of angiogenic basic fibroblast growth factor with endothelial cell heparan sulfate proteoglycans. *International journal of clinical & laboratory research* 26(1):15-23.
8. Arakawa T, Wen J, Philo J 1994. Stoichiometry of heparin binding to basic fibroblast growth factor. *Archives of biochemistry and biophysics* 308(1):267-273.
9. Faham S, Hileman R, Fromm J, Linhardt R, Rees D 1996. Heparin structure and interactions with basic fibroblast growth factor. *Science(Washington)* 271(5252):1116-1116.
10. Wong P, Hampton B, Szylobryt E, Gallagher A, Jaye M, Burgess W 1995. Analysis of putative heparin-binding domains of fibroblast growth factor-1. *Journal of Biological Chemistry* 270(43):25805.
11. Ruoslahti E, Yamaguchi Y 1991. Proteoglycans as modulators of growth factor activities. *Cell* 64(5):867.
12. Saksela O, Moscatelli D, Sommer A, Rifkin D 1988. Endothelial cell-derived heparan sulfate binds basic fibroblast growth factor and protects it from proteolytic degradation. *The Journal of cell biology* 107(2):743.
13. Sommer A, Rifkin D 1989. Interaction of heparin with human basic fibroblast growth factor: protection of the angiogenic protein from proteolytic degradation by a glycosaminoglycan. *Journal of cellular physiology* 138(1):215-220.
14. Lu W, Luo Y, Kan M, McKeehan W 1999. Fibroblast growth factor-10. *Journal of Biological Chemistry* 274(18):12827.
15. Emoto H, Tagashira S, Mattei M, Yamasaki M, Hashimoto G, Katsumata T, Negoro T, Nakatsuka M, Birnbaum D, Coulier F 1997. Structure and expression of human fibroblast growth factor-10. *Journal of Biological Chemistry* 272(37):23191.
16. Gillis P, Savla U, Volpert O, Jimenez B, Waters C, Panos R, Bouck N 1999. Keratinocyte growth factor induces angiogenesis and protects endothelial barrier function. *Journal of Cell Science* 112:2049-2057.
17. Ishiwata T, Naito Z, Ping Lu Y, Kawahara K, Fujii T, Kawamoto Y, Teduka K, Sugisaki Y 2002. Differential Distribution of Fibroblast Growth Factor (FGF)-7 and FGF-10 in-Arginine-Induced Acute Pancreatitis. *Experimental and molecular pathology* 73(3):181-190.
18. Jimenez P, Rampy M 1999. Keratinocyte growth factor-2 accelerates wound healing in incisional wounds. *Journal of Surgical Research* 81(2):238-242.
19. Robson M, Phillips T, Falanga V, Odenheimer D, Parish L, Jensen J, Steed D 2001. Randomized trial of topically applied repifermin (recombinant human

keratinocyte growth factor 2) to accelerate wound healing in venous ulcers. *Wound Repair and Regeneration* 9(5):347-352.

20. Derrick T, Grillo A, Vitharana S, Jones L, Rexroad J, Shah A, Perkins M, Spitznagel T, Middaugh C 2007. Effect of polyanions on the structure and stability of repifermin(tm)(keratinocyte growth factor 2). *Journal of Pharmaceutical Sciences* 96(4):761-776.

21. Sung C, Parry T, Riccobene T, Mahoney A, Roschke V, Murray J, Gu M, Glenn J, Caputo F, Farman C 2002. Pharmacologic and pharmacokinetic profile of repifermin (KGF-2) in monkeys and comparative pharmacokinetics in humans. *The AAPS Journal* 4(2):24-33.

22. Chen BL, Arakawa T 1996. Stabilization of recombinant human keratinocyte growth factor by osmolytes and salts. *Journal of Pharmaceutical Sciences* 85(4):419-422.

23. Fan H, Li H, Zhang M, Middaugh C 2007. Effects of solutes on empirical phase diagrams of human fibroblast growth factor 1. *Journal of Pharmaceutical Sciences* 96(6):1490-1503.

24. Fan H, Vitharana S, Chen T, O'Keefe D, Middaugh C 2007. Effects of pH and polyanions on the thermal stability of fibroblast growth factor 20.

25. Kajio T, Kawahara K, Kato K 1992. Stabilization of basic fibroblast growth factor with dextran sulfate. *FEBS letters* 306(2-3):243-246.

26. Larramendy-Gozaló C, Barret A, Daudigeos E, Mathieu E, Antonangeli L, Riffet C, Petit E, Papy-Garcia D, Barritault D, Brown P 2007. Comparison of CR36, a new heparan mimetic, and pentosan polysulfate in the treatment of prion diseases. *Journal of General Virology* 88(3):1062.

27. Nickel J, Kaufman D, Zhang H, Wan G, Sand P 2008. Time to initiation of pentosan polysulfate sodium treatment after interstitial cystitis diagnosis: effect on symptom improvement. *Urology* 71(1):57-61.

28. Rusnati M, Urbinati C 2009. Polysulfated/Sulfonated Compounds for the Development of Drugs at the Crossroad of Viral Infection and Oncogenesis. *Current pharmaceutical design* 15(25):2946-2957.

29. Tsai P, Volkin DB, Dabora JM, Thompson KC, Bruner MW, Gress JO, Matuszewska B, Keogan M, Bondi JV, Middaugh CR 1993. Formulation design of acidic fibroblast growth factor. *Pharmaceutical research* 10(5):649-659.

30. Harada M, Murata J, Sakamura Y, Sakakibara H, Okuno S, Suzuki T 2001. Carrier and dose effects on the pharmacokinetics of T-0128, a camptothecin analogue-carboxymethyl dextran conjugate, in non-tumor-and tumor-bearing rats. *Journal of Controlled Release* 71(1):71-86.

31. Zhang R, Tang M, Bowyer A, Eisenthal R, Hubble J 2005. A novel pH-and ionic-strength-sensitive carboxy methyl dextran hydrogel. *Biomaterials* 26(22):4677-4683.

32. Kurfurst MM 1992. Detection and molecular weight determination of polyethylene glycol-modified hirudin by staining after sodium dodecyl sulfate-polyacrylamide gel electrophoresis. *Analytical biochemistry* 200(2):244-248.

33. Lee KC, Tak KK, Park MO, Lee JT, Woo BH, Yoo SD, Lee HS, DeLuca PP 1999. Preparation and characterization of polyethylene-glycol-modified salmon calcitonins. *Pharmaceutical development and technology* 4(2):269-275.

34. Zhai Y, Zhao Y, Lei J, Su Z, Ma G 2009. Enhanced circulation half-life of site-specific PEGylated rhG-CSF: Optimization of PEG molecular weight. *Journal of biotechnology* 142(3-4):259-266.

35. Jiao Q, Liu Q, Sun C, He H 1999. Investigation on the binding site in heparin by spectrophotometry. *Talanta* 48(5):1095-1101.
36. Antonov Y, Sato T 2009. Macromolecular complexes of the main storage protein of *Vicia faba* seeds with sulfated polysaccharide. *Food Hydrocolloids* 23(3):996-1006.
37. Michon C, Konat K, Cuvelier G, Launay B 2002. Gelatin/carrageenan interactions in coil and ordered conformations followed by a methylene blue spectrophotometric method. *Food Hydrocolloids* 16(6):613-618.
38. Ottoy MH, V rum KM, Christensen BE, Anthonsen MW, Smidsr d O 1996. Preparative and analytical size-exclusion chromatography of chitosans. *Carbohydrate polymers* 31(4):253-261.
39. Copeland R, Ji H, Halfpenny A, Williams R, Thompson K, Herber W, Thomas K, Bruner M, Ryan J, Marquis-Omer D 1991. The structure of human acidic fibroblast growth factor and its interaction with heparin. *Archives of biochemistry and biophysics* 289(1):53-61.
40. Gosavi S, Jennings P, Onuchic J 2007. The folding of an "average" beta trefoil protein. *Bulletin of the American Physical Society* 52.
41. Giger K, Vanam R, Seyrek E, Dubin P 2008. Suppression of insulin aggregation by heparin. *Biomacromolecules* 9(9):2338-2344.
42. Ostaci RV, Dameron D, Al Akhrass S, Grohens Y, Drockenmuller E 2010. Poly (ethylene glycol) brushes grafted to silicon substrates by click chemistry: influence of PEG chain length, concentration in the grafting solution and reaction time. *Polym Chem*.
43. Zdyrko B, Varshney SK, Luzinov I 2004. Effect of molecular weight on synthesis and surface morphology of high-density poly (ethylene glycol) grafted layers. *Langmuir* 20(16):6727-6735.
44. Juhasz P, Biemann K 1994. Mass spectrometric molecular-weight determination of highly acidic compounds of biological significance via their complexes with basic polypeptides. *Proceedings of the National Academy of Sciences of the United States of America* 91(10):4333.
45. Chattopadhyay K, Mandal P, Lerouge P, Driouich A, Ghosal P, Ray B 2007. Sulphated polysaccharides from Indian samples of *Enteromorpha compressa* (Ulvales, Chlorophyta): Isolation and structural features. *Food Chemistry* 104(3):928-935.
46. Middaugh CR, Mach H, Burke CJ, Volkin DB, Dabora JM, Tsai P, Bruner MW, Ryan JA, Marfia KE 1992. Nature of the interaction of growth factors with suramin. *Biochemistry* 31(37):9016-9024.
47. Kamerzell TJ, Joshi SB, McClean D, Peplinskie L, Toney K, Papac D, Li M, Middaugh CR 2007. Parathyroid hormone is a heparin/polyanion binding protein: Binding energetics and structure modification. *Protein Science* 16(6):1193-1203.
48. Mach H, Volkin DB, Burke CJ, Middaugh CR, Linhardt RJ, Fromm JR, Loganathan D, Mattsson L 1993. Nature of the interaction of heparin with acidic fibroblast growth factor. *Biochemistry* 32(20):5480-5489.
49. Chen B, Arakawa T, Hsu E, Narhi L, Tressel T, Chien S 1994. Strategies to suppress aggregation of recombinant keratinocyte growth factor during liquid formulation development. *Journal of Pharmaceutical Sciences* 83(12):1657-1661.
50. Onesippe C, Lagerge S 2009. Study of the complex formation between sodium dodecyl sulphate and gelatin. *Colloids and Surfaces A: Physicochemical and Engineering Aspects* 337(1-3):61-66.

51. Vinayahan T, Williams PA, Phillips G 2010. Electrostatic Interaction and Complex Formation between Gum Arabic and Bovine Serum Albumin. *Biomacromolecules*:420-476.
52. Dhalluin C, Ross A, Huber W, Gerber P, Brugger D, Gsell B, Senn H 2005. Structural, kinetic, and thermodynamic analysis of the binding of the 40 kDa PEG-interferon- 2a and its individual positional isomers to the extracellular domain of the receptor IFNAR2. *Bioconjugate chemistry* 16(3):518-527.
53. Wen J, Hsu E, Kenney W, Philo J, Morris C, Arakawa T 1996. Characterization of keratinocyte growth factor binding to heparin and dextran sulfate. *Archives of biochemistry and biophysics* 332(1):41-46.

Chapter 5

Conclusions

5.1 Summary and conclusions

Polymeric drug delivery systems hold promise in the 21st century. Polymers are versatile, easy to produce at the industrial scale, and amenable to conjugation reactions. Passively or actively targeted drug delivery has been made possible by using well-controlled size or by grafting targeting ligands to polymers.¹⁻³ Furthermore, pharmacokinetics, biodistribution, and/or therapeutic indexes of some drugs have been improved by PEGylation or by other types of polymer conjugation.⁴ The increasing number of polymeric drugs commercially available or being evaluated in clinical trials demands an enhanced effort to produce innovative and more efficient polymers.

In this thesis, we have explored the potential uses of some tailor-made polyelectrolytes in gene and protein delivery. In chapter 2, the cytotoxicity and transfection efficiency of a synthetic polyvinylamine (PVAm) nanogel was probed as a function of particle charge and degradability. We found that non-degradable nanogels with high charge densities yielded higher gene expression compared to nanogels with low charge densities. Interestingly, acid-labile nanogels with low charge densities yielded extended gene expression while maintaining lower cytotoxicity. The data reiterated that balancing transfection efficiency and toxicity is a key that should be further explored in order to develop suitable gene vectors. Furthermore, the data also suggested that gene expression studies should be extended for longer periods of time to account for delays in transfection or cell viability.

Cationic nanoparticles have been reported to be cleared from the body quickly due to an increased hydrodynamic diameter resulting from serum protein adsorption.⁵ Neutralization of the nanoparticle surface via PEGylation was shown to be effective in preventing serum protein adsorption.⁶ Therefore, the synthetic PVAm was replaced

with the biodegradable CPP TAT conjugated with PEG in an effort to improve plasma compatibility and ultimately, *in vivo* performance.

Chapter 3 presented these PEGylated TAT/DNA complexes and explored targeted versions as a means to transfect ICAM-1 expressing cells. ICAM-1 upregulation is associated with many diseases. TAT polyplexes with DNA have historically shown relatively poor gene delivery, but the transfection efficiency was enhanced by condensing TAT/DNA complexes to a small particle size using calcium. LABL peptide targeting ICAM-1 was conjugated to the TAT peptide using a PEG spacer. We found that PEGylation reduced the transfection efficiency of TAT as expected, but targeted TAT complexes formulated with an optimal calcium concentration regained much of the lost transfection efficiency in activated A549 cells (overexpressing ICAM-1). There are, however, several concerns about the use of this gene vector. Complexes were produced manually, thus batch to batch consistency will be of concern when conducting studies in animals. Although the targeted TAT complexes showed selectivity to ICAM-1 on activated cells, however these effects seem to be small. Therefore, it is necessary to compare the transfection efficiency between non-targeted and targeted formulations and, more importantly, placebo in an early *in vivo* screen. Lastly, dilution effect may hinder the targetability of these complexes when administered intravenously, hence local administration may be explored at an initial stage of animal trials.

In chapter 4, another polyelectrolyte vehicle was explored for protein delivery. Electrostatic interactions between polyanions and several FGFs have been reported to enhance the thermal stability of these proteins as well as other ‘heparin-binding’ proteins. PEG was grafted to the polyanions, PPS and DS, as a novel means to non-covalently PEGylate KGF-2. PPS-PEG and DS-PEG conjugates were able to stabilize

KGF-2 by increasing the melting temperature. It is possible that micro-aggregation occurs simultaneously with electrostatic binding when conducted ITC experiments. The thermodynamics of microaggregation may be superimposed upon the measured thermodynamic binding parameters making interpretations difficult. Therefore, alternative approaches such as analytical ultracentrifugation may be used to identify KGF2:polyanion conjugate stoichiometry. Also, acrylamide gel electrophoresis seemed not to be suitable to investigate the interaction affinity in this system, alternative approaches such as surface plasmon resonance may be used to elucidate the binding affinity.

Furthermore, there are several concerns about the utilization of these conjugates. PEG may sterically hinder receptor binding affinity of the protein. In addition, polyanion conjugate binding may interfere the presentation of KGF-2 to their cell surface receptors, which may diminish signal transduction, thus receptor binding assays are needed. The observed structural changes upon binding may affect protein activity, mitogenic activity in fibroblast cells will be helpful to predict the activity of protein conjugates.

However, these conjugates are encouraging excipients that can improve the stability of heparin-binding proteins based on this work and the generality of polyanions and protein interactions known from the literature.

5.2 Future directions

With respect to the continued development of targeted TAT/DNA complexes, the next key task is to evaluate the transfection efficiency of these complexes in primary human cells. Even though, the correlation between *in vitro* and *in vivo* efficiency of gene vectors has been elusive, the efficiency data from primary human cells will provide critical information for these complexes. In addition,

immunogenicity (cytokine and chemokine induction) and an early *in vivo* screen of antigenicity (e.g. IgG, IgM production) will be essential when evaluating transfection efficiency of these complexes in an animal model of human disease. It is worth noting that production of PEGylated TAT or targeted TAT complexes with DNA is laborious, therefore, production scale-up should be taken into consideration in order to transition from the laboratory bench to the clinic.

To further develop PPS-PEG and DS-PEG conjugates, the next step should be to carry out preclinical pharmacokinetic and biodistribution tests in an animal model. This data will be crucial to determine whether key benefits of PEGylation are maintained by this electrostatic PEGylation approach. In addition, immunogenicity assays should be conducted in an animal model (e.g. mice) to monitor specific IgG levels. These should be explored for both polyanion-PEG conjugates and for protein complexes. In the next step of formulation development, short- and long-term stability tests of the protein and protein complexes in both solution and lyophilized forms should be explored. Furthermore, studies to find optimized reconstitution mediums or conditions will also be necessary to enhance the recovery of the protein.

5.3 Bibliography

1. Kim S, Kim JH, Jeon O, Kwon IC, Park K 2009. Engineered polymers for advanced drug delivery. *European journal of pharmaceutics and biopharmaceutics: official journal of Arbeitsgemeinschaft fur Pharmazeutische Verfahrenstechnik eV* 71(3):420.
2. Maeda H, Bharate G, Daruwalla J 2009. Polymeric drugs for efficient tumor-targeted drug delivery based on EPR-effect. *European Journal of Pharmaceutics and Biopharmaceutics* 71(3):409-419.
3. Xie Y, Bagby TR, Cohen M, Forrest ML 2009. Drug delivery to the lymphatic system: importance in future cancer diagnosis and therapies.
4. Haag R, Kratz F 2006. Polymer therapeutics: concepts and applications. *Angewandte Chemie International Edition* 45(8):1198-1215.
5. Longmire M, Choyke PL, Kobayashi H 2008. Clearance properties of nano-sized particles and molecules as imaging agents: considerations and caveats. *Nanomedicine* 3(5):703-717.
6. Sato A, Choi SW, Hirai M, Yamayoshi A, Moriyama R, Yamano T, Takagi M, Kano A, Shimamoto A, Maruyama A 2007. Polymer brush-stabilized polyplex for a siRNA carrier with long circulatory half-life. *Journal of Controlled Release* 122(3):209-216.